POLITECNICO DI MILANO

School of Industrial and Information Engineering

MSc in Energy Engineering

Development of a quasi-2D dynamic model for simulation of Solid Oxide Fuel Cells

Supervisor: Prof. Stefano Campanari

Co-supervisor: Prof. Luca Mastropasqua

Author:

Alberto Cammarata, 877181

Academic year 2018 - 2019

Abstract

The purpose of the present work is to extend and improve an existing code capable of simulating the stationary performance of a high temperature planar SOFC in co-flow configuration, and to make it dynamic. Now, the code is much more accurate and efficient than it was, and it is now capable of simulating the transient after a load connection, starting from the hot cell at OCV. Anyway, the model can be easily adapted to run several type of dynamic simulations. One of the aim of the code will be the integration with a wider program for the simulation of advanced power systems, thus one of the focus has been the improvement of its velocity so as not to slow down the overall simulation. As a matter of fact, the calculations are now 20-200 times faster, depending on the type of simulation run. The code has been widely revised and extended in all its parts, indeed the revision process represents a considerable share of the work done. For instance, an iterative method to account for axial conduction within the cell has been implemented. Thus, a final results comparison against an already validated code has been performed, showing good matching. One of the work highlights is the developing of a direct carbon monoxide oxidation model defining a single reversible voltage, which proved to give realistic results in line with expectations. Moreover, a low temperature SOFC Macro-Scale model has been implemented, the comparison of its polarization curves with experimental data gave good results. Nevertheless, solving the charge conservation equations within the electrodes would enhance the model performance, due to an accurate evaluation of ohmic ionic losses and activation losses within the electrodes. Finally, the interest in investigating the SOFC dynamic in certain situations such as startup and dynamic load-following has led to the implementation of a dynamic model, which gave realistic results consistent with the stationary model ones.

Abstract

Lo scopo di questo lavoro è di migliorare ed estendere un codice esistente in grado di lanciare simulazioni stazionarie di celle SOFC planari ad alta temperatura in configurazione co-flow, e di implementare un modello dinamico. Allo stato attuale il codice è di gran lunga più accurato e veloce di quanto non fosse in partenza, ed è inoltre in grado di simulare il transitorio dopo la connessione di un carico, partendo dalla situazione stazionaria di cella calda. Il modello può comunque essere facilmente adattato a lanciare svariati tipi di simulazioni dinamiche. Uno dei principali obiettivi del codice sarà quello di essere integrato in un più ampio programma atto a simulare sistemi energetici avanzati, per questo motivo è stata posta un'attenzione particolare all'efficienza del codice, di modo che non rallenti l'intera simulazione. A seguito delle modifiche apportate in tal senso, la velocità di calcolo del codice è aumentata di 20-200 volte, a seconda del tipo di simulazione considerata. Il codice è stato ampiamente revisionato ed esteso in ogni sua parte, tanto che il processo di revisione ha ricoperto una parte molto considerevole del lavoro svolto. Ad esempio, è stato implementato un metodo iterativo per considerare la conduzione assiale interna alla cella. Considerando quanto sopra, si è ritenuto necessario validare i risultati del codice comparandoli con quelli di un codice già validato, ottenendo ottimi risultati. Inoltre, è stato introdotto un modello per l'ossidazione diretta del monossido di carbonio, la cui peculiarità è quella di definire un'unica tensione reversibile. I risultati del modello si sono dimostrati realistici e allineati con le aspettative. Nel codice è anche stato implementato un modello per la simulazione di celle SOFC a bassa temperatura, il confronto delle curve di polarizzazione ottenute con dati sperimentali ha dato buoni risultati. Nonostante ciò, risolvere le equazioni di conservazione della carica negli elettrodi esalterebbe le prestazioni del modello, sia per quanto riguarda i risultati che per quanto concerne la stabilità dei risultati stessi. Questo sarebbe dovuto ad una più accurata analisi delle perdite ohmiche e di attivazione negli elettrodi. Infine, l'interesse nel valutare la dinamica della cella in situazioni come lo startup e il load-following di un carico variabile, ha portato all'implementazione di un modello dinamico nel codice. Questo ha dimostrato di dare risultati realistici e consistenti con i risultati forniti dal modello stazionario.

Contents

Extended abstract

1. Introduction

Fuel cells are widely acknowledged to be a very promising technology, mainly due to their high efficiency, low emissions and absence of moving parts compared to conventional power systems. The main fuel considered to run these devices is hydrogen, which ideally determines just water as final product.

The present work focuses on Solid Oxide Fuel Cells (SOFCs), characterized by high operating temperature and fuel flexibility. As a matter of fact, SOFC anodes may catalyze both Methane Steam Reforming (MSR) and electrochemical reactions. The high operating temperature benefits the cell efficiency, plus it could bust the efficiency of a combined cycle, leading to unsurpassed electric efficiency levels [1]. Nevertheless, the high operating temperature limits SOFCs commercialization due to materials degradation, high manufacturing cost, and both time and energy consuming startup [2][3]. The latter is one of the reason for which SOFCs transients should be investigated, together with the need to assess thermal stresses and load-following behaviour. Thus, nowadays efforts are aimed at lowering their temperature to switch to metallic construction materials. Nevertheless, the electrolyte would likely be a Mixed Ionic and Electronic Conducting (MIEC) material, which introduces intrinsic losses in the system.

Considering the above, the aim of the present work is to revise and extend an existing stationary high temperature SOFC model, and to adapt it to run dynamic simulations. The revision step has probably been the most time-consuming: among others, an iterative method to account for axial conduction has been introduced in the code. Nevertheless, in this context the focus is put on the innovative and more interesting models implemented: a direct carbon monoxide oxidation model, a low temperature SOFC model and the dynamic model. Finally, one of the goals of the work has been to improve the code efficiency for integration with another code to simulate advanced power plants. As it will be said, great results have been achieved from that perspective.

2. Models and Methodology

2.1. General code functioning

The existing stationary model has been extensively revised and updated in all its parts. As a matter of fact, a great share of the work has been directed towards the revision of the existing code. This is mainly made up by an electrochemical model, a chemical one, and a module devoted to applying mass, momentum and energy balance to each Control Volume (CV). With the term "Control Volume" one refers to the discretization unit of the channel, as shown in the following figure.

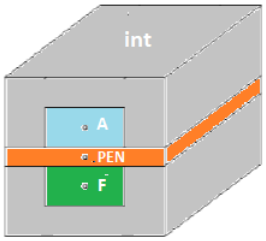

Figure 1: *Control Volume definition from reference [4]*

The figure shows the cell PEN structure (Positive-Electrolyte-Negative), and the discretized air (A) and fuel (F) channels. The rest of the figure represents the CV interconnection, which will always be treated as a single entity, with its own lumped temperature. This is one of the main weaknesses of the code. Thus, dividing the air side interconnection from the fuel one could be one of the next step to improve the model in the future. Moreover, the PEN structure of the CV has a lumped temperature as well.

The code initially solved one CV at a time from the inlet towards the outlet of the cell to compute the stationary performance. This was done by using the PEN temperature of the previous CV to assess the electrochemical and chemical rates in a CV, which defined the species exchange between PEN and both fuel and air channels. Then the balances could be applied to find the CV outlet concentrations, velocities, pressures and temperatures (fuel and air). Moreover, PEN and interconnection temperatures were found through the balances as well. Therefore, there were $8 + N_{sp,f} + N_{sp,a}$ unknowns, with the same number of equations which are listed below.

- Mass balances on A and F, one for each species
- Momentum balances on A and F. Actually, the fluids behave as incompressible, thus a simple pressure loss equation has been seen to give exactly the same results. 2 equations in total

- Ideal gas equations of state at the outlet of A and F, 2 equations (the inlet variables are known from solving the previous CV)
- Energy balances on the channels A and F, 2 equations
- Energy balance on PEN and interconnection structures, 2 equations

The found values were given as input of the next CV, until the last CV was solved. The problem with the explained algorithm is that axial conduction could not be accounted properly within PEN and interconnection energy balances, as PEN and interconnection temperatures in the next CV were not known. Thus, a method which iterates PEN and interconnection temperature distributions has been implemented. A certain guess is provided by solving the equations without axial conduction. Then, the channel is solved from inlet to outlet using the guessed PEN temperature distribution to assess electrochemical and chemical rates. The updated temperature distributions come from solving the energy balances, which can now account for axial conduction using the guessed distribution. The updated distribution is then used in a next iteration to evaluate electrochemical rates, and so on until convergence is reached.

2.2. CO electroxidation

One of the highlights of the present work is the implementation of a novel model to account for direct carbon monoxide electroxidation. The most used model in the literature [5][6] defines an equivalent electric circuit associated with the CV by setting a parallel configuration at the anode side and by defining two different Nernst voltages (hydrogen and carbon monoxide). On the other hand, the present model defines a single reversible voltage. This is done by making stationary considerations on the reversible system and relating it with hydrogen alone and carbon monoxide alone reversible systems. Thus, the first step is to impose a null net current drawn from anode in the reversible system. This is done by setting to zero the sum of the Butler-Volmer expressions ([6]) for activation polarization of hydrogen and carbon monoxide.

$$i = i_{0,H_2}[\exp(\frac{F\eta_{act,H_2,rev}}{RT}) - \exp(-\frac{F\eta_{act,H_2,rev}}{RT})] + i_{0,CO}[\exp(\frac{F\eta_{act,CO,rev}}{RT}) - \exp(-\frac{F\eta_{act,CO,rev}}{RT})] = 0 \quad (1)$$

Thus, in the reversible system with both species present, one between hydrogen and carbon monoxide activation overpotentials would be positive, the other one would be negative to satisfy equation (1). Therefore, those species would be respectively consumed and produced also in the ideal reversible situation. This means that it does not

really exist an equilibrium condition, but a stationary one occurs. Assuming that the electric potential difference between cathode and electrolyte is the same in the three reversible situations (H_2 alone, CO alone, combined system), starting from the definition of activation overpotential one can demonstrate that:

$$\eta_{act,H_2,rev} = (\phi_{an} - \phi_{elec})_{rev} - (\phi_{an} - \phi_{elec})_{rev,H_2} \tag{2}$$

$$\eta_{act,CO,rev} = (\phi_{an} - \phi_{elec})_{rev} - (\phi_{an} - \phi_{elec})_{rev,CO} \tag{3}$$

$$\eta_{act,H_2,rev} = \frac{|\Delta G_{H_2}|}{2F} - \Delta V_{rev,comb} \tag{4}$$

$$\eta_{act,CO,rev} = \frac{|\Delta G_{CO}|}{2F} - \Delta V_{rev,comb} \tag{5}$$

Where the activation overpotentials are evaluated in the reversible system including both hydrogen and carbon monoxide, and the Nernst voltage of the species alone are computed using bulk flow molar fractions. In the right-hand side of equations (2) and (3) the electric potential difference between anode and electrolyte in the reversible systems with hydrogen alone and carbon monoxide alone appears. The term $\Delta V_{rev,comb}$ is the searched combined reversible voltage, which can be found putting equations (4) and (5) inside equation (1). Then, one can define losses depending both on hydrogen and carbon monoxide currents to be subtracted from the reversible voltage, together with the power output. The following is the resulting system of equations.

Sub-model	Governing equations
Energy conservation	$\Delta V_{rev,comb} = V_{cell} + \eta_{ohm} + \eta_{act,an} + \eta_{act,O_2} + \eta_{conc}$
Ohmic loss [4]	$\eta_{ohm} = iAR$
Activation loss [6]	$i_{0,H_2}[\exp(\frac{F\eta_{act,H_2}}{RT}) - \exp(-\frac{F\eta_{act,H_2}}{RT})]A_{act,an} = i_{H_2}A \qquad i_{0,H_2} = 1.344 \cdot 10^{10}(\frac{P_{H_2}}{P_{ref}})(\frac{P_{H_2O}}{P_{ref}})\exp(-\frac{1\cdot 10^5}{RT})$
	$i_{0,CO}[\exp(\frac{F\eta_{act,CO}}{RT}) - \exp(-\frac{F\eta_{act,CO}}{RT})]A_{act,an} = i_{CO}A \qquad i_{0,CO} = \frac{1.344}{3} \cdot 10^{10}(\frac{P_{CO}}{P_{ref}})(\frac{P_{CO_2}}{P_{ref}})\exp(-\frac{1\cdot 10^5}{RT})$
	$i_{0,O_2}[\exp(2\frac{F\eta_{act,O_2}}{RT}) - \exp(-2\frac{F\eta_{act,O_2}}{RT})]A_{act,cat} = iA \qquad i_{0,O_2} = 2.051 \cdot 10^9(\frac{P_{O_2}}{P_{ref}})^{0.25}\exp(-\frac{1.2\cdot 10^5}{RT})$
	$A_{act,an} = 650At_{an} \qquad A_{act,cat} = 6500At_{cat}$
	$\eta_{act,H_2} = \eta_{act,an} + \frac{\|\Delta G_{H_2}\|}{2F} - \Delta V_{rev,comb} \qquad \eta_{act,CO} = \eta_{act,an} + \frac{\|\Delta G_{CO}\|}{2F} - \Delta V_{rev,comb}$
Currents	$i = i_{H_2} + i_{CO}$

Table 1: *CO electroxidation governing equations*

Where R is the CV electric resistance, computed with the model proposed in [4], and A is the area to which the current is specific, equal to PEN geometrical surface within the CV. Finally, the term $\Delta V_{rev,comb} - \eta_{conc}$ is computed as $\Delta V_{rev,comb}$, but using

active site molar fractions to compute $\frac{\Delta G_{H_2}}{2F}, \frac{\Delta G_{CO}}{2F}, i_{0,H_2}, i_{0,CO}$ instead of channels ones.

2.3. Low temperature model

The low temperature model implemented, is an attempt of capturing the cell behaviour using a Macro-Scale model as done in high temperature operation. The model employs the equations of references [7][8][9] for the calculations of electrolyte electronic and ionic currents. The reference cell has a Samaria-Doped-Ceria (SDC) electrolyte, which is known to be a MIEC material. The aim is to reproduce the isothermal *button cell* polarization curves of reference [7], which actually solves the charge conservation equations within the electrodes, thus it is inherently more accurate. As a matter of fact, the reference work succeeds in reproducing experimental polarization curves. The code is not generally capable of simulating a button cell configuration, since there are not channels as the ones in figure 1 and the streams are actually directed perpendicularly to the PEN structure. Nevertheless, the electrochemical solver can easily tackle equations of table (2) setting a unique operating temperature (which replaces T_f, T_a, T_{PEN}) and the button cell geometry (interconnection is not considered). This way, equations in table 2 are believed to capture the polarization behaviour of a button cell. Once the model have proven to give reliable polarization curves, it could be used to simulate low temperature cells with a co-flow channels configuration.

Sub-model	Governing equations
Energy conservation	$V_{rev,H_2} i^{ely}_{O^{2-}} = V_{cell} i_{load} + i^{ely}_{O^{2-}} (\eta_{ohm,O^{2-}} + \eta_{act,O_2} + \eta_{act,H_2} + \eta_{conc}) + i^{ely}_{el} \eta_{ohm,el}$
Concentration loss	$\eta_{conc} = \eta_{conc,H_2} + \eta_{conc,O_2}$ $\quad \eta_{conc,H_2} = \frac{RT}{2F} \ln(\frac{x_{H_2,b} x_{H_2O,r}}{x_{H_2,r} x_{H_2O,b}})$ $\quad \eta_{conc,O_2} = \frac{RT}{4F} \ln(\frac{x_{O_2,b}}{x_{O_2,r}})$ $x_{H_2,r} = x_{H_2,b} - \frac{i^{ely}_{O^{2-}} RT t_{an}}{2FP_f D_{p,H_2}}$ $\quad x_{H_2O,r} = x_{H_2O,b} + \frac{i^{ely}_{O^{2-}} RT t_{an}}{2FP_f D_{p,H_2O}}$ $\quad x_{O_2,r} = x_{O_2,b} - \frac{i^{ely}_{O^{2-}} RT t_{cat}}{4FP_a D_{p,O_2}}$
Ohmic loss	$\eta_{ohm,O^{2-}} = \frac{i^{ely}_{O^{2-}} L}{\sigma_{O^{2-}(T)}}$ $\quad \eta_{ohm,el} = \frac{RT}{4F} \ln(\frac{P^L_{O_2}}{P^0_{O_2}}) - \eta_{ohm,O^{2-}}$ $\eta_{act,H_2} = \frac{RT}{4F} \ln(\frac{P^0_{O_2}}{P^I_{O_2}})$ $\quad \eta_{act,O_2} = \frac{RT}{4F} \ln(\frac{P^{II}_{O_2}}{P^L_{O_2}})$ $\quad \frac{P^I_{O_2}}{P_{ref}} = (\frac{x_{H_2O,r}}{x_{H_2,r} K_{eq,H_2ox}})^2$ $\quad P^{II}_{O_2} = x_{O_2,r} P_a$
Activation loss	$i_{0,H_2} [\exp(\frac{F\eta_{act,H_2}}{RT}) - \exp(-\frac{F\eta_{act,H_2}}{RT})] A_{act,an} = i^{ely}_{O^{2-}} A$ $\quad i_{0,H_2} = 23.8 T \exp(-\frac{73000}{RT})(\frac{P_{H_2}}{P_{ref}})^{0.47}$ $i_{0,O_2} [\exp(1.3\frac{F\eta_{act,O_2}}{RT}) - \exp(-0.7\frac{F\eta_{act,O_2}}{RT})] A_{act,cat} = i^{ely}_{O^{2-}} A$ $\quad i_{0,O_2} = 2.8 \cdot 10^7 T \exp(-\frac{139000}{RT})(\frac{P_{O_2}}{P_{ref}})^{0.33}$
Currents	$i^{ely}_{O^{2-}} = i_{load} + i^{ely}_{el}$ $\quad i^{ely}_{el} = \frac{i^{ely}_{O^{2-}}}{\sigma_{O^{2-}}} \frac{\sigma^0_{el}}{1-M_0} [M_0 (P^0_{O_2})^{-1/4} - (P^L_{O_2})^{-1/4}]$ $\quad M_0 = \exp(-\frac{F}{RT} \frac{i^{ely}_{O^{2-}}}{\sigma_{O^{2-}}} L)$

Table 2: *Low temperature SOFC model governing equations*

In the above table, L is the electrolyte thickness. The above set of equations does

not account any electrodes ohmic loss, as they will be discussed separately. All the missing parameters of the equations may be found in reference [7]. The term $x_{i,r}$ is the species molar fraction at the active site, computed by considering porous diffusion from the bulk flow molar fraction. In general, also the diffusion from the channel to the electrode should be considered. Nevertheless, the validation will consider a button cell, thus just the porous diffusion will be accounted.

To somehow account for electrodes ohmic losses one can make the assumption of electrochemical reactions occurring just at the interface electrode/electrolyte, in this way the ohmic electrode loss to add in the energy balance equation would be:

$$i_{load}(\eta_{ohm,an}+\eta_{ohm,cat}) = i_{load}^2(\frac{t_{an}}{\sigma_{el,an}}+\frac{t_{cat}}{\sigma_{el,cat}}) \tag{6}$$

Where t is the electrodes thickness and σ is their electric conductivity, which can be found in reference [7]. Nevertheless, this assumption is practically equal to assuming no electrode loss at all (low electronic loss) and the risk is to achieve just a limited matching with the reference. Thus, one should somehow consider ionic loss within the electrodes to get more accurate results, as the following is a typical ionic current distribution within the cell:

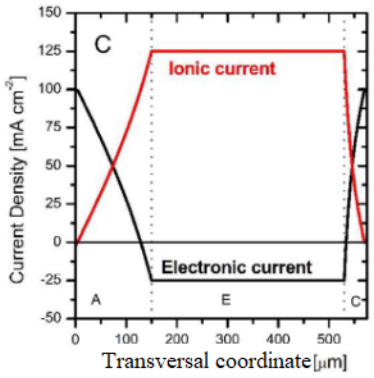

Figure 2: *Example of currents distributions.* $i_{load} = 1000\frac{A}{m^2}$ *[7]*

Therefore, one may assume that ionic and electronic currents have a linear distribution within the electrodes. Thus, the ionic current ranges from 0 to $i_{O^{2-}}^{ely}$, whereas the electronic one from i_{load} to i_{el}^{ely}. The resulting ohmic losses to be added in the energy balance right-hand side would be:

$$-\int_0^{L_{an/cat}} \frac{i_{O^{2-}}^2(x)}{\sigma_{O^{2-},an/cat}} dx \tag{7}$$

$$-\int_0^{L_{an/cat}} \frac{i_{el}^2(x)}{\sigma_{el,an/cat}} dx \tag{8}$$

This assumption is not generally true, but now the aim is to investigate the assumption on electrodes ohmic loss, and to get closer as possible to the reference to check the model implementation.

2.4. Dynamic model

The dynamic model considered a specific case study as reference, but it can be easily adapted to simulate several kind of dynamic simulations. The case considered is the transient after a load connection, starting from a stationary condition in which hot fuel and air streams are passed through the cell. This is modeled by a voltage step to a certain value, which is kept constant throughout the simulation. The main assumptions of the model is that electrochemical and mass diffusion transients are negligible, as they are supposed to be much faster than the thermal one.

The time step of the dynamic simulation is the main parameter affecting its accuracy and stability. Nevertheless, a too low time step would determine an unacceptable required computational time. Therefore, an adjustable time step is used, which drops when time gradients are too high or when the variables show too large instability over time. Otherwise, the time step increases.

The algorithm to solve the transient simulation is the following. The length of each CV is defined by a code internal function, the same used in the stationary simulation. The starting point is an initial distribution of all the variables of interest at the CVs faces, except interconnection and PEN temperatures which are lumped parameters within the CV. These variables of interest are 2 faces temperatures, pressures and velocities (outlet fuel and air), $N_{sp,f} + N_{sp,a}$ concentrations ($\frac{mol}{m^3}$), and PEN and interconnection temperatures. Then, the voltage is set to a constant value, and electrochemical and chemical rates are computed for the first time step and CV, using the initial temperature and concentrations distributions. The equations in table 3 provide the values of the above cited variables at the end of the first time step in the first CV. Electrochemical and chemical rates of the second CV are computed using time averaged molar fractions (between $t = 0$ and $t = \Delta t$) at the outlet of the first CV, this has been seen to be really important for the simulation stability. All the CVs of the channel are solved this way. Finally, all the variables of interest at $t = \Delta t$ become the initial condition of the second time step, and so on until reaching the stationary condition.

In table 3, V is the volume of fuel (or air) channel included in the CV. Moreover, all the inlet variables evaluated at $t + \Delta t$ and the ones evaluated at instant t are known, as

the previous CV has just been solved and the initial condition is known.

	Discretized governing equations
Mass F x $N_{sp,f}$	$[\frac{(\dot{n}_t+\dot{n}_{t+\Delta t})_{i,in}}{2}+\dot{n}_{i,PEN\rightarrow f}-\dot{n}_{i,f\rightarrow PEN}-\frac{(\dot{n}_t+\dot{n}_{t+\Delta t})_{i,out}}{2}]\Delta t=V[\frac{(C_{in}+C_{out})_{i,t+\Delta t}}{2}-\frac{(C_{in}+C_{out})_{i,t}}{2}]$
Mass A x $N_{sp,a}$	$[\frac{(\dot{n}_t+\dot{n}_{t+\Delta t})_{j,in}}{2}-\dot{n}_{j,a\rightarrow PEN}-\frac{(\dot{n}_t+\dot{n}_{t+\Delta t})_{j,out}}{2}]\Delta t=V[\frac{(C_{in}+C_{out})_{j,t+\Delta t}}{2}-\frac{(C_{in}+C_{out})_{j,t}}{2}]$
Momentum x2 [10]	$P_{out,t+\Delta t}=P_{in,t+\Delta t}-\frac{2C_f\rho_{in,t}v_{in,t}^2L}{D_{hydro}}\qquad C_f=\frac{Po}{Re}\qquad Re=\frac{\rho_{in,t}v_{in,t}}{\nu_{fluid}}$
Energy F	$\{\frac{[(\dot{n}h_{tot})_t+(\dot{n}h_{tot})_{t+\Delta t}]_{in}}{2}-\frac{[(\dot{n}h_{tot})_t+(\dot{n}h_{tot})_{t+\Delta t}]_{out}}{2}+\dot{H}_f+\dot{Q}_f\}\Delta t=V\Delta(Ch_{tot})$
Energy A	$\{\frac{[(\dot{n}h_{tot})_t+(\dot{n}h_{tot})_{t+\Delta t}]_{in}}{2}-\frac{[(\dot{n}h_{tot})_t+(\dot{n}h_{tot})_{t+\Delta t}]_{out}}{2}+\dot{H}_a+\dot{Q}_a\}\Delta t=V\Delta(Ch_{tot})$
	$\Delta(Ch_{tot})=\{\frac{[(Ch_{tot})_{in}+(Ch_{tot})_{out}]_{t+\Delta t}}{2}-\frac{[(Ch_{tot})_{in}+(Ch_{tot})_{out}]_t}{2}\}\qquad h_{tot}=h+\frac{v^2}{2}MM$
	$\dot{H}_{f/a}=\sum_{i/j}\dot{n}_{i/j,PEN\rightarrow f/a}h_{i/j}(T_{PEN})-\dot{n}_{i/j,f/a\rightarrow PEN}h_{i/j}(T_{f/a})\qquad \dot{Q}_{f/a}=\dot{Q}_{PEN\rightarrow f/a}+\dot{Q}_{int\rightarrow f/a}$
Energy (PEN)	$(\dot{Q}_{ax,PEN}-V_{cell}I-\dot{H}_f-\dot{H}_a-\dot{Q}_{PEN\rightarrow f}-\dot{Q}_{PEN\rightarrow a}-\dot{Q}_{PEN\rightarrow int})\Delta t=[Mc_p(T_{t+\Delta t}-T_t)]_{PEN}$
	$\dot{Q}_{ax,PEN}=(\dot{Q}_{ax,n-1\rightarrow n}-\dot{Q}_{ax,n\rightarrow n+1})_{PEN}$
Energy (int)	$(\dot{Q}_{ax,int}-\dot{Q}_{int\rightarrow f}-\dot{Q}_{int\rightarrow a}+\dot{Q}_{PEN\rightarrow int}-\dot{Q}_{loss})\Delta t=[Mc_p(T_{t+\Delta t}-T_t)]_{int}$
	$\dot{Q}_{ax,int}=(\dot{Q}_{ax,n-1\rightarrow n}-\dot{Q}_{ax,n\rightarrow n+1})_{int}$
Equation of state x2	$P_{out,t+\Delta t}=R(CT)_{out,t+\Delta t}$

Table 3: *Discretized dynamic governing equations of the n^{th} CV*

One can demonstrate that all the variables in the above equations are dependent on the $8+N_{sp,f}+N_{sp,a}$ independent unknowns. Along with the discretization, comes the fact that instantaneous mass and energy flows should be averaged within the time step for accuracy and numerical stability, this can be easily seen in the mass conservation equations. This has been done everywhere it was possible, for instance the heat exchange between PEN and interconnection is computed with the following equation.

$$\dot{Q}_{PEN\rightarrow int}=\frac{[\frac{(T_t+T_{t+\Delta t})_{PEN}}{2}-\frac{(T_t+T_{t+\Delta t})_{int}}{2}]}{R_{PEN/int}} \tag{9}$$

Moreover, the fuel and air temperature used in the above equations have been averaged both in time and space, to consider both inlet and outlet temperature. Actually, the space averaging was already done before the dynamic model was implemented.

3. Results and discussion

As first result, it is important to stress the outstanding improvement of the code efficiency. The computational time required by the code is estimated to be 20-200 times lower with respect to the initial situation, depending on operating condition and

type of run simulation (stationary with or without axial conduction, dynamic). Several measures have been undertaken to achieve that result, such as replacing of numerical integrals with analytical ones, improvement of the balance module algorithm (and equations), and guess variables of the electrochemical non-linear solver.

The code has been deeply modified, thus its general validation will be performed. Then the carbon monoxide oxidation model, the low temperature model, and the dynamic model will be validated. Unfortunately, for the carbon monoxide and dynamic model, the literature lacks of suitable and reliable works to make a comparison, thus the validation will only be limited to show the physical consistency of the results.

3.1. General code validation

To validate the final code an existing and already validated code has been used. The final purpose is to reproduce the reference code results by using its electrochemical and chemical models. The details of the reference code can be seen in the first part of reference [4]. Tables 1 and 4 in the same reference define the input geometry, operating conditions and models parameters. Actually, in the present simulation just one channel is considered, and the heat loss is set to zero (thus no matter how many channels). The following table resumes the results of the validation.

	Axial conduction validation				Final validation	
	Reference		New code		Reference	New code
ax cond.	off	on	off	on	on	on
$\eta_{el,LHV}$ [%]	56.08	56.98	54.54	55.60	56.15	55.60
Power [W]	0.886	0.9	0.8974	0.9148	0.9236	0.9148
U_f [%]	85.36	86.74	86.49	88.16	89.01	88.16
U_{ox} [%]	14.23	14.46	14.41	14.69	14.84	14.69
i [A m^{-2}]	2274	2311	2306	2350	2373	2350

Table 4: *Validation of results enabling (on) and disabling (off) axial conduction*

The axial conduction validation is successful, as the impact of its introduction within the simulation affects the reference and the new code results in an analogous way. The final validation is made to check the actual matching of the results. Indeed, during the axial conduction validation, the reference code was affected by some little inaccuracies which influenced the results, thus it has been corrected and the new outcome has been compared with the new code one, with axial conduction switched on. The in-

herent differences between the codes justify the little mismatch of the final validation results. The main difference is in the treatment of the fuel and air side interconnections, which are merged in a single entity in the new code. The channel distribution of some variables of interest related to this stationary simulation will be shown in section 3.4., as results of the dynamic simulation which has reached the stationary condition.

3.2. CO electroxidation

Unfortunately, the literature lacks of reliable models accounting for carbon monoxide oxidation, as the Water Gas Shift reaction (WGS) is usually assumed to be very fast:

$$CO + H_2O \rightleftharpoons H_2 + CO_2 \tag{10}$$

Thus, oxidation is assumed to proceeds via hydrogen electroxidation. As a matter of fact, a lot of authors assume WGS to be at equilibrium throughout the cell. Nevertheless, several authors claim that WGS is not at equilibrium [11][12]. Therefore, the latter reference has been considered to implement a WGS model to investigate the effect of WGS rate on the benefit gained by introducing CO direct oxidation. The cited reference shows that the following parameter never overcomes the value of 0.85 (it is 1 for WGS at equilibrium), under a wide range of operating conditions:

$$\eta_{eq} = \frac{K_p}{K_{eq}(T)} = \frac{x_{H_2} x_{CO_2}}{x_{CO} x_{H_2O}} \left(\frac{x_{H_2} x_{CO_2}}{x_{CO} x_{H_2O}}\right)_{eq}^{-1} \tag{11}$$

Where x_i is the molar fraction of species i. Thus, a model allowing to set a certain η_{eq} has been implemented within the code. The following table summarizes the results of the simulations, with same input as in 3.1., changing just the electrochemical model.

	$\eta_{eq} = 1$		$\eta_{eq} = 0.8$		$\eta_{eq} = 0.6$	
CO ox	off	on	off	on	off	on
$\eta_{el,LHV}$ [%]	55.78	55.92	55.28	55.50	54.54	54.86
U_f [%]	88.45	88.68	87.66	88.00	86.48	87.00
U_{ox} [%]	14.74	14.78	14.61	14.67	14.41	14.50
i [A m^{-2}]	2358	2364	2337	2346	2306	2319

Table 5: *CO direct oxidation results, switching on and off CO oxidation*

Considered the low inlet CO molar fraction (2.94%), the results do not change much with the introduction of direct CO oxidation. Nevertheless, the performance when CO oxidation is off, is slightly more penalized by a lower WGS reaction rate, as there would

generally be less hydrogen in the channel, which is the only active species. Therefore, the model results are aligned with expectations. Eventually, it has been checked that the energy balance in table 1 is equivalent to writing the following energy balance:

$$V_{rev,H_2} i_{H_2} + V_{rev,CO} i_{CO} = (V_{cell} + \eta_{ohm} + \eta_{act,O_2} + \eta_{conc,O_2}) i + (\eta_{act,H_2} + \eta_{conc,H_2}) i_{H_2} + (\eta_{act,CO} + \eta_{conc,CO}) i_{CO} \quad (12)$$

3.3. Low temperature model validation

As for the carbon monoxide oxidation it is rather difficult, if not impossible, to find in the literature reliable models of well functioning low temperature SOFC for validation, as this technology is not really mature. Thus, the model will be used to reproduce the polarization curves of reference [7], which considers an isothermal button cell. In case the polarization behaviour is well reproduced, cells with normal fuel and air channels could be simulated by the model in the future. Several assumptions on the ohmic loss within the electrodes will be investigated in the simulations:

- Only electronic loss: assumption of electrochemical reactions occurring just at electrode/electrolyte interface. This is equivalent to assuming that just electric current (the drawn current) flows within the electrodes, with no ionic loss. This has been seen to be equivalent to setting null electrodes loss (low electronic loss).
- Null anodic ionic loss: the above assumption applies just within the anode (its ionic conductivity is not really available in the reference). In the cathode the assumption of linear ionic and electronic currents has been made.
- Linear currents: linear electronic and ionic currents in both electrodes. The electrolyte ionic conductivity and the anode one are assumed to be equal.

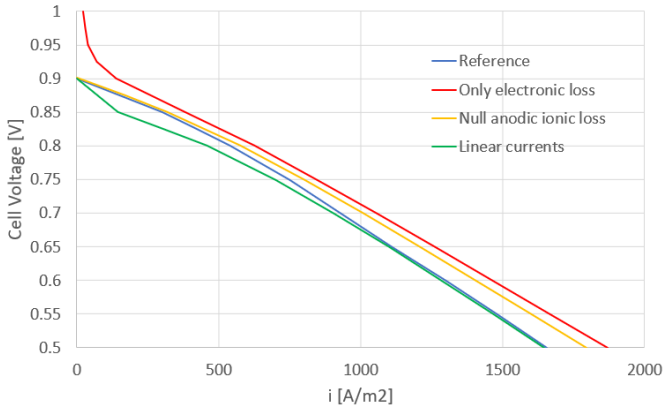

Figure 3: *Electrodes ohmic loss assumption effect. 97% H_2, 3% H_2O, 650°C*

Figure 3 shows the results of the simulation. Considering only electronic loss within the electrodes seems to be the worse assumption concerning the matching with the

reference. Moreover, the useful current does not really become zero, differently from the other cases. This means that ionic losses are important also when approaching OCV. Considering linear ionic and electronic currents in both electrodes gives a very good agreement with reference at low voltages, but it shows instability at higher voltages. Thus, considering ionic loss just within the cathode (for which ionic conductivity is available) may be the best choice, due to a general good matching with reference and stable results. Several operating conditions available in the reference have been investigated: the model showed to be able of catching temperature and composition changes, and the curves generally behave as the ones in figure 3. The assumption of linear currents is not generally realistic, solving the charge conservation equations within the electrodes would give a reliable ionic current distribution to better assess ohmic and activation losses. This would definitely improve the model accuracy and stability.

3.4. Dynamic simulation

Unfortunately, the literature lacks of suitable works to make a comparison, also because the majority of the works applies a current step instead of a voltage one. Therefore, the validation will be limited to showing the plausibility of the results and their consistency with the stationary model results. The input geometry and models used are the same of section 3.1., as it will be shown that the results achieved by the stationary and dynamic models perfectly match. The distributions along the channel of some variables of interest have been recorded every 500s throughout the simulation.

As expected, the composition distribution transient is the quicker one, almost stop changing after about 2000s. The current density distribution almost reaches the stationary distribution after about 3000s. As expected, the thermal transient is the longest one, lasting more than 4000s.

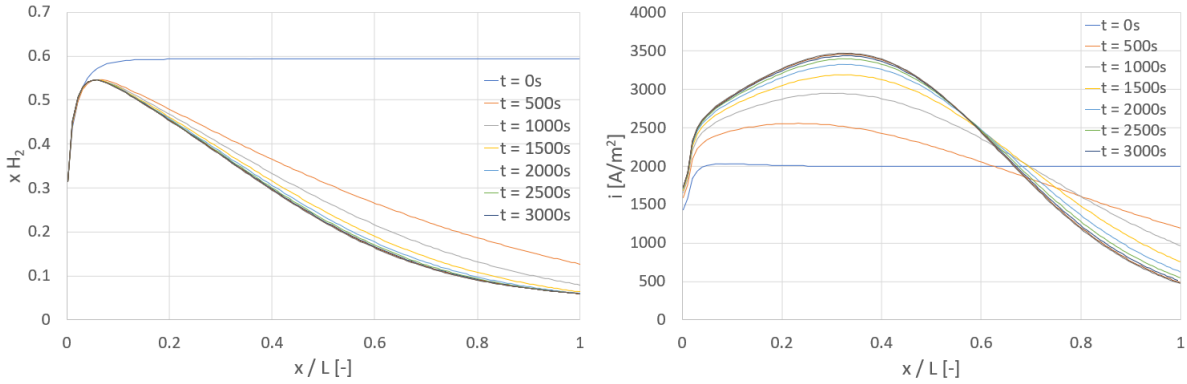

Figure 4: *On the left the hydrogen molar fraction distribution, on the right the current one*

The distribution of hydrogen grows until about 10% of the channel because of the rapid steam reforming kinetic. This kind of hydrogen molar fraction distribution using a methane-rich fuel (17.1%) is also confirmed by graphs shown at the end of reference [4]. Moreover, in reference [13] it is claimed that methane is generally consumed in the very first part of the channel in high-temperature SOFCs, which is what happens here. At $t = 0$, when the fuel runs out of methane, the hydrogen composition stop changing. During the simulation, the molar fraction in the part of the channel where methane is not present drops sensibly until stationary condition is reached. This is obviously due to hydrogen electrochemical oxidation.

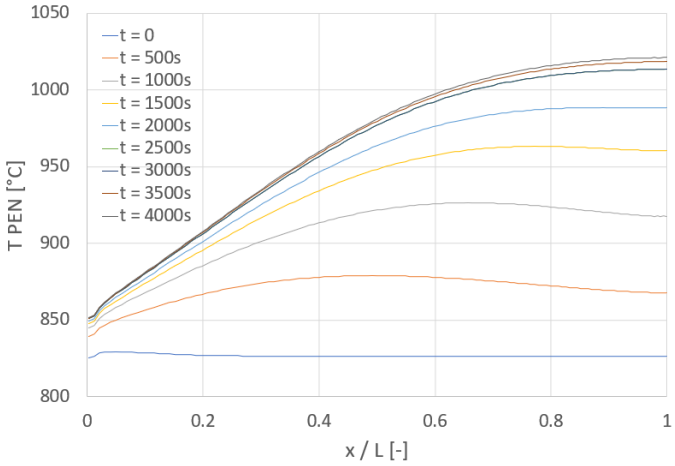

Figure 5: *PEN temperature distribution throughout the simulation*

The initial distribution of current density (right after the voltage step from OCV condition to 0.7 V) is plain throughout the cell except from the very beginning, where it is sensibly lower. The steep current increase at the inlet is actually a common feature to all the current distributions recorded in the simulation. The current is generally higher where the temperature and the presence of hydrogen is larger. The temperature increase at the inlet of the cell does not justify the rapid current increase, thus it must be due to the rapid increase of hydrogen molar fraction. Nevertheless, the maximum of the current density occurs considerably after the hydrogen molar fraction one. This may due to temperature, which generally increases along the channel. This is confirmed by the fact that the current maximum keeps moving towards the channel end and to grow in value, even if hydrogen molar fraction drops and remains constant after a while. This is because of the continuous spacial temperature gradient increase, which implies higher temperatures far from the channel inlet. Nevertheless, after the plateau the current sensibly drops, this must be due to the lower hydrogen concen-

tration, as the temperatures are generally the highest. Moreover, thanks to the general temperature increase, the mean current density increases throughout the simulation:

t [s]	0	500	1000	1500	2000	2500	3000	3500	4000
i [A m^{-2}]	1998	2076	2282	2350	2364	2364	2362	2360	2359

The above results seem physically realistic. Another check can be done verifying the consistency between the results of the stationary model and the dynamic model ones which has reached the stationary condition: the variables profiles should perfectly match. For instance, this is the current profile computed with both models:

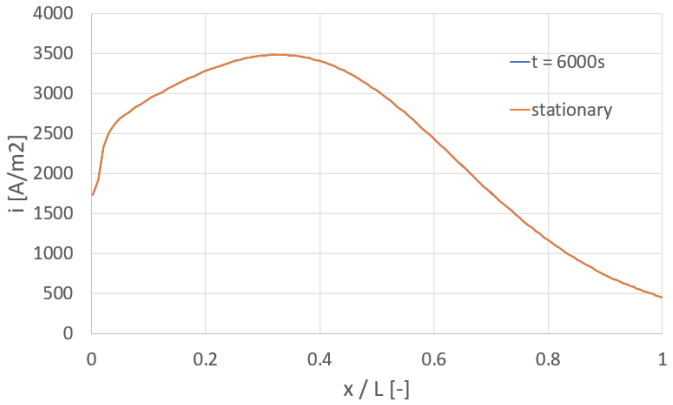

Figure 6: *Comparison between current profile at 6000s and the the stationary one*

The matching is flawless, thus the two models are consistent. It is not necessary to show the PEN temperature and the hydrogen molar fraction profiles along the channel, as the current is dependent from these two variables, as said above. These profiles are basically the stationary ones in figures 4 (left) - 5.

4. Conclusions

The work has started from an existing stationary SOFC model, which has been adapted to run dynamic simulations. The accuracy and the efficiency of the code has been deeply improved, as a consistent share of work done has been directed at revising the existing code. The required computational time is estimated to be 20-200 times lower, depending on the type of simulation run. This would be extremely helpful in case of integration with a wider program for simulation of advanced power cycles. A novel model to account for carbon monoxide direct oxidation has been implemented, which proved to give consistent results in line with expectations. Moreover, a model to simulate a low temperature SOFC has been added to the code, this has shown to give

good polarization curves compared to a button cell experimental results. Nevertheless, solving the charge conservation equations within the electrodes would make the model more accurate and robust to handle whatever operating condition. Finally, the dynamic model implemented has given realistic results in line with expectations, and showed to be consistent with the stationary model.

Chapter 1

Introduction

Fuel cells are generally known to be a really promising technology, mainly because of their high efficiency and low environmental impact due to using hydrogen as fuel, which ideally gives just water as final product [14][15]. In the following picture, a trivial schematisation of a specific type of fuel cell is shown. This is the Solid Oxide Fuel Cell (SOFC), and it is the one considered throughout the present work.

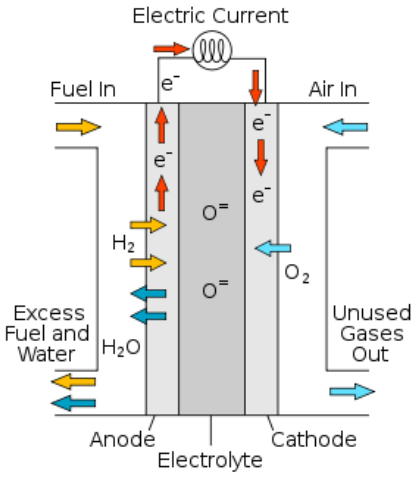

Figure 1.1: *SOFC functioning [16]*

All types of fuel cells are characterized by common features such as the presence of anode, cathode and electrolyte. These three layers have a supporting function, as they provide mechanical strength to the structure. Together they form the PEN structure of the cell (Positive-Electrolyte-Negative). As a matter of fact, fuel cells can be divided based on the thicker layer, thus they could be anode-supported, electrolyte-supported or cathode-supported. Another common feature is that all fuel cells can be

fueled by hydrogen. For instance, figure 1.1 shows oxygen moving towards the electrolyte/cathode interface and splitting up via the following electrochemical reaction (oxygen reduction):

$$\frac{1}{2}O_2 + 2e^- \rightleftharpoons O^{2-} \tag{1.1}$$

Oxygen ions flow through the electrolyte which is always an ions conductor. Then, they react with hydrogen on the anode/electrolyte surface via the following electrochemical reaction (hydrogen oxidation):

$$H_2 + O^{2-} \rightleftharpoons H_2O + 2e^- \tag{1.2}$$

Electrolyte electric resistivity is generally high, so that electrons are collected by the anode and flow towards the cathode via an external circuit, driven by cathode high electric potential. Thus, a desirable feature of anode and cathode is high electrons conductivity. Putting together reactions (1.1) and (1.2) one concludes that the overall reaction is totally similar to the conventional hydrogen combustion:

$$H_2 + \frac{1}{2}O_2 \rightleftharpoons H_2O \tag{1.3}$$

Thus one may wonder what are the intrinsic differences between the oxidation occurring within a fuel cell and the combustion of hydrogen which may occur in conventional systems. Inside a fuel cell the chemical energy enclosed in the fuel species is directly turned into electricity, without the need of raising the fuel temperature. In conventional systems the driving force is the temperature of the heat source, whilst in a fuel cell the temperature is just a parameter which benefits reactions kinetic. Indeed, some type of fuel cells may reach good efficiencies working only at about 100°C. If in a conventional system one managed to exploit a heat source at the adiabatic flame temperature of the fuel, then the maximum producible work would be much higher. Unfortunately, materials thermal resistance is limited, and that temperature must be lowered. This last step sensibly *degrade* the energy used in conventional systems.

Moreover, the efficiency of a fuel cell is not affected by its size, unlike what happens for conventional systems. The main reason for that is that the internal losses of a fuel cell are mainly determined by electrochemical phenomenons, which are primarly affected by the operating temperature. On the other hand, the performance of

the conventional energy production systems, such as internal combustion engines and gas turbines, are heavily affected by their size (because of fluid dynamics losses). The above are not the only common advantages of fuel cell systems. Another important one is the total absence of moving parts. This would of course tackle the problems of noise and vibrations which is rather important in gas or steam turbines or internal combustion engines.

Fuel cells can actually be of many types based on their main features such as construction materials, operating temperature and fuel composition restraints. Some fuel cells work at low temperature and some not, ranging from 100 to 1000 °C. Plus, the operating temperature would likely put restraints on the construction materials. Some kinds can only work with hydrogen due to catalyst poisoning problems, others can even function as hydrocarbons reformers. Depending on the fuel composition, several reactions may occur inside the cell, with WGS (Water Gas Shift) and MSR (Methane Steam Reforming) being of major importance. These reactions provide to carbon monoxide (CO) and methane (CH4) a path to be turned into hydrogen which could then be oxidized.

$$CO + H_2O \rightleftharpoons CO_2 + H_2 \tag{1.4}$$

$$CH_4 + H_2O \rightleftharpoons CO + 3H_2 \tag{1.5}$$

As said above, the present work focuses on the stationary and dynamic simulation of SOFCs (Solid Oxide Fuel Cells), whose temperature range is generally about 800-1000 °C. These kind of cells are capable of using several hydrocarbons as fuel, because of their high operating temperature. In that case, the hydrocarbons may be easily reformed within the cell itself. Moreover, the high temperature lowers all kind of internal losses, determining a substantial efficiency increase (whereas the ideal efficiency drops!). The high operating temperature is beneficial also for an eventual bottom cycle: the combination of a high-temperature fuel cell with a gas turbine leads to unsurpassed electric efficiency levels [1].

Judging by the above paragraphs, the high operating temperature may seem an essential element to design efficient SOFCs. Nevertheless, the high temperature is the major obstacle to SOFCs commercialization, because of relatively low long-term sta-

bility and high manufacturing costs [2][3]. Thus, nowadays efforts are also aimed at reducing the operating temperature of these devices, which is lowered to 500-800°C. The expensive materials universally used for high temperature operation are replaced with metals which could also lower the startup time [2]. For instance the metal oxide Yttrium Stabilized Zirconia (YSZ) electrolyte used in high temperature operation could be turned into a Cerium-based material to raise ionic conductivity at low temperature. The low-temperature configuration would bring also disadvantages, for instance there would very likely be a MIEC (Mixed Ionic and Electronic Conducting) electrolyte. These kind of electrolytes, differently from the ones used at higher temperature, conduct both electrons and ions. Thus, the overall ions current would split in a useful and a leakage current which comes back to the cathode, attracted from its high electric potential.

Therefore, the objective of this work is to develop a stationary and dynamic model for SOFCs. The interest in the dynamic model is due to the need of predicting transients in certain moments of the cell life-time. For instance the startup (or shutdown) performance, in which one wants to know the transient time and the maximum thermal gradients (thermal stresses limitation). Moreover, it is of great interest the simulation of load-following situations to assess if the cell is capable of following a dynamic load. The starting point is an already existing *Fortran* code capable of predicting the stationary performance of a high temperature SOFC.

In chapter 2 changes and uptdates made on the stationary model will be presented, including the implementation of the (relatively) low temperature model. This chapter includes all the corrections applied to the existing code, the revision process has actually been the most time-consuming one. In chapter 3 the dynamic model is explained and presented. Finally, chapter 4 deals with the results, validations and discussion about the previous chapters.

Chapter 2

Stationary model

This work has started from an existing stationary model, which has been deeply revised and extended. The aim of the present chapter is to present the corrections, changes and updating applied to the initial code. The revision process has been a major step of the overall work, as a consistent amount of time has been spent in correcting the initial code. The general changes made in the code will be presented as first. Then the main modules of the model will be considered: the *mass, momentum and energy balances* module, the *electrochemical model* and finally the *chemical model*, where a novel direct CO oxidation model will be presented. Eventually, the implementation of the low-temperature model will be addressed.

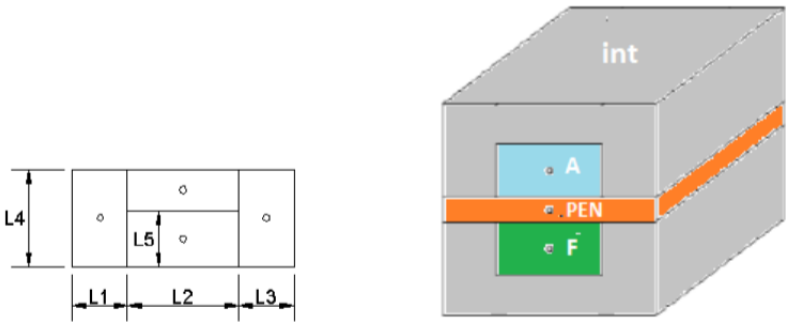

Figure 2.1: *On the left the channel schematisation, on the right a single-channel CV is shown [4]*

As figure 2.1 shows, the spacial discretization of the model is based on dividing each channel in several Control Volumes (CVs), so that the mass, momentum, and energy balance equations could be written independently for each of them. If several channels are simulated, then a single CV is defined by "cutting" the whole cell transversally in two specified planes. Thus a CV actually includes all the channels, whose balance

equations are solved altogether. On the other hand, if only one channel is simulated, then a CV represents the discretization unit of that channel. Thus, figure 2.1 actually shows the schematisation of a single-channel CV. However, *the single channel configuration is taken as reference*, thus the "CV" is meant to be the one in the right-hand side of the figure, unless otherwise told.

In figure 2.1 the grey structure called "int" represents the interconnection included in the CV. As one can see, the interconnections in the air and fuel sides are treated as a single entity, with its own lumped temperature. This is probably the main approximation made by the code, fixing that would probably be the next step in the code development. Finally, A and F are the discretized air and fuel channels within the CV. In the following sections the geometrical dimensions of the CVs will be widely used, thus the following table defines the correspondence among the name of the variables and figure 2.1.

Parameter	Named as	Corresponds to
Channel width	W	L2
Channel height	H	L5
Interconnection thickness	t_{int}	L1 or L3
Interconnection height	H_{int}	L4 - L5
PEN thickness	t_{PEN}	-
CV length	L_{CV}	3^{rd} dimension

Table 2.1: *Definition of channel and CV geometry*

Throughout the following work a very important geometrical area A_n related to the n^{th} CV will be extensively used. Thus it is worth to define it now:

$$A_n = L_{CV,n}(W + 2t_{int}) \tag{2.1}$$

This surface is important because it is generally the one to which the current densities are specific. Moreover, in several electrochemical models, it also defines the available active area within the electrode. Summing up the contributions of the N CVs within a channel, the geometrical surface associated to one channel is obtained:

$$A_{channel} = \sum_{n=1}^{N} A_n \tag{2.2}$$

2.1 General changes

In this section the modifications applied to the code which are not directly related to the main modules of the code will be explained. Apart from what will be presented, it is worth to say that a lot of little changes have been done in order to improve the code general functioning. For instance, now an allocatable variable will be actually allocated just if needed. The needed variables would of course depend on the general settings made by the user (e.g. CO oxidation activated or not). This would save virtual memory which can be used for computations.

2.1.1 Grid generation

The computational grid is generated once two constants B and C are provided. The following are the equations which were used in the existing code to define the length of each CV.

$$A = \frac{L_{channel}}{\int_1^N \frac{1}{\exp(-\frac{n-N/B}{N/C})+1} dn} \tag{2.3}$$

$$L_{CV,n} = \frac{A}{\exp(-\frac{n-N/B}{N/C}) + 1} \tag{2.4}$$

Where N is the total number of CVs. The problem arose when summing up the length of each CV, which was not equal to the length of the channel given by the user. This could of course be a source of inaccuracy because of the deviation of the simulation with respect to reality (e.g. different active area). Using equations (2.3) and (2.4) the relative difference between the sum of CVs length and the input channel length could be about 1.25 %. In the existing code, the integration was performed until $N+0.5$ instead of N, probably to reduce that relative difference which goes to 0.5 %.

The problem with the above grid generation is in equation (2.3). Indeed, one can easily demonstrate that if the integration was replaced by a summation between the same extremes (extended to all CVs), then $\sum_{n=1}^{N} L_{CV,n} = L_{channel}$. Therefore, the following is the equation which replaces (2.3).

$$A = \frac{L_{channel}}{\sum_{n=1}^{N} \frac{1}{\exp(-\frac{n-N/B}{N/C}) + 1}} \tag{2.5}$$

2.1.2 Post-processing and check equations

After the resolution of the cell channels the performance of the SOFC is computed, together with the mass and energy balances of each channel to check that the unbalance is below a certain threshold. Thus, the following is referred to the balances applied to a single channel.

All the unbalances were computed in absolute term, so that one could not really tell whether the unbalance was high or not. Therefore, all the unbalances are now evaluated in relative term.

The overall mass balance presented an inaccuracy in the definition of the input air mass flow rate. This was taken to be the one at the outlet of the first CV. Now both the fuel and air mass rates are the inlet ones. The relative mass defect has gone from 10^{-4} to 10^{-10}.

The calculation of the energy unbalance of each channel had to be deeply revised. First of all the heat exchanged with the adjacent channels through the interconnection was not considered, thus it has been added. Moreover, the energy flow related to inlet air and fuel streams should be computed as:

$$A_{cross}\{C_f v_f[h(T_f, x_{f,i}) + \frac{v_f^2}{2} MM_f] + C_a v_{a,}[h(T_a, x_{a,i}) + \frac{v_a^2}{2} MM_a]\}_{in} \tag{2.6}$$

$$A_{cross} = W \cdot H \tag{2.7}$$

Where C is the total concentration of the inlet flows ($\frac{mol}{m^3}$) and h is the molar enthalpy of the inlet mixture. The problem was that T_f, x_f, C_f, v_f, MM_f, T_a, x_a, C_a, v_a, MM_a used in equation (2.6) were the ones at the inlet of the last CV. Thus those values have been replaced by the corresponding inlet variables.

Another step of the post-processing is to compute the fuel and air utilizations. The code output actually gives two fuel utilizations computed in different ways, which has to perfectly match. However, the difference between these two figures was about 2%. The same thing was true for the air utilization. One of the two ways of computing the utilizations was to calculate the difference of equivalent hydrogen molar rate (or

oxygen molar rate) between the inlet and outlet of each CV. Then, one sums up all those differences and divides by the inlet equivalent hydrogen molar rate (or oxygen molar rate). There was an inaccuracy in the first CV, where instead of the inlet equivalent hydrogen molar rate there was the equivalent hydrogen molar rate at the outlet of that CV. The same thing was done for the oxygen utilization. After the correction the two ways of computing the utilizations has given the same results. However, the second way of computing the fuel utilization is using the following equation instead of the difference of equivalent hydrogen molar rate, for the n^{th} CV:

$$\frac{i_n \cdot A_n}{2 \cdot F} \tag{2.8}$$

Where i_n is the current density and F is the Faraday constant (96485 $\frac{C}{mol}$). A similar equation is used for the oxygen utilization.

One of the aims of the post-processing is to compute the overall efficiency. As done for the utilizations, this is calculated in two different ways, which have to match each other. Unfortunately, the output of the existing code simulating just one channel gave slightly different overall efficiencies (e.g. 35.27% against 34.75%). Moreover, if one tryed to simulate more than one channel, the difference really increased (e.g. 35.27% against 69.50%). The first way of computing the electric efficiency is to sum up the power provided by each CV and to divide by the input power of the fuel:

$$\eta_{el} = \frac{V_{cell}}{(\dot{m}LHV)_{f,in}} \sum_{n=1}^{N} i_n A_n \tag{2.9}$$

Where N is the total number of CVs in a channel. The other way is to multiply the following figures:

$$\eta_{el,ideal} = \frac{\overline{V}_{Nernst} i_{max} A_{channel}}{(\dot{m}LHV)_{f,in}} = \frac{2\overline{V}_{Nernst} F(x_{H_2,in} + 4x_{CH_4,in} + ...)}{(MM \cdot LHV)_{f,in}} \tag{2.10}$$

$$\eta_{voltage} = \frac{V_{cell}}{\overline{V}_{Nernst}} \tag{2.11}$$

$$\eta_i = \frac{\overline{i}}{i_{max}} \tag{2.12}$$

Where $\eta_{el,ideal}$, $\eta_{voltage}$ and η_i are respectively the ideal electric efficiency, the voltage efficiency and the current efficiency. The term $A_{channel}$ has been already explained in equation (2.2). considering equation (2.10), in the existing code the term regarding the equivalent hydrogen in the inlet fuel was not considered, thus it has been added.

$\overline{V}_{Nernst}$ is the mean Nernst voltage along the channel and it was computed as:

$$\overline{V}_{Nernst} = \frac{\sum_{n=1}^{N} V_{Nernst,n} \cdot L_{CV,n}}{L_{channel}} \tag{2.13}$$

This definition has been changed, since the mean Nernst voltage should represent the ideal mean energy per unit charge released from the reversible system. Therefore, it should be weighed on the current instead of the CV lengths. Thus:

$$\overline{V}_{Nernst} = \frac{\sum_{n=1}^{N} V_{Nernst,n} \cdot i_n \cdot L_{CV,n}}{\sum_{n=1}^{N} i_n \cdot L_{CV,n}} \tag{2.14}$$

The mean current density was computed in the right way, weighing on the CV length.

$$\overline{i} = \frac{\sum_{n=1}^{N} i_n \cdot L_{CV,n}}{L_{channel}} \tag{2.15}$$

On the other hand, the maximum available current density was computed considering the overall active area of the cell:

$$i_{max} = \frac{\dot{m}_{f,in} \cdot MM_{f,in} \cdot (x_{H_2,in} + 4 \cdot x_{CH_4,in} + ...)}{N_{channels} \cdot A_{channel}} \tag{2.16}$$

This led to a i_{max} lower by a factor $N_{channels}$. Thus one had η_i higher by the same factor (it could go over unity), and so the electric efficiency. The factor $N_{channel}$ has now been deleted.

After the above changes, the electric efficencies still did not exactly match each other. The last step has been explained in section 2.1.1. The channel length given by the user and the one computed as the sum of the CVs lengths were both used in those

calculations. This led to discrepancies in the results. After this last modification, the electric efficiencies have finally exactly matched each other.

2.2 Mass, Momentum and Energy balances

A considerable amount of the efforts aimed at revising the code has been addressed to this module. This is both because it was the one that needed to be revised the most, and because it is crucial from the point of view of the temperature and molar fraction distribution, which deeply affects the electrochemical and chemical calculations.

2.2.1 Momentum balances

To be sure of calculating things right in whatever operating condition, one should write the axial global momentum balances for air and fuel channels in each CV. The following is the fuel momentum balance as it was written in the existing code:

$$\dot{m}_{out} v_{out} - \dot{m}_{in} v_{in} - (p_{out} - p_{in}) A_{cross} - F_{friction} - \overline{v} \sum_i \dot{n}_{i,PEN \to f} \cdot MM_i = 0 \tag{2.17}$$

Where $F_{friction}$ is evaluated using a simple relationship for the pressure loss, which is presented in section 2.2.3. The term $\dot{n}_{i,PEN \to f}$ is positive if electrochemical and chemical reactions together determines a net passage of i from PEN to the fuel channel. It is negative otherwise. To account for the momentum of the species exchanged with the PEN an average velocity is used ($\overline{v}$). This is the arithmetic mean between the inlet and the outlet one.

The first thing to be noted is the sign of the pressure term. The outlet momentum should be higher where the inlet pressure is higher. Thus the before the pressure term a plus should be put instead of a minus. Considering that, also the friction force should change its sign, because its direction is the same one as the outlet pressure. Finally, only the species going from the channel to the PEN should be considered in the balance, this is because the species entering from the PEN do not have any axial velocity component. Therefore, $\dot{n}_{i,PEN \to f}$ should be considered only if negative. Thus the following is the resulting equation:

$$\dot{m}_{out} v_{out} - \dot{m}_{in} v_{in} + (p_{out} - p_{in}) A_{cross} + F_{friction} - \overline{v} \sum_i \dot{n}^-_{i,PEN \to f} \cdot MM_i = 0 \tag{2.18}$$

The above considerations and modifications have been applied also to the air channel. In this case the only species exchanged with the PEN is the oxygen, whose outgoing momentum was already treated in the right way. The outgoing oxygen due to the eventual CO oxidation has been added to the one related to H_2.

2.2.2 Energy balances

The equations defining the energy balances of the system are the ones which have been changed the most. The energy balances are written for the PEN structure, interconnection, and air and fuel channels. This is done in order to find the 4 relevant temperature in the considered CV, $T_{int}, T_{PEN}, T_f, T_a$. The last two are the ones at the outlet of the CV, since the ones at the inlet are known from solving the previous CV. On the other hand, the PEN and interconnection temperatures are a sort of average throughout the solid part (lumped parameters).

Thermal resistances

In this paragraph, the modifications applied to the thermal resistances of the CVs will be explained. $R_{an}, R_{cat}, R_{elec}, R_{int}$ are the axial thermal resistance between adjacent CVs. R_{trans} is the resistance between the PEN structure and the interconnection structure within a certain CV. Finally, $R_{int,ch}$ is the thermal resistance between the interconnection of one channel and the one of the adjacent channel. This last thermal resistance is the only kind of interaction modeled between adjacent channels.

The axial thermal resistances of anode, cathode and electrolyte for the n^{th} CV (Control Volume) were initially evaluated as:

$$R_{an} = \frac{L_{CV,n}}{\sigma_{th,an} \cdot W \cdot t_{an}} \tag{2.19}$$

$$R_{cat} = \frac{L_{CV,n}}{\sigma_{th,cat} \cdot W \cdot t_{an}} \tag{2.20}$$

$$R_{elec} = \frac{L_{CV,n}}{\sigma_{th,elec} \cdot W \cdot t_{an}} \tag{2.21}$$

The above equations contain several inaccuracies. The first one is a trivial typo, indeed the anode thickness (t_{an}) should be replaced by the cathode and electrolyte thickness in the respective resistances. Then, to get the area through which the heat flows,

one should add to the channel width (W) the interconnection thickness (counted double). Finally, for a certain CV, one should evaluate two thermal resistances, related to the previous and the subsequent CV. Therefore, the following are the resistances evaluated for the nth CV and the subsequent one:

$$R_{an,n,n+1} = \frac{L_{CV,n} + L_{CV,n+1}}{2\sigma_{th,an}(W + 2t_{int})t_{an}} \tag{2.22}$$

$$R_{cat,n,n+1} = \frac{L_{CV,n} + L_{CV,n+1}}{2\sigma_{th,cat}(W + 2t_{int})t_{cat}} \tag{2.23}$$

$$R_{elec,n,n+1} = \frac{L_{CV,n} + L_{CV,n+1}}{2\sigma_{th,elec}(W + 2t_{int})t_{elec}} \tag{2.24}$$

Then, the three resistances have been put together, as it was done in the existing code, to get the PEN axial resistance.

$$R_{PEN,n,n+1} = (\frac{1}{R_{an,n,n+1}} + \frac{1}{R_{cat,n,n+1}} + \frac{1}{R_{elec,n,n+1}})^{-1} \tag{2.25}$$

The interconnection axial resistance was initially evaluated as:

$$R_{int} = \frac{L_{CV,n}}{\sigma_{th,int} \cdot W \cdot t_{an}} \tag{2.26}$$

which has been changed to:

$$R_{int,n,n+1} = \frac{L_{CV,n} + L_{CV,n+1}}{2\sigma_{th,int}A_{int}} \tag{2.27}$$

where A_{int} is computed as:

$$A_{int} = 4t_{int}H + 2H_{int}(W + 2t_{int}) \tag{2.28}$$

The reader must have noticed that the surface through which the heat flows in the interconnection is computed summing up the contributions of the air and the fuel side. Indeed, a weakness of the code which persists up to the actual version is considering the interconnection of the air and fuel sides as a single entity which has its own single temperature. This is of course a source of inaccuracy. I the future, this may be fixed. Nevertheless, it is not a trivial task as all the energy balances should be rewritten.

The thermal resistance between PEN and interconnection has been totally changed, and it is now evaluated as:

$$R_{trans} = \frac{1}{4L_{CV,n}t_{int}}(\frac{H}{\sigma_{th,int}} + \frac{t_{PEN}}{2\sigma_{th,PEN}}) \tag{2.29}$$

where t_{PEN} is the thickness of the PEN structure and $\sigma_{th,PEN}$ is the arithmetic mean between the conductivities of anode, cathode and electrolyte.

Finally, also the thermal resistance between the interconnections of adjacent channel has been totally changed. It is now computed as:

$$R_{int,ch} = \frac{t_{int}}{2\sigma_{th,int}L_{CV,n}(H + H_{int})} \tag{2.30}$$

The factor 2 at the denominator is due to the same reason as before. Being the interconnections at fuel and air sides a single entity, the interconnection contact surface at both sides should be considered in a single resistance.

The above thermal resistances were initially calculated each time that the code entered the balances module. Now they are computed and recorded in "field" variables only the first time that a CV is solved. The "field" variables are generally used within the code to store important paramaters associated to each CV. In this way, they can be used throughout the simulation (axial conduction iterations or dynamic simulation). Thus the efficiency of the code has been improved.

Axial conduction

The way axial conduction is accounted for has been deeply changed. Indeed, in the energy balance written for each CV, the heat flowing along the axial direction was considered to be just the one coming from (or going to) the previous CV. One could not actually account for the heat coming from (or going to) the next CV because the channel is solved one CV at a time, so that one knows the temperature in the previous CV (just solved) but not the one in the next one.

In the first place, the axial conduction was completely erased. Indeed, with the assumption that in a certain position the heat flows in a preferential direction, one could assume, as a first approximation, that the heat coming from an adjacent CV and the

one going to the other one simply cancel out. This is not a realistic hypothesis, but at least 0 is likely to be closer to the difference of the two axial contribution compared to one of the contribution itself.

Eventually, the axial conduction has been introduced in a more rigorous way by using an iterative method, and the possibility to turn it off is given to the user. The first step of the iterative method is to provide a first guess temperature distribution by solving the channel without axial conduction. The temperature distributions of the PEN and of the interconnection is then recorded, in order to compare them with the updated distributions and to provide a criteria to stop the iterations. Thus the old distribution is used both for the electrochemical calculations and to solve the energy balances accounting for axial conduction. This leads to new temperature profiles, which are then compared to the old ones. Thus the maximum relative temperature difference in each CV must be below certain non user-defined threshold. Another condition which must be fulfilled for the iterations to be stopped is a small enough total energy unbalance computed in one of the channels. This tolerance is user-provided, and a good threshold to get accurate results is 0.1%. In case convergence is not reached at the required tolerance, one can either raise the tolerances, or decrease the relaxation factor, which is user-provided.

The constants B and C play a major role in the computational time required to get axial conduction to convergence. These constants define the length given to each CV. Indeed, one usually wants a finer grid in the initial part of the channel, to cope with high gradients due to steam reforming. In the case without axial conduction, the parameters B and C did not play a very important role, because one could easily use more than 300 CVs without significantly increasing the computational time. In this way the CVs were small everywhere, and one could just give a slight increase of the CVs length setting for instance B = 20 and C = 2.

When dealing with axial conduction, the computational time may be rather higher than the previous case. Thus the number of CVs used is crucial, and the reason is twofold: the time required to perform each iteration approximately increases proportionally with the CVs number, and the number of iterations required to get to the same tolerance level increases as well. Therefore, one should minimize the number of CVs used by making a good choice of the constants B and C, refining the grid where it is

required by the higher gradients.

A possible improvement of the implemented algorithm is to solve the channel as a whole, in each iteration. This would likely improve the "effectiveness" of each iteration (now depending on the conditions one may need up to 10^4 iterations). The reason is that solving the channel one CV at a time, does not allow the solution of a CV to see the updated temperatures of the following CV. If one solved the channel altogether, all the updated temperatures, which depend on each other through axial conduction, would be solved together. Nevertheless, the non-linear solver may have troubles in solving such a big system of equations ($4 \cdot N_{CV}$). Another solution could be to solve the channel several times during just one iteration, so that the temperature distribution at least approaches the one arising from solving the channel altogether.

Channels energy balances

Both the fuel and air channel balances considered 4 energy exchanges in the existing code. These were the mass flow coming from the previous CV, the one going to the next one, and the heat exchange with PEN and interconnection. Thus, the species exchange with the PEN structure should be added, both for the fuel and the air side. For instance, for the fuel channel:

$$+\sum_i \dot{n}_{i,PEN\to f} h_i(T_{PEN}) \tag{2.31}$$

$$-\sum_i \dot{n}_{i,f\to PEN} h_i(\overline{T}_f) \tag{2.32}$$

Where the signs are put to stress whether they introduce or not energy in the channel. The term h_i is the molar enthalpy of species i, and $\overline{T}_f$ is the mean temperature of the fluid across the CV. The molar rates are always positive in this case. Moreover, the mean temperature of the fuel across the CV has been turned from a logarithmic temperature to an arithmetic one. Thus the previous and the actual temperatures are respectively:

$$\overline{T}_f = \frac{T_{in} - T_{out}}{\ln \frac{T_{in}}{T_{out}}} \tag{2.33}$$

$$\overline{T}_f = \frac{T_{in} + T_{out}}{2} \tag{2.34}$$

In the existing code there was not the possibility to get a vector containing the molar enthapies of each species given the temperature. Thus, a function has been created in the module devoted to the computation of thermochemical properties.

As far as the air channel balance is concerned, the enthalpy flux due to oxygen crossing the PEN boundaries has been added, it corresponds to an outgoing energy flux:

$$-\frac{\dot{n}_{H_2 f\rightarrow PEN}+\dot{n}_{COf\rightarrow PEN}}{2}h_{O_2}(\overline{T}_a) \tag{2.35}$$

What was said for the fuel average temperature applies also to the air one.

Moreover, the enthalpy of the fuel and air species, which was computed when calculating the mix molar enthalpy, had to be changed since enthalpy of formation was not considered. The mix molar enthalpy, which is used to assess the energy flow associated with streams ingoing and outgoing a CV was computed as:

$$h_i(T)=\int_0^T c_p(T)dT \tag{2.36}$$

$$h_{mix}=\sum_i h_i\cdot x_i \tag{2.37}$$

The equation defining the enthalpy of mix has been left unchanged, whilst the molar enthalpy of a species has been recalculated as:

$$h_i(T)=\Delta h^\circ_{f,i}+\int_{T_{ref}}^T c_{p,i}(T)dT \tag{2.38}$$

where the reference temperature T_{ref} is the temperature at which the enthalpies of formation are evaluated, namely 298.15 K.

In the existing code, the integral in equation (2.38) was actually computed by the code. This reduced both the accuracy and the velocity of the code itself. The former because a numerical integral is always less accurate than an analytical one, the latter because a huge quantity of integrals where computed throughout the simulation. Indeed, also enthalpies of C_2H_6, C_3H_8, C_4H_{10}, CH_3OH and N_2 where computed each time, also if they where not present in the fuel mixture. Now the calculation of a species

enthalpy is much more straightforward. For instance, the specific heat of H_2 is computed with a 9^{th} grade polynomial expression:

$$c_{p,H_2} = aT^9 + bT^8 + cT^7 + ... + l \tag{2.39}$$

Which had to be numerically integrated by the code each time the enthalpy of the fuel (or of the air) was needed. Therefore, the enthalpy of H_2 is now directly computed as:

$$h_{H_2}(T) = \Delta h^{\circ}_{f,H_2} + \frac{a}{10}(T^{10} - T^{10}_{ref}) + \frac{b}{9}(T^9 - T^9_{ref}) + \frac{c}{8}(T^8 - T^8_{ref}) + ... + l(T - T_{ref}) \tag{2.40}$$

With this modification, the *computational time has become 1-2 order of magnitude lower*.

PEN structure energy balance

This energy balance already included the convective heat transfer with air and fuel side, the radiative heat transfer with the interconnection (if radiative heat transfer is switched-on), and the electric power delivered. Plus, the energy introduced by chemical and electrochemical reactions occurring inside the PEN structure was accounted as follows, in the n^{th} CV.

$$-\dot{n}_{H_2,f\rightarrow PEN} \cdot \Delta h_{ox,H2}(T_{PEN,n}) \tag{2.41}$$

$$-\dot{n}_{CO,f\rightarrow PEN} \cdot \Delta h_{ox,CO}(T_{PEN,n}) \tag{2.42}$$

$$-r_{WGS} \cdot A_n \cdot \Delta h_{WGS}(T_{PEN,n-1}) \tag{2.43}$$

$$-r_{MSR} \cdot A_n \cdot \Delta h_{MSR}(T_{PEN,n-1}) \tag{2.44}$$

One may think about just replacing $T_{PEN,n-1}$ with $T_{PEN,n}$, but still an energy unbalance would be present in the system. Indeed, the species enter the PEN structure at $\overline{T}_f$ and $\overline{T}_a$ (O_2), and come out from it at T_{PEN}, as stated by equation (2.31). Also, species are supposed to react at T_{PEN}, as stated in the above equations. Therefore, one should add to the PEN structure energy balance a power loss equal to the one required by the

reacting species to be brought from $\overline{T}_f$ and $\overline{T}_a$ to $T_{PEN,n}$.

Nevertheless, the method explained above is thought to be less intuitive then just considering the species crossing the PEN boundaries with their molar enthalpies. Thus, contributions (2.41) - (2.44) have been replaced by the following enthalpy flows:

$$+\sum_i \dot{n}_{i,f\rightarrow PEN} \cdot h_i(\overline{T}_f) \tag{2.45}$$

$$-\sum_i \dot{n}_{i,PEN\rightarrow f} \cdot h_i(T_{PEN}) \tag{2.46}$$

$$+\frac{(\dot{n}_{H_2}+\dot{n}_{CO})_{f\rightarrow PEN}}{2} \cdot h_{O_2}(\overline{T}_a) \tag{2.47}$$

before that modification the energy unbalance on the whole channel was about 0.05 %. After the change the unbalance dropped to $2 \cdot 10^{-8}$ %.

Another addition which has been made to the PEN structure balances, which applies only when the axial conduction iterations are performed, is the heat loss of the first and last CVs towards the surroundings. This is computed as:

$$-q_{loss} \cdot t_{PEN} \cdot (W + 2 \cdot t_{int}) \tag{2.48}$$

Where q_{loss} is the energy lost in the unit time specific to the exposed surface. This value can be computed by making some assumptions regarding the emissivity of the PEN and of the case around the stack, assuming an average emitting temperature of the PEN and a temperature difference with the case (e.g. 900° and 5°). Thus a reasonable value could be 1000 $\frac{W}{m^2}$ [4].

Interconnection energy balance

Apart from the thermal resistance explained in section 2.2.2, and possibility to account for axial conduction presented in section 2.2.2, only one more change has been introduced in this balance. This is how the heat loss is accounted for. In the existing code this was given by the user, specific to the volume of the fuel channel, if the whole cell was made up by just one channel. The default value was calibrated from previous experiences, but that figure is thought to be not very realistic for different cell geometries.

This is because the heat loss is mainly proportional to the surface exposed to the surroundings. The user may now give a heat loss specific to that surface, and the *total* interconnection heat loss in a certain CV will be computed as:

$$\dot{Q}_{loss} = 4 \cdot q_{loss} \cdot L_{CV,n} \cdot H \cdot H_{int} \tag{2.49}$$

Where H is the channel height and H_{int} is the height of the interconnection above the channel height. The heat loss has been multiplied by 2 because one has to account for both sides, fuel and air. That loss is all applied to one channel if just one channel is simulated, and it is spread equally between the first and last channel if the cell is made up by more than one channel. The surface where the adjacent cell should be located is supposed to be adiabatic.

As done for the PEN structure energy balance, a heat loss for the first and last CVs has been added when axial conduction is activated. That loss is computed as:

$$-2 \cdot q_{loss}[2 \cdot t_{int}(H + H_{int}) + H_{int} \cdot W] \tag{2.50}$$

Where the first factor 2 is to account for interconnection loss in both the air and fuel sides.

2.2.3 Simplified balances

The existing code solved the complete mass, momentum and energy balances for each CV, resulting in a system of 20 equations and 20 unknowns. This system was then solved with a non-linear equations solver. The unknowns were 12 outlet concentrations (10 for the fuel and 2 for the air), 2 pressures, 2 velocities and 4 temperatures. This worked fine because without axial conduction the computational time was relatively low. Nevertheless, introducing the iterations for axial conduction involves the need for a more efficient way of solving the mass, momentum and energy equations, due to the higher computational time which may be required. Therefore, the user may set the input 'mom_detail' to 'off' to pass to a quicker and more efficient mode. This mode turns out to be about *3 times quicker* than the standard mode, achieving right the same results.

The crucial point is that the detailed momentum equations are not solved anymore, instead a very simple equation is used to compute the pressure loss across the CV. This equation is the same one used in the existing code to account for the friction force in the momentum balance equation. The reason for doing this is that the fluids move with a very low speed, which results in low Mach numbers. Thus the fluids can be considered incompressible. Therefore, the pressure loss can be directly evaluated with an equation which accounts for the friction with the channel walls. Moreover, the mass balances and pressure losses are directly computed outside the non-linear equations solver, so that the system is now made up of just 4 energy balances used to find the 4 relevant temperatures of a CV.

Another source of inefficiency is that one does not really have to go through the species concentrations to solve the balances. One can solve the equations in a more efficient way, and calculate the species concentrations afterwards.

Either when one is iterating for axial conduction or not, one has the input flows from the previous CVs and a PEN temperature which can be used to evaluate the chemical and electrochemical species production and consumption. If one is iterating for axial conduction, the PEN temperature used is the one at the previous iteration in that CV, otherwise it is the PEN temperature in the previous CV. Given that, one can directly evaluate the outlet streams and molar fractions, without making use of the non-linear solver.

$$\dot{n}_{f,i,out} = \dot{n}_{f,i,in} + \dot{n}_{i,PEN \rightarrow f} \tag{2.51}$$

$$\dot{n}_{f,out} = \sum_{i} \dot{n}_{f,i,out} \tag{2.52}$$

Where $\dot{n}_{i,PEN \rightarrow f}$ is the net production of species i by chemical and electrochemical reactions. Thus, it is positive if the species is produced, negative otherwise. One can write similar equations for the air channel:

$$\dot{n}_{N_2,out} = \dot{n}_{N_2,in} \tag{2.53}$$

$$\dot{n}_{O_2,out} = \dot{n}_{O_2,in} - \frac{(\dot{n}_{H_2} + \dot{n}_{CO})_{f \rightarrow PEN}}{2} \tag{2.54}$$

$$\dot{n}_{a,out} = \sum_i \dot{n}_{a,i,out} \tag{2.55}$$

Thus one can easily evaluate the molar fractions at the outlet of the considered CV, which could then be used in chemical and electrochemical calculations for the subsequent CV.

$$x_{f,i,out} = \frac{\dot{n}_{f,i,out}}{\dot{n}_{f,out}} \tag{2.56}$$

$$x_{a,i,out} = \frac{\dot{n}_{a,i,out}}{\dot{n}_{a,out}} \tag{2.57}$$

Moreover, one can compute the outlet molar masses (both for air and fuel) of the mixtures, and the total mass flows.

$$MM_{out} = \sum_i x_{i,out} \cdot MM_i \tag{2.58}$$

$$\dot{m}_{out} = \dot{n}_{out} \cdot MM_{out} \tag{2.59}$$

The next step is to take care of the pressure loss, which is actually not very important in the considered operating condition (low velocity). The following equations can be written for the nth CV, and they are valid both for the fuel and the air channels:

$$Re = \frac{\rho_{in} \cdot v_{in}}{\nu_{fluid,in}} \tag{2.60}$$

$$C_f = \frac{Po}{Re} \tag{2.61}$$

$$p_{out} = p_{in} - \frac{2C_f \rho_{in} v_{in}^2 L_{CV}}{D_{hydro}} \tag{2.62}$$

Where C_f is the friction factor. The Posuille number (Po) is computed as a function of the channel aspect ratio, its exact definition is reported in reference [10]. The outlet partial pressures can now be computed at the outlet of the considered CV (both for air and fuel channel).

$$p_{i,out} = p_{out} \cdot x_{i,out} \tag{2.63}$$

The last step is to solve the 4 energy balances (PEN, interconnection, fuel and air channels) with a non-linear equations solver. In the energy balances the outlet velocities of the fluids appear, so that one should solve the following equations together with the balances (both for the air and the fuel channels):

$$v_{out} = \frac{\dot{n}_{out}}{A_{cross} \cdot C_{out}} \tag{2.64}$$

$$C_{out} = \frac{p_{out}}{R \cdot T_{out}} \tag{2.65}$$

Where C_{out} is the outlet total concentration of fuel or air channels. Now that outlet velocities has been found, the outlet concentrations can be evaluated as well.

$$C_{i,out} = \frac{\dot{n}_{i,out}}{A_{cross} \cdot v_{out}} \tag{2.66}$$

As said above, this approach reduces of about 3 times the computational time required by the code. Nevertheless, there is still margin for improvement. For instance, one can think of making the enthalpy of a species a linear function of temperature:

$$h_i = a_i + b_i T \tag{2.67}$$

This same approach has been followed in reference [4] and it likely does not introduce big inaccuracies if the linerarization temperature range is limited. The main advantage of this simplification would be the possibility to solve the system with a linear solver, which could sensibly improve the code efficiency. Moreover, the linear solver could probably tackle an eventual system of $4 \cdot N_{CV}$ equations arising from solving the channel altogether, as explained at the end of section 2.2.2.

2.3 Electrochemical and Chemical models

The electrochemical model is of major importance for the calculation of fuel cell performance. The chemical model also can be important depending on the operating condition (e.g. methane content in the fuel flow). Whereas the balance equations on the CV are rather straightforward, the chemical and electrochemical models are subject to a certain degree of uncertainty. Indeed, the literature is full of models describing H_2 electroxidation, MSR and WGS reaction rates. These models can also vary a lot from

each other, especially for what is concerned the chemical reaction rates.

One of the highlight of the present work is the implementation of a novel way to account for CO electroxidation, which is based on the definition of a combined Nernst potential, and on the loss which must be subtracted from that potential. Unfortunately, the literature lacks of works considering the carbon monoxide as electrochemically active, as it is supposed to be readily turned into hydrogen via WGS.

2.3.1 General changes

Variables used in electrochemical and chemical calculations

In the existing code there was a bit of confusion regarding the variables used throughout the electrochemical and chemical models. The code solves one CV at a time, providing as a first step the electrochemical and chemical reaction rates in a certain CV. Afterwards, the mass, momentum and energy balances are solved, and the results are recorded in the correspondent field variables. The field variables represent temperatures, pressures, velocities, concentrations, mass flows and molar flows at the interface of each CV. The PEN and interconnection temperatures are the only variables not computed at the interface of each CV.

At the beginning of the electrochemical model, which is the first module to be treated in each CV, the variables used for chemical and electrochemical calculations must be given. For instance one has to write for the nth CV:

$$T_f = T_{f,field,n-1} \tag{2.68}$$

to set the fuel temperature used in the chemical and electrochemical models as the one at the outlet of the previous CV. This was done right for temperature, pressures and molar fractions. Other variables used in the chemical calculations are:

$$\dot{n}_{f,i} = \dot{n}_{f,i,field,n-1} \tag{2.69}$$

$$\dot{n}_f = \dot{n}_{f,field,n-1} \tag{2.70}$$

$$p_{f,i} = p_{f,i,field,n-1} \tag{2.71}$$

The first two variables are used in the chemical module when calculating the equilibrium reactions rate. This is done to check whether a model overcomes the equilibrium condition or not across a CV. Without adding equation (2.70), the total fuel molar rate used in equilibrium calculations was always the one at the inlet of the channel. $\dot{n}_{f,i}$ was actually adjourned, but it was done at the beginning of the balances module. Thus the equilibrium calculations of the nth CV was performed using the species molar rates at the outlet of (n-2)th CV. The same thing was done for $p_{f,i}$, which in the existing code was used to compute the MSR and WGS reaction rates. Other variables where adjourned with $\dot{n}_{f,i}$ at the beginning of the balances module, they all have been moved at the beginning of the electrochemical module.

As said above, the existing code solved one control volume at a time, using the T_{PEN} of the previous CV to make electrochemical and chemical calculations. One of course has the problem of dealing with the first CV, because it seems that PEN temperatures are not available at all. The trick has been to compute the energy balances of a fictitious CV before the first one, and to use the PEN temperature arising from those balances. In the existing code that PEN temperature was not used to enter the chemical and electrochemical calculations of the first CV, thus it has been added.

Electrochemical guess variables

The aim of the electrochemical calculations is to find, for each CV, the current which determines the voltage losses from the Nernst potential so as to match the given operating voltage. This is done by giving a certain guess of the unknowns of the system of equations, and to let a non-linear solver to find the solution. It is well-known that the closer the guess to the real solution, the quicker will be the solver to reach the required accuracy. The following are the unknowns of the system in the case H_2 is the only electrochemically active species.

$$\eta_{ohm}, \eta_{act,H_2}, \eta_{act,O_2}, \eta_{conc}, i_{an} \tag{2.72}$$

For the first CV it is right to make a guess based on the overall ohmic resistance of the cell, like it was done in the existing code.

$$i_{guess} = \frac{(V_{Nernst} - V_{cell})}{R_{ohm,tot}} \tag{2.73}$$

From a guess on the current density, one could easily give a guess on the other voltage losses. When one is considering the successive CVs, a more efficient guess choice exists, namely to use the solution from the previous CV. This was done just for the current density, now all the unknowns are guessed based on the results of the just solved CV. After this modification, the total computational time to solve the channel has dropped by about 30%.

2.3.2 Voltage losses

Concentration losses

The concentration losses have a little influence in normal SOFC operating condition [8]; Nevertheless, several modifications and corrections have been made, so that it is worth to mention them.

The concentration losses are generally computed once the molar fractions of electrochemically active species in the active site are known. If H_2 is considered the only active species, the following are the equations defining the reduction of Nernst potential.

$$\eta_{conc,an} = \frac{RT_{PEN}}{2F} \ln\left(\frac{x_{H_2,b} x_{H_2O,r}}{x_{H_2,r} x_{H_2O,b}}\right) \tag{2.74}$$

$$\eta_{conc,cat} = \frac{RT_{PEN}}{4F} \ln\left(\frac{x_{O_2,b}}{x_{O_2,r}}\right) \tag{2.75}$$

Where $x_{i,r}$ represents the molar fraction at the active site, $x_{i,b}$ is the one in the bulk flow. The above equations have been left unchanged, whilst changes have been made on the way $x_{i,r}$ is computed. The following were the equations used in the initial code:

$$x_{H_2,r} = x_{H_2,l} - \frac{iRT_f t_{an}}{2Fp_f D_{p,H_2}} \tag{2.76}$$

$$x_{H_2,l} = x_{H_2,b} - \frac{iRT_f D_h}{2Fp_f D_{m,H_2}} \tag{2.77}$$

$$x_{H_2O,r} = x_{H_2O,l} - \frac{iRT_f t_{an}}{2Fp_f D_{p,H_2O}} \tag{2.78}$$

$$x_{H_2O,l} = x_{H_2O,b} - \frac{iRT_f D_h}{2Fp_f D_{m,H_2O}} \tag{2.79}$$

Where D_p is the diffusivity accros the porous electrode and D_m is the diffusivity of a species in a gaseous mixture. The term x_l is the molar fraction at the interface between channel and electrode. If hydrogen is consumed the current density i is positive, and according to equations (2.76) and (2.77) the molar fraction of hydrogen is lower towards the PEN structure. The higher molar fraction of hydrogen in the channel guarantees a flux of hydrogen towards the active site, and according to equation (2.74) the anode concentration loss due to hydrogen is positive. Likewise, the molar fraction of water should be higher in the active site and lower in the bulk. This would determine a flux of water from the anode to the channel and an increase of concentration loss computed with equation (2.74). The above reasoning is true only if the signs in equations (2.78) and (2.79) are positive. Thus, the following are the right equations:

$$x_{H_2O,r} = x_{H_2O,l} + \frac{iRT_f t_{an}}{2Fp_f D_{p,H_2O}} \tag{2.80}$$

$$x_{H_2O,l} = x_{H_2O,b} + \frac{iRT_f D_h}{2Fp_f D_{m,H_2O}} \tag{2.81}$$

The same modification has been applied also to the equation defining CO_2 molar fractions, considering the current density due to CO oxidation:

$$x_{CO_2,r} = x_{CO_2,l} + \frac{i_{CO}RT_f t_{an}}{2Fp_f D_{p,CO_2}} \tag{2.82}$$

$$x_{CO_2,l} = x_{CO_2,b} + \frac{i_{CO}RT_f D_h}{2Fp_f D_{m,CO_2}} \tag{2.83}$$

Before the modification, negative concentration losses occurred, this does not happen anymore.

Moreover, the temperature used to solve equations (2.76), (2.77), (2.78) and (2.79) is the fuel one at the inlet of the CV. This is considered to be accurate for equations (2.77) and (2.79), but one should use the PEN temperature for equations (2.76) and (2.78), because the porous diffusion occurs within the PEN structure. This was probably done because without axial conduction activated, one did not know the temperature of the PEN in the considered CV, because the electrochemical calculations are always performed before the energy balances. With the possibility to account for axial conduction one can simply use the PEN temperature at the previous iteration in the

considered CV, thus this change has been applied.

In the existing code, the porous diffusion coefficient D_p was computed as:

$$D_{p,i} = \frac{\epsilon}{\tau}[\frac{3}{4 \cdot r_p}(\frac{\pi MM_i}{2RT})^{0.5} + \frac{1}{D_{m,i}}] \tag{2.84}$$

Where ϵ and τ are respectively the porosity and the tortuosity of the electrode. Equation (2.84) comes from reference [17], but an inaccuracy is present in the cited paper. Indeed, the right equation is:

$$D_{p,i} = \frac{\epsilon}{\tau}[\frac{3}{4 \cdot r_p} \cdot (\frac{\pi MM_i}{2RT})^{0.5} + \frac{1}{D_{m,i}}]^{-1} \tag{2.85}$$

After this correction the concentration loss becomes several times higher than before, but it still remains relatively low.

A little error has been found also in the equation defining the diffusivity coefficient of O_2 in N_2. The following is the equation used, which is taken from reference [18].

$$D_{AB} = \frac{0.00143 \cdot T^{1.75}}{pM_{AB}^{0.5}[(\sum_v)_A^{1/3} + (\sum_v)_B^{1/3}]} \tag{2.86}$$

$$M_{AB} = 2(\frac{1}{MM_A} + \frac{1}{MM_B})^{-1} \tag{2.87}$$

As shown in the reference, the pressure should have the unit of [bar], and the result is in unit $[\frac{cm^2}{s}]$. Thus the pressure, which was given in [Pa] in the existing code has been divided by 10^5 and the overall result has been devided by 10^4 to get $[\frac{m^2}{s}]$. This last error was present just in the oxygen diffusivity, the fuel species diffusivities were computed right.

Ohmic losses

The ohmic loss model used is taken from reference [4].

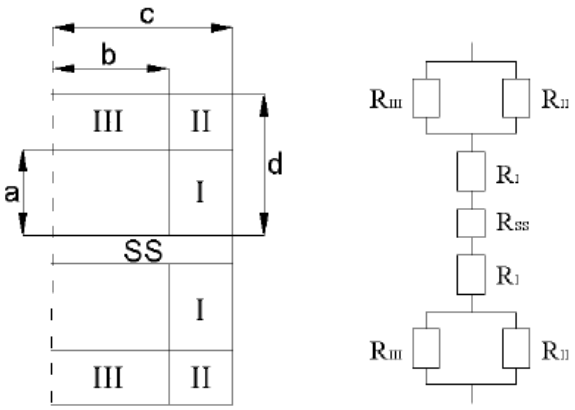

Figure 2.2: *Half ohmic circuit of a CV [4]*

The electrical scheme in the figure represents the interconnection (I,II,II) and electrolyte (SS) ohmic resistances of half a CV. Indeed, two set of resistances like the one in the figure put in parallel would represent the overall ohmic resistance in a certain CV. In the existing code, R_{III} was counted just one time both at the anode and the cathode side. Thus, at the anode two R_{II} and two R_{III} should be present (all in parallel), but only 3 resistances in parallel were present, one R_{III} was missing. The same thing was done for the cathode.

Moreover, until now the model always considered that $c-b$ (t_{int}) was equal to $d-a$. The possibility for the user to give the quantity $d-a$ (H_{int}) has now been added, so that electrical (and thermal) resistances could be more accurately evaluated.

2.3.3 CO electroxidation

A model accounting for the oxidation of carbon monoxide was already present in the code. This model defined an equivalent electric circuit, in which the activation and concentration losses of CO and H_2 were considered to occur in parallel. The equivalent circuits both with and without CO oxidation can be seen in reference [5]. The main problem with this model is the definition of two different Nernst potentials, both for H_2 and CO. Therefore, the aim of the developed model has been to define just one reversible Nernst voltage. Thus, the activation loss which is subctracted from the Nernst voltage in the energy balance equation is only one.

The first step is to compute the reversible voltage by imposing a *null overall current*

drawn from anode in the reversible system were both species are considered active. To do that, one can use the well known Butler-Volmer equations for activation polarization both for H_2 and CO electrochemistry, which are taken from reference [6].

$$i = i_{0,H_2}[\exp(\frac{F\eta_{act,H_2,rev}}{RT}) - \exp(-\frac{F\eta_{act,H_2,rev}}{RT})] + i_{0,CO}[\exp(\frac{F\eta_{act,CO,rev}}{RT}) - \exp(-\frac{F\eta_{act,CO,rev}}{RT})] = 0 \tag{2.88}$$

Where i_0 is the exchange current density which can be easily evaluated by making use of an Arrheius-like equation [6].

$$i_{0,H_2} = \gamma_{an}(\frac{p_{H_2}}{p_{ref}})(\frac{p_{H_2O}}{p_{ref}})\exp(-\frac{E_{act,an}}{RT}) \tag{2.89}$$

$$i_{0,CO} = \frac{\gamma_{an}}{3}(\frac{p_{CO}}{p_{ref}})(\frac{p_{CO_2}}{p_{ref}})\exp(-\frac{E_{act,an}}{RT}) \tag{2.90}$$

$$i_{0,O_2} = \gamma_{cat}(\frac{p_{O_2}}{p_{ref}})^{0.25}\exp(-\frac{E_{act,cat}}{RT}) \tag{2.91}$$

For completeness also the oxygen exchange current has been shown. The partial pressures of the species appearing in equations (2.91) and (2.90) are taken to be the ones in the bulk fuel flow, because concentration losses are not considered now. If one imagines to reach a stationary OCV condition, neither $\eta_{act,H_2,rev}$ or $\eta_{act,CO,rev}$ is null, they would assume a certain non-zero value so as to satisfy equation (2.88). Thus, in that stationary condition there would be a certain net production/consumption of H_2 and consumption/production of CO. The objective now is to write the activation overpotentials of H_2 and CO in the reversible system as functions of the Nernst combined voltage, to find that voltage from equation (2.88). Thus the following is the definition of the considered activation overpotentials:

$$E = \phi_{anode} - \phi_{electrolyte} \tag{2.92}$$

$$\eta_{act,H_2,rev} = E_{rev,comb} - E_{rev,H_2} \tag{2.93}$$

$$\eta_{act,CO,rev} = E_{rev,comb} - E_{rev,CO} \tag{2.94}$$

Where ϕ is the electrical potential, and E_{rev,H_2} and E_{rev,H_2} are evaluated in a condition where H_2 or CO are electrochemically active alone. One can now express all

the anode potentials as function of the cathode potentials. The equations (2.93) and (2.94) both refer to reversible conditions, so that the following are the expressions for the anode potentials.

$$\phi_{anode,rev,comb} = \phi_{cathode,rev,comb} - \Delta V_{rev,comb} \tag{2.95}$$

$$\phi_{anode,rev,H_2} = \phi_{cathode,rev,H_2} - \frac{|\Delta G_{H_2}|}{2 \cdot F} \tag{2.96}$$

$$\phi_{anode,rev,CO} = \phi_{cathode,rev,CO} - \frac{|\Delta G_{CO}|}{2 \cdot F} \tag{2.97}$$

Where $\Delta V_{rev,comb}$ is the combined Nernst voltage that occur when both hydrogen and carbon monoxide are present as active species, thus it is the figure that we are looking for. Putting (2.95), (2.96) and (2.92) into (2.93) and (2.95), (2.97) and (2.92) into (2.94) one gets the following expressions for the activation overpotentials:

$$(\phi_{cathode} - \phi_{electrolyte})_{rev,comb} - \Delta V_{rev,comb} - (\phi_{cathode} - \phi_{electrolyte})_{rev,H_2} + \frac{|\Delta G_{H_2}|}{2 \cdot F} \tag{2.98}$$

$$(\phi_{cathode} - \phi_{electrolyte})_{rev,comb} - \Delta V_{rev,comb} - (\phi_{cathode} - \phi_{electrolyte})_{rev,CO} + \frac{|\Delta G_{CO}|}{2 \cdot F} \tag{2.99}$$

The term $\phi_{cathode} - \phi_{electrolyte}$ is supposed to be the same in all three reversible conditions. Thus the above equations reduce to:

$$\eta_{act,H_2,rev} = \frac{|\Delta G_{H_2}|}{2F} - \Delta V_{rev,comb} \tag{2.100}$$

$$\eta_{act,CO,rev} = \frac{|\Delta G_{CO}|}{2F} - \Delta V_{rev,comb} \tag{2.101}$$

Finally, one can combine equations (2.88), (2.100) and (2.101) to get $\Delta V_{rev,comb}$ which respects the zero current condition. This reversible Nernst voltage is always located somewhere in the middle between the Nernst voltages of H_2 and CO. This is trivial, because from (2.88) one knows that $\eta_{act,H_2,rev}$ and $\eta_{act,CO,rev}$ should have opposite signs. The only way to respect that, looking at equations (2.100) and (2.101) is that $\Delta V_{rev,comb}$ has a value between the two reversible voltages.

Once the reversible Nernst voltage has been found, the equations defining the voltage losses should be written for the nth CV. The usual energy balance (which is turned into a voltage balance) is still valid, as done when only H_2 is the active species.

$$\Delta V_{rev,comb} = V_{cell} + \eta_{ohm} + \eta_{act,O_2} + \eta_{act,an} + \eta_{conc} \tag{2.102}$$

The ohmic loss is computed by making use of the model explained in section 2.3.2.

$$\eta_{ohm} = i R_{ohm,tot} A_n \tag{2.103}$$

Where i is the current density specific to the electrode geometric surface, which is computed with equation (2.1). The concentration overpotential is simply calculated as difference between the Nernst potential referred to channel molar fractions and the one computed with active site molar fractions, as done when hydrogen was the only active species. The reversible voltage computed with the active site concentrations is different because $\frac{|\Delta G_{H_2}|}{2F}$, $\frac{|\Delta G_{CO}|}{2F}$, i_{0,H_2} and $i_{0,CO}$ change. Finally, one has to deal with the activation overpotentials. As said above, reference [6] could be used for that.

$$I_{H_2} = i_{0,H_2}[\exp(\frac{F\eta_{act,H_2,rev}}{RT}) - \exp(-\frac{F\eta_{act,H_2,rev}}{RT})] \cdot A_{act,an} = i_{H_2} \cdot A_n \tag{2.104}$$

$$I_{CO} = i_{0,CO}[\exp(\frac{F\eta_{act,CO,rev}}{RT}) - \exp(-\frac{F\eta_{act,CO,rev}}{RT})] \cdot A_{act,an} = i_{CO} \cdot A_n \tag{2.105}$$

$$I = i_{0,O_2} \cdot [\exp(2\frac{F\eta_{act,O_2,rev}}{RT}) - \exp(-2\frac{F\eta_{act,O_2,rev}}{RT})] \cdot A_{act,cat} = i \cdot A_n \tag{2.106}$$

$$i = i_{H_2} + i_{CO} \tag{2.107}$$

The surface A_n is computed with equation (2.1). The terms $A_{act,an}$ and $A_{act,cat}$ are the active surfaces within the electrodes provided by the reference. It is important to use the values provided as the kinetic parameters of the exchange current densities may have been calibrated using those active areas. These are computed through a constant defining the ratio between the active area and the volume of the electrode.

$$A_{act,an} = a_{v,an} \cdot V_{an} = a_{v,an} \cdot A_n \cdot t_{an} \tag{2.108}$$

$$A_{act,cat} = a_{v,cat} \cdot V_{cat} = a_{v,cat} \cdot A_n \cdot t_{cat} \tag{2.109}$$

Parameter	Value	Unit
γ_{an}	$1.344 \cdot 10^{10}$	$[\frac{A}{m^2}]$
γ_{cat}	$2.051 \cdot 10^{9}$	$[\frac{A}{m^2}]$
$E_{act,an}$	$1 \cdot 10^{5}$	$[\frac{J}{mol}]$
$E_{act,cat}$	$1.2 \cdot 10^{5}$	$[\frac{J}{mol}]$
$a_{v,an}$	650	$[\frac{m^2}{m^3}]$
$a_{v,cat}$	6500	$[\frac{m^2}{m^3}]$

The only thing missing is a relation between H_2 and CO activation overpotentials and the actual anodic overpotential ($\eta_{act,an}$) referred to the reversible combined potential difference between anode and electrolyte. Starting from the definitions of H_2 and CO activation overpotentials one can write:

$$\eta_{act,H_2} = E - E_{rev,H_2} \tag{2.110}$$

$$\eta_{act,CO} = E - E_{rev,CO} \tag{2.111}$$

The above expressions are equivalent to the following:

$$\eta_{act,H_2} = E - E_{rev,comb} + E_{rev,comb} - E_{rev,H_2} \tag{2.112}$$

$$\eta_{act,CO} = E - E_{rev,comb} + E_{rev,comb} - E_{rev,CO} \tag{2.113}$$

Where the first two terms in both equations represent $\eta_{act,an}$. Therefore, using also equations (2.93), (2.94), (2.100) and (2.101), one can finally write:

$$\eta_{act,H_2} = \eta_{act,an} + \frac{|\Delta G_{H_2}|}{2F} - \Delta V_{rev,comb} \tag{2.114}$$

$$\eta_{act,CO} = \eta_{act,an} + \frac{|\Delta G_{CO}|}{2F} - \Delta V_{rev,comb} \tag{2.115}$$

Thus one can easily solve the arising system of equations using a non-linear solver.

2.3.4 Equilibrium composition

One of the duties of the chemical module is to compute the equilibrium composition given the CV inlet molar flow rates. This is done in order to find the maximum rates of the considered chemical reactions. If the kinetic model for a certain reaction overcomes the equilibrium rate, then the latter would be taken as the real one. In order to compute the equilibrium reaction rate one has to find the number of reaction advancement grades to be considered. The other advancement grades are dependent parameters. The number of independent advancement grades is equal to the difference between the number of atoms involved in the reactions and the number of different chemical species. In the existing code a chemical species was considered to be present in the mixture if its molar fraction was above 10^{-15}. At the beginning of the code, the molar fraction of CH_4 was actually set to 10^{-15} if the user gave a null molar fraction (for numeric reasons). Moreover, if the sum of molar fractions given by the user was different from unity, a re-normalization was performed. Therefore, if the sum of molar fractions was even slightly below unity, the molar fraction of methane was always set to a number higher that 10^{-15}, thus it was always counted as a present species. Therefore, now a species is considered to be present in the mixture if its molar fraction is above 10^{-9}. In this way, just the WGS advancement grade is considered when computing the equilibrium composition with null methane concentration.

A similar reasoning applies to the routine defining the equations to be used when solving the equilibrium composition. The code solved the equations relative just to the WGS advancement grade when the molar fraction of CH_4 was zero. This was never the case since its molar fraction was set to 10^{-15} at the beginning of the code.

Moreover, now all the molar fractions set to 0 by the user are set to 10^{-15} for numerical reasons.

2.3.5 WGS reaction rate

In the existing code, several chemical models were implemented, so that one could easily choose which one to use. Nevertheless, it is difficult to find in the literature relations for reaction rates (WGS and MSR) which are widely shared. At least for MSR several correlations have been found which give analogous results in certain operat-

ing conditions [4][19][5][20]. For WGS reaction the debate on whether it is necessary to consider a reaction rate equation or not is still open, also because little work has been done to investigate the approach to equilibrium of WGS. Indeed, a lot of author make the assumption that it is fast enough to be considered always at equilibrium, but still some works demonstrate that WGS is not at equilibrium at normal SOFC operating condition [11]. Therefore, one of those works has been used to try to improve the assumption of WGS being at equilibrium. The paper is the one of Ahmed and Föger [12], where the approach to equilibrium of the WGS reaction on a Ni/Zirconia anode is investigated under normal high temperature SOFC conditions. A wide range of fuel utilization has been simulated, and the approach to equilibrium is never complete. On the contrary, the maximum η_{eq} is about 0.85, where η_{eq} is defined as:

$$\eta_{eq} = \frac{K_p}{K_{eq}(T)} \tag{2.116}$$

$$K_p = \frac{p_{H_2} \cdot p_{CO_2}}{p_{CO} \cdot p_{H_2O}} \tag{2.117}$$

Thus, a WGS model allowing to impose a certain η_{eq} at the outlet of a CV has been implemented. Setting $\eta_{eq} = 0.85$ is at least believed to improve the assumption of imposing WGS to be at equilibrium. If η_{eq} at the inlet of a certain CV is higher than 0.85 but lower than 1 then the WGS is supposed to be too close to equilibrium, and its reaction rate is set to 0. This is done to be sure WGS moves towards equilibrium. The above reasoning holds when K_p at the inlet of a CV is lower than K_{eq}. If it is higher, η_{eq} is set to 1.15, and the discussion just done still applies in a symmetrical way. This same model could be used to set the outlet composition to the equilibrium one. This is done by setting $\eta_{eq} = 1$

2.3.6 Chemical functions

In the chemical module a set of functions which could be used in the simulation are provided. Those functions are the reaction enthalpies and the equilibrium constants of several important chemical reactions:

$$H_2 + \frac{1}{2}O_2 \rightleftharpoons H_2O \tag{2.118}$$

$$CO + \frac{1}{2}O_2 \rightleftharpoons CO_2 \tag{2.119}$$

$$CO + H_2O \rightleftharpoons H_2 + CO_2 \tag{2.120}$$

$$CH_4 + H_2O \rightleftharpoons 3H_2 + CO \tag{2.121}$$

$$C_2H_6 + 2H_2O \rightleftharpoons 5H_2 + 2CO \tag{2.122}$$

$$C_3H_8 + 3H_2O \rightleftharpoons 7H_2 + 3CO \tag{2.123}$$

$$C_4H_{10} + 4H_2O \rightleftharpoons 9H_2 + 4CO \tag{2.124}$$

$$CH_3OH \rightleftharpoons 2H_2 + CO \tag{2.125}$$

In the following two section the changes and simplifications to reaction enthalpies and equilibrium constants calculations will be explained.

Reaction enthalpies calculation

The reaction enthalpy of the just listed chemical reactions was used in the existing code to compute the chemical heat released to the PEN structure. At the moment this is not done anymore, as explained in section 2.2.2. Nevertheless, the changes applied to reaction enthalpy calculations will be explained for completeness. The following reasoning (and modifications) apply also to the Gibbs energy of a certain reaction.

The reaction enthalpy is easily computed as:

$$\Delta h_r(T) = \sum_{j=1}^{NS} \nu_j \cdot h_j(T) = \sum_{j=1}^{NS} \nu_j \cdot (\Delta h^\circ_{f,j} + \int_{T_{ref}}^{T} c_{p,j}(T)\,dT) \tag{2.126}$$

Where h_j is the molar enthalpy of a species, which is just a function of temperature since all the species can be considered ideal gases. The term ν_j is the stoichiometric coefficient of species j, positive for products and negative for reactants. Finally, NS is the number of species involved in the considered reaction. The term $\Delta h^\circ_{f,j}$ is the standard enthalpy (i.e. computed at a certain reference temperature $T_{ref} = 298.15$ K) of formation of the species j, and it can be easily found in the literature for all the species.

This figure is conventionally set to zero for pure species, whereas it is the opposite of the heat of formation at T_{ref} for a compound. Thus the following is the standard reaction enthalpy:

$$\sum_{j=1}^{NS} \nu_j \cdot \Delta h^{\circ}_{f,j} \tag{2.127}$$

The value of the standard reaction enthalpy was readily computed for all reactions except for methanation (which was considered apart from methane steam reforming), thus it has been added. Moreover, the standard reaction enthalpy of CO oxidation was computed as:

$$\Delta h^{\circ}_{r,COox} = \Delta h^{\circ}_{f,CO_2} \tag{2.128}$$

Therefore, the term related to CO formation enthalpy has been added:

$$\Delta h^{\circ}_{r,COox} = \Delta h^{\circ}_{f,CO_2} - \Delta h^{\circ}_{f,CO} \tag{2.129}$$

The oxygen does not appear in equation (2.129) since it is a pure species.

Moreover, in the existing code the following integral, which appears in equation (2.126), was computed numerically.

$$\int_{T_{ref}}^{T} \sum_{j=1}^{NS} \nu_j c_{p,j}(T)\, dT \tag{2.130}$$

As explained is section 2.2.2, the numerical integration could substantially increase the computational time required. Thus, as done in section 2.2.2 the integral have been resolved analytically and it has been directly given to the code as a function of temperature. An example of the analytical integration result is shown in the next section addressed to equilibrium constants calculation.

Equilibrium constants calculation

The equilibrium constants of the considered reactions could be evaluated by simple relations taken from the literature [5][19]. Those relations are just functions of the temperature at which they are evaluated. This can easily be demonstrated by considering the following equation, valid for whatever reaction at equilibrium:

$$\Delta G_r = \Delta G_r^\circ(T) + RT \cdot \ln(K_{eq}) = 0 \tag{2.131}$$

$$K_{eq} = \exp(-\frac{\Delta G_r^\circ(T)}{RT}) \tag{2.132}$$

Despite one could get a good estimation of the equilibrium constant of a reaction by using an equation taken from the literature, the code has its own set of functions aimed at computing equilibrium constants. The equilibrium constant functions of WGS and MSR are used to compute the reaction rates in one of the chemical model which are available in the code. Moreover, those functions are used also to compute the equilibrium composition of section 2.3.4. Actually, if one wanted to compute the equilibrium composition with the existing code to check the consistency of kinetic relations, the computational time substantially increased, and the reason is readily explained. The code employs the integrated Van't Hoff equation to derive an expression for the equilibrium constant of a certain reaction:

$$-\frac{\Delta G_r^\circ(T)}{RT} = (\frac{\Delta h_r^\circ(T) - \Delta G_r^\circ(T)}{RT})_{T_{ref}} - \frac{\Delta h_r^\circ(T_{ref})}{RT} + \int_{T_{ref}}^{T} \frac{\int_{T_{ref}}^{T} \sum_{j=1}^{NS} \nu_j c_{p,j}(T) dT}{RT^2} dT \tag{2.133}$$

As explained in the previous sections, computing integrals numerically could be really time consuming for the code. This is actually the reason why computing the equilibrium condition at the outlet of a CV was so detrimental for the performance of the code. The integrals in equation (2.133) are actually much worse than the ones encountered until now. The reason is that for each point in which the first integral is divided, another integral has to be evaluated. Thus the double integral has been computed analytically and given to the code as a function of temperature T. For instance, let us consider the following integral:

$$\int_{T_{ref}}^{T} \frac{\int_{T_{ref}}^{T} c_{p,H2}(T) dT}{T^2} dT \tag{2.134}$$

Which should be evaluated for the WGS reaction equilibrium constant as part of the summation inside the internal integral. As said in a previous section, the specific heat of hydrogen is computed with a 9^{th} grade polynomial expression. Therefore, equation (2.134) becomes:

$$\int_{T_{ref}}^{T} \frac{\frac{a}{10}(T^{10}-T_{ref}^{10})+\frac{b}{9}(T^{9}-T_{ref}^{9})+...+l(T-T_{ref})}{T^2}dT \tag{2.135}$$

The above equation can be further developed as follow:

$$\frac{a}{10}[\frac{T^9-T_{ref}^9}{9}-T_{ref}^9+\frac{T_{ref}^{10}}{T})]+\frac{b}{9}[\frac{T^8-T_{ref}^8}{8}-T_{ref}^8+\frac{T_{ref}^9}{T})]+...+l[\ln(\frac{T}{T_{ref}})-1+\frac{T_{ref}}{T})] \tag{2.136}$$

This last expression is evaluated for each species involved in a certain reaction and put in equation (2.133). Thus the equilibrium constant is now a simple function of the temperature at which it is evaluated, therefore it is computed in a much more efficient and fast way. The resulting equilibrium constants perfectly match the ones computed using the numerical integrals. There was a little discrepancy with the methanol dissociation constant, this was due to a mistaken stoichiometric coefficient of H_2 used in the existing code (1 was used instead of 2).

2.4 Low Temperature SOFC model

As said in the introduction, reducing the operating temperature of a SOFC would very likely bust the commercialization process of this device. The cell could entirely be made of metals, bringing benefits from the economic and startup point of view (both time and energy need related). Moreover, the degradation process of the materials would be a much less serious problem. Therefore, the aim of the present section is to develop a Macro-Scale model to compute the performance of a Ceria-based low-temperature SOFC. Specifically, the models used have been developed for a Samaria-Doped Ceria (SDC) electrolyte fuel cell.

The equations employed have been taken from references [7][9][8]. Hereafter, those equations will be presented. The main difference with the usual high temperature cells is that the electrolyte is also an electronic conductor (MIEC material), thus also the leakeage current should be assessed. The electrochemical energy balance within the CV is written as [8]:

$$V_{rev,H_2} i_{O^{2-}}^{ely} = V_{cell} i_{load} + i_{O^{2-}}^{ely}(\eta_{ohm,O^{2-}}+\eta_{act,O_2}+\eta_{act,H_2}+\eta_{conc}) + i_{el}^{ely}\eta_{ohm,el} \tag{2.137}$$

$$\eta_{conc} = \eta_{conc,H_2} + \eta_{conc,O_2} \tag{2.138}$$

$$i^{ely}_{O^{2-}} = i_{load} + i^{ely}_{el} \tag{2.139}$$

Where all the currents are the ones within the electrolyte (constants), as the associated ohmic losses. At the end of this section, also the ohmic losses within the electrodes will be discussed. Moreover, the currents are all taken as positive even if the electrons and oxygen ions currents have opposite direction within the electrolyte. The reason for that is that electrons are moved by electric potential, whereas oxygen ions are subject also to chemical forces. The electronic current density is evaluated as:

$$i^{ely}_{el} = \frac{i^{ely}_{O^{2-}}}{\sigma_{O^{2-}}} \frac{\sigma^0_{el}}{1 - M_0} [M_0 (P^0_{O_2})^{-1/4} - (P^L_{O_2})^{-1/4}] \tag{2.140}$$

$$M_0 = \exp(-\frac{F}{RT} \cdot \frac{i^{ely}_{O^{2-}}}{\sigma_{O^{2-}}} L) \tag{2.141}$$

Where L is the thickness of the electrolyte. The term $\sigma_{O^{2-}}(T)$ is the ionic conductivity of the electrolyte and $\sigma^0_{el}(T)$ is the temperature-dependent part of the electrolyte electronic conductivity:

$$\sigma_{el} = \sigma^0_{el}(T) \cdot P^{-1/4}_{O_2} \tag{2.142}$$

The parameters $P^0_{O_2}$ and $P^L_{O_2}$ are the partial pressure of oxygen at the anode and cathode side within the electrolyte.

The concentration losses are computed with equations (2.74) and (2.75). Likewise, the relations between hydrogen oxidation and oxygen reduction currents and their respective activation overpotentials are evaluated via Butler-Volmer equations. One has to be careful about the active area used when dealing with those equations. In the code, the active area in a CV is generally the geometrical one (A_n). Nevertheless, in more sophisticated model, it may happen that the active area is calculated based on the electrode characteristics, as done in reference [7]. This reference will be used to validate the present model, thus its Butler-Volmer equations are empolyed. Taking the cited article as a reference one may write:

$$I_{0,H_2} = \gamma_{pre,H_2} \cdot T \cdot \exp(-\frac{E_{act,H_2}}{RT}) \cdot (\frac{P_{H_2}}{P_{ref}})^{0.47} \cdot V_{an} \cdot a_{v,an} \tag{2.143}$$

$$I_{0,O_2} = \gamma_{pre,O_2} \cdot T \cdot \exp(-\frac{E_{act,O_2}}{RT}) \cdot (\frac{P_{O_2}}{P_{ref}})^{0.33} \cdot V_{cat} \cdot a_{v,cat} \tag{2.144}$$

The above currents unit of measure is [A]. The terms V_{an} and V_{cat} are respectively the anode and cathode volumes. Finally, $a_{v,an}$ and $a_{v,cat}$ are the square meters of active area per unit volume of anode and cathode respectively. To find those terms one of the standard models is to consider the electrode made up by a ordered cluster of particles. By trivial geometrical considerations one could conclude that:

$$a_v = \frac{6 \cdot (1-\epsilon)}{d_p} \tag{2.145}$$

Where d_p is the mean particle diameter of an electrode and ϵ is its porosity. The reference article applies a coefficient to equation (2.145), leading to the following values:

Parameter	Value	Unit
$a_{v,an}$	$5.4 \cdot 10^5$	$[\frac{m^2}{m^3}]$
$a_{v,cat}$	$2.2 \cdot 10^5$	$[\frac{m^2}{m^3}]$

Thus, the Butler-Volmer equations assume the following form:

$$I_{H_2} = I_{0,H_2} \cdot [\exp(\frac{F\eta_{act,H_2}}{RT}) - \exp(-\frac{F\eta_{act,H_2}}{RT})] = i^{ely}_{O^{2-}} \cdot A_n \tag{2.146}$$

$$I_{O_2} = I_{0,O_2} \cdot [\exp(1.3\frac{F\eta_{act,O_2}}{RT}) - \exp(-0.7\frac{F\eta_{act,O_2}}{RT})] = i^{ely}_{O^{2-}} \cdot A_n \tag{2.147}$$

The activation overpotentials are also related to the oxygen partial pressures by the following equations:

$$\eta_{act,H_2} = \frac{RT}{4F} \cdot \ln(\frac{P^0_{O_2}}{P^I_{O_2}}) \tag{2.148}$$

$$\eta_{act,O_2} = \frac{RT}{4F} \cdot \ln(\frac{P^{II}_{O_2}}{P^L_{O_2}}) \tag{2.149}$$

Where $P^I_{O_2}$ and $P^{II}_{O_2}$ are the oxygen partial pressures respectively at anode and cathode active sites. The latter can be easily evaluated by starting from the oxygen bulk

partial pressure, accounting for mass diffusion towards the active site. The former is estimated by assuming that the hydrogen oxidation reaction (2.118) is at equilibrium within the anode. Thus:

$$\frac{P^I_{O_2}}{P_{ref}} = \left(\frac{\frac{P_{H_2O}}{P_{ref}}}{\frac{P_{H_2}}{P_{ref}} \cdot K_{eq,H_2ox}}\right)^2 = \left(\frac{x_{H_2O,r}}{x_{H_2,r} \cdot K_{eq,H_2ox}}\right)^2 \tag{2.150}$$

Where P_{ref} is the ambient pressure (1 atm). The equilibrium constant is temperature-dependent, and can be easily computed by making use of the correspondent function presented in section 2.3.6. This function is a very complex expression depending on temperature, made up by three contribution as (2.136). In the following table are reported the values of that constant for several temperatures, calculated by the code function:

T [°C]	$K_{eq} \cdot 10^{-10}$[−]
500	6570.014
525	1978.331
550	640.1852
575	221.2273
600	81.18272
625	31.47866
650	12.84003
675	5.487632
700	2.448627
725	1.137058
750	0.5479048
775	0.2732431
800	0.1406955

For instance, Shen et al. consider a 3% humidified hydrogen fuel mixture at 600 °C and ambient pressure. Thus, by using equation (2.150), $P^I_{O_2}$ should be around $1.45 \cdot 10^{-27}$ atm. This figure fairly matches the oxygen partial pressure at point 0 (anode) in the following graph taken from reference [8].

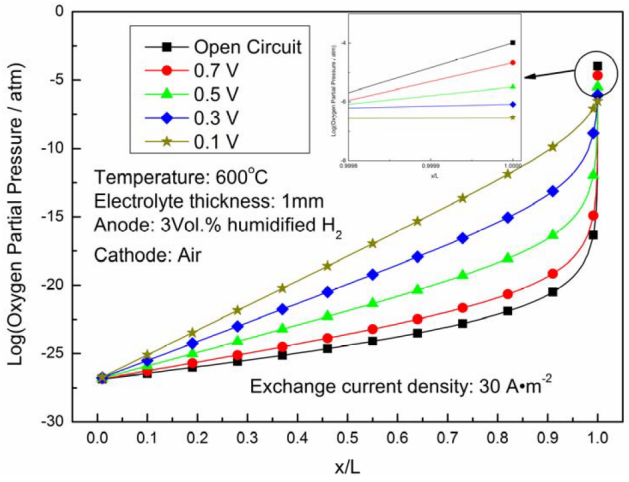

Figure 2.3: *O_2 partial pressure distribution within the elctrolyte from [8]*

Actually, the pressure in point 0 is $P^0_{O_2}$ and $P^I_{O_2}$ should be lower than the number shown in the figure (the former is the pressure within the electrolyte, the latter in the anode). Nevertheless, the order of magnitude is thought to be the same. Therefore, the equilibrium constant calculation and the methodology used until now are thought to be fine.

Considering equation (2.137), one can see that ohmic losses are the only ones which still need to be evaluated. The following equation holds true both for oxygen ions and electrons.

$$\eta_{ohm} = \int_0^L \frac{i}{\sigma} dx \tag{2.151}$$

The integration of this expression within the electrolyte is easy in the case of oxygen ions, as the conductivity is just a function of temperature and the ions current is constant within the electrolyte.

$$\eta_{ohm,O^{2-}} = \frac{i^{ely}_{O^{2-}} L}{\sigma_{O^{2-}}(T)} \tag{2.152}$$

On the other hand, the conductivity of electrons depends on oxygen partial pressure within the electrolyte, which is a function of the distance from the anode as one can see from figure 2.3. The actual form of this function is available in all the cited references, thus the integration of electronic ohmic loss within the electrolyte can actually be performed, as done in reference [8].

$$\eta_{ohm,el} = \int_0^L \frac{i_{el}^{ely}}{\sigma_{el}(T, P_{O_2})} dx = \frac{RT}{4F} \ln(\frac{P_{O_2}^L}{P_{O_2}^0}) - \eta_{ohm,O^{2-}} \tag{2.153}$$

The ohmic losses considered until now are the ones occurring within the electrolyte. To investigate the low temperature operation, one should properly account for all the present losses. Thus, the terms related to cathodic, anodic and interconnection ohmic losses should be added in the right-hand side of equation (2.137). The paper taken as reference simulates a button cell, thus the interconnection one will not be considered.

In the following, an attempt of modeling the ionic and electronic ohmic losses within the electrodes will be explained. A possibility could be to assume that within the electrodes only the current i_{load} flows, as done in the high temperature SOFC model. This is equivalent to assuming that all the oxygen reacts at the interfaces cathode/electrolyte and electrolyte/anode. In this way, one does not have to consider the ionic ohmic losses within the the electrodes, thus only their electronic conductivities would be needed. This is not what actually happens in reality, as one can see in picture 2.4. Nevertheless, in this case the loss to add to the energy balance (2.137) would be:

$$i_{load}(\eta_{ohm,an} + \eta_{ohm,cat}) = i_{load}^2(\frac{t_{an}}{\sigma_{el,an}} + \frac{t_{cat}}{\sigma_{el,cat}}) \tag{2.154}$$

The cathode is made by LSCF-GDC (Lanthanum Strontium Cobalt Ferrite - Gadolina Doped Ceria), which are considered respectively as the electronic and ionic conductive phase (even though LSCF is a MIEC material). Their intrinsic electronic and ionic conductivities are given [7]. The effective conductivity has to be found by assessing the volume fraction Ψ of the two phases, which have both been set to 50% (as the wheight fraction).

$$\sigma_{eff} = \sigma \Psi^{3/2} \tag{2.155}$$

Moreover, the anodic electronic conductivity is given, whereas the ionic one could be assumed to be the electrolyte one as a first approximation. Indeed, a considerable amount of Ceria is present also within the anode. Moreover, the anode is very thick, thus its ohmic loss should be considered somehow. In the following table, the conductivities of the materials are summarized:

Parameter	Value	Unit
SDC ionic conductivity	$9.85{\cdot}10^6/T\exp(-65200/R/T)$	[S m^{-1}]
SDC electronic conductivity	$2.5{\cdot}10^{10}/T\exp(-220000/R/T)\cdot P_{O_2}^{-1/4}$	[S m^{-1}]
Cathode ionic conductivity	$\Psi_{GDC}^{3/2}\cdot 1.09\cdot 10^7/T\exp(-61700/R/T)$	[S m^{-1}]
Cathode electronic conductivity	$\Psi_{LSCF}^{3/2}(98325-62.7\cdot T)$	[S m^{-1}]
Anode ionic conductivity	As SDC	[S m^{-1}]
Anode electronic conductivity	400	[S m^{-1}]

Table 2.2: *Materials conductivities [7]*

The electronic ohmic losses in the electrodes have been seen not to be very important, so let us start from the ionic losses. One should add to the right-hand side of equation (2.137) the following term, both for anode and cathode:

$$-\int_0^{L_{an/cat}} \frac{i_{O^{2-}}^2(x)}{\sigma_{O^{2-},an/cat}}dx \tag{2.156}$$

Where the cathode conductivity is the one of GDC accounting for its volume fraction. However, it is a constant (isothermal assumption is used when simulating a button cell). Thus, one should now guess a certain current distribution within the electrode, knowing that it is null at $x=0$ and $i_{O^{2-}}=i_{O^{2-}}^{ely}$ at $x=L_{an/cat}$ ($x=L_{an/cat}$ is the interface between electrode and electrolyte, also for cathode) .

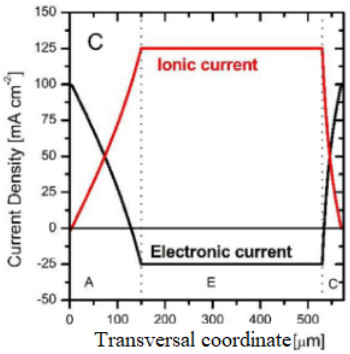

Figure 2.4: *Example of currents distributions. $i_{load}=1000\frac{A}{m^2}$ [7]*

Therefore, assuming a linear relationship, one may write:

$$i_{O^{2-}}(x)=\frac{i_{O^{2-}}^{ely}}{L_{an/cat}}x \tag{2.157}$$

Thus equation (2.156) can actually be integrated. The same reasoning can be conducted for the electrons current:

$$-\int_0^{L_{an/cat}} \frac{i_{el}^2(x)}{\sigma_{el,an/cat}} dx \tag{2.158}$$

Where the electronic currents at $x = 0$ are equal in module to i_{load} and at $x = L_{an/cat}$ they become i_{el}^{ely}. Thus one may write:

$$i_{el}(x) = i_{load} - \frac{(i_{load} + i_{el}^{ely})}{L_{an/cat}} x \tag{2.159}$$

Remember that in this model all currents are taken as positive. Moreover, in equation (2.159) it is not important the sign of the current but its absolute value, as it will be raised to the power of 2 in equation (2.158). Actually, once the current $i_{O^{2-}}(x)$ is known, one can compute $i_{el}(x)$ as follow to (charge conservation):

$$i_{el}(x) = i_{load} - i_{O^{2-}}(x) \tag{2.160}$$

Chapter 3

Dynamic model

One of the objectives of the work has been to develop a dynamic model aimed at evaluating the system response to boundary condition changes. The change taken as reference to develop the dynamic model has been the passage from the stationary OCV condition to the one after a load connection. This situation has been modeled via a voltage step from the maximum to the final one. The voltage is actually kept constant throughout the dynamic simulation. The model main objective is to predict the temperature distribution along the channel throughout time, and to assess the duration of the transient. Therefore, the dynamic electrochemical and mass transport equations are not solved, as those phenomenons are assumed to be much faster than the thermal transient.

After the computation of the initial condition, the electrochemical and chemical reactions at $t = 0$ are computed by using the initial molar fractions and temperatures distribution. To compute the electrochemical reaction rates the imposed voltage is also used. Thus the mass, momentum, and energy balance equations are solved. The updated variables are then used to evaluate again the electrochemical and chemical rates, this is done until the stationary condition is reached.

Despite the model has been developed by focusing on one specific case, it can be easily adapted to simulate other kind of transients. It would just be necessary to include some modifications in the calculation of the initial stationary condition, and then to impose a certain step change at the beginning of the dynamic module. Then the dynamic balance equations would still be capable of evaluating the system evolu-

tion.

Moreover, one may want to begin the simulation with a non-stationary condition. For instance, during a transient a certain boundary condition change could be imposed. It is also possible to give a value to the variables aimed at defining the initial condition at the beginning of the dynamic module. Of course, in that case it could be difficult to forecast the system evolution, since the transient would be affected both from the boundary condition change and the fact that the system was not stationary (thus it was already evolving).

Finally, one may also want to give a time-dependent boundary condition. This would also be possible by updating its value before solving each time step. Likewise, in principle one could assign different values to each variable defining a boundary condition at the beginning of each time step.

3.1 General considerations

3.1.1 Initial condition

The initial condition is computed with the same models presented in the previous chapter. As explained in the introduction, the initial condition is supposed to be the stationary OCV condition. The air and fuel flows are passed through the cell with chemical reactions normally occurring, but with no net current density drawn from the system. Thus the modification applied to the normal stationary code is mainly concerned with the electrochemical model. Particularly, the *net* current density which was found solving the voltage balance in the electrochemical module has been set to zero.

In case only H_2 is considered as the active species, electrochemical reactions do not occur at all. On the other hand, setting the net current density to zero in case CO oxidation is activated does not suppress electrochemical reactions. The model predicts the establishment of a stationary condition where a net production/consumption of H_2 occurs. The opposite is true for CO. The species that will be produced and consumed will be determined by the Nernst voltages of H_2 and CO (i.e. on the composition of

the fuel). As explained in section 2.3.3, the combined reversible voltage in a certain CV stands between the reversible voltages of H_2 and CO. If the molar fraction of H_2 was much higher with respect to CO, its reversible voltage would be higher. Thus the anode electric potential if only H_2 at that molar fraction was present would be more negative than the case of only CO. Thus the overpotential of H_2 would be negative based on the definition given in equation (2.93). In other words the potential of anode gets closer to the electrolyte one with respect to the case of only H_2 at that molar fraction to the case of combined electroxidation, this means that H_2 is consumed.

3.1.2 Adjustable time step

The amplitude of each time step is the main parameter which determines the accuracy of the solution and its stability, together with the definition of the grid (see section 2.1.1). The user will provide an initial step which is better to be low. Then the time step will automatically adapt based on the variations of the variables of interest such as temperatures and molar fractions. After time step t is performed, the following conditions have to occur to let the time step increase:

- The relative variations of molar fraction of each species in all points where the initial molar fraction is above a certain threshold should be below a certain threshold. This practically means that in all the points where the initial molar fraction of a substance is enough higher than zero the relative variation should be low enough. In this way, one avoids a time step drop in situations where the molar fraction change from 10^{-9} to 10^{-7} for instance. This condition is usually the most restrictive one at the beginning of the simulation (for the investigated cases), because of the electrochemical reactions occuring after the load connection.

- The maximum relative variation of the relevant temperatures should be below a certain threshold. This condition is generally always fulfilled for maximum relative variations of the order of 0.2% (a couple of degrees).

- Only little oscillations of the variables of interest are allowed. The parameters more prone to oscillate are the temperatures, this conclusion has been reached after a good number of trials. Therefore, when one of the relevant temperatures in a certain point has not a monotonic trend when looking at 3 subsequent instants, then only a certain absolute difference is allowed between the last 2 tem-

peratures in that point. If one wants to completely get rid of oscillations, the time step may have to decrease a lot, and this would not really affect the results of the simulation. Thus one has to find a good compromise between accuracy and required computational time. For instance, a maximum oscillation of 0.1°C has been found to be ok for the considered operating conditions.

- The last condition which should be respected is that the non-linear solver has found a solution for each CV. This is the case if all the variables change from the previous instant. If the solver does not converge with the required accuracy, it gives as the solution the initial guess, which is actually made up by the variables at the previous instant. Thus it is checked that a certain variable (no matter which one) changes in all points from one instant to the next one. If this is not the case, the time step is lowered and the accuracy required by the solver is loosened. Both the above measures have been proven to help the convergence of the solver. Another measure could be to increase the CVs number. This is probably due to the fact that the lower the time step and the higher the CVs number, the more accurate the spatial and temporal discretization of the balance equations. Nevertheless, it can happen that none of the above measures is successful, and the solver does not manage to converge to a solution. This may be due to the time oscillations explained in the last point, which may give inconsistent values of a certain variable (usually a temperature). Therefore, in this case one should lower the limit put on the variables oscillation (which is not directly available for the user as an input value).

3.2 Mass, momentum and energy balances

During each time step all the CVs of the cell are solved starting from the inlet one until the outlet of the cell. The main variables used to solve the mass, momentum and energy balances are the same used in the existing code to solve the stationary problem. Therefore, for each CV solved a system of $20 \cdot N_{channels}$ non-linear equations is solved. The unknowns of the system are the variables of interest at the end of the considered time step. For each CV there are 12 outlet concentrations (10 possible species for fuel and 2 for the air), 2 outlet pressures, 2 outlet velocities, 2 outlet temperatures (fuel and air) and the PEN and interconnection temperatures.

All the following balances are of course derived from the same equations used to evaluate the stationary condition, the only difference is the inclusion of the accumulation term and its temporal discretization. The spatial discretization is the same used in the stationary case, thus the following balances are meant to be applied on a discrete CV.

3.2.1 Mass balances

Considering a fuel or air CV in one of the cell channels one can write the following differential equation (the spatial discretization has already been performed):

$$\dot{n}_{i,in} + \dot{n}_{i,PEN\rightarrow ch} - \dot{n}_{i,out} = V\frac{dC_i}{dt} \tag{3.1}$$

Where C_i is the mean concentration of the i^{th} species inside the CV ($\frac{mol}{m^3}$), and V is its volume. The term $\dot{n}_{i,PEN\rightarrow ch}$ is the net production of species i by chemical and electrochemical reactions (negative if species i is consumed). Therefore, it also corresponds to the net molar rate of the considered species from the PEN to the CV. Equation (3.1) is valid both for air and fuel channels, in the air case $\dot{n}_{i,PEN\rightarrow ch}$ would represent the net consumption of O_2. When considering the stationary problem, the accumulation term (right hand side of the equation) is null, whereas in the dynamic simulation it must be discretized.

$$(\dot{n}_{i,in} + \dot{n}_{i,PEN\rightarrow ch} - \dot{n}_{i,out}) \cdot \Delta t = V \cdot (C_{i,t+\Delta t} - C_{i,t}) \tag{3.2}$$

Since the concentrations are computed at the faces of each CV (they are used to evaluate the molar rates together with the velocities and the cross area), one has to interpolate the faces values to get the mean value across the CV.

$$(\dot{n}_{i,in} + \dot{n}_{i,PEN\rightarrow ch} - \dot{n}_{i,out}) \cdot \Delta t = V \cdot [\frac{(C_{i,in} + C_{i,out})_{t+\Delta t}}{2} - \frac{(C_{i,in} + C_{i,out})_t}{2}] \tag{3.3}$$

The finer the computational grid, the more valid is this interpolation, the more close is (3.3) to accurately describe the real behaviour of the system. This may be the reason why increasing the number of CVs may help the convergence of the solver, as said at the end of section 3.1.2.

Along with the discretization comes the fact that the molar rates could vary within the time step. Therefore, the molar rates in the left-hand side of equation (3.3) should be averaged in the time step.

$$\overline{\dot{n}}_{i,in} = \frac{\dot{n}_{i,in,t} + \dot{n}_{i,in,t+\Delta t}}{2} \tag{3.4}$$

$$\overline{\dot{n}}_{i,out} = \frac{\dot{n}_{i,out,t} + \dot{n}_{i,out,t+\Delta t}}{2} \tag{3.5}$$

At the moment it is not possible to do the same with $\dot{n}_{i,PEN\rightarrow ch}$ because this figure is evaluated before performing the balances module. To evaluate $\dot{n}_{i,PEN\rightarrow ch,t+\Delta t}$ one should know the PEN temperature at the end of the time step before solving the balances, and this is not possible. Nevertheless, to compute $\dot{n}_{i,PEN\rightarrow ch}$ one needs also the molar fractions at the inlet of the considered CV. These molar fractions have been averaged in the time step to calculate the electrochemical and chemical rates. This is possible because the previous CV has been just solved, thus the averaged inlet molar fractions are known. As a matter of fact, this has been seen to be of major importance for the stability of the simulation, as all the cited averaging processes.

In the above equations, all the variables evaluated at instant t and the inlet variables are known (the initial condition is known from the previous time step and the previous CV has just been solved). Therefore, the only unknowns are $\dot{n}_{i,out,t+\Delta t}$ and $C_{i,out,t+\Delta t}$, but one can also write the following:

$$\dot{n}_{i,out,t+\Delta t} = C_{i,out,t+\Delta t} \cdot v_{out,t+\Delta t} \cdot A_{cross} \tag{3.6}$$

Therefore, the unknown variables until now are $C_{i,out,t+\Delta t}$ and $v_{out,t+\Delta t}$. Thus there are 14 overall unknowns (10 fuel concentrations, 2 air concentrations, 2 outlet velocities) and 12 equations have been written.

3.2.2 Momentum balances

The momentum balance equations have been written in their whole form as it was done in the stationary part of the existing code. However, one can easily simplify them by just introducing a pressure loss term in both fuel and air sides of the CV using equation (2.62). The following is the differential equation describing the momentum conservation in either the air or fuel channel:

$$(\dot{m}v)_{in} - (\dot{m}v)_{out} - (p_{out} - p_{in})A_{cross} - F_{friction} - \bar{v} \cdot \sum_i \dot{n}_{i,ch \to PEN} \cdot MM_i = V \frac{d\rho v}{dt} \tag{3.7}$$

Where $\dot{n}_{i,ch \to PEN}$ is different from zero just if a species moves from the channel to the PEN structure: as explained in section 2.2.1 the species moving in the opposite direction have a null axial velocity component. The usual discretization process gives the following left-hand term:

$$[(\dot{m}v)_{in} - (\dot{m}v)_{out} - (p_{out} - p_{in})A_{cross} - F_{friction} - \overline{v} \cdot \sum_i \dot{n}_{i,ch \to PEN} \cdot MM_i]\Delta t \tag{3.8}$$

As done in the mass balances, the terms in equation (3.8) has to be averaged in the time step, because their values are actually continuously changing.

$$(\overline{\dot{m}v})_{in} = \frac{(\dot{m}v)_{in,t} + (\dot{m}v)_{in,t+\Delta t}}{2} \tag{3.9}$$

$$(\overline{\dot{m}v})_{out} = \frac{(\dot{m}v)_{out,t} + (\dot{m}v)_{out,t+\Delta t}}{2} \tag{3.10}$$

$$(\overline{p})_{in} = \frac{p_{in,t} + p_{in,t+\Delta t}}{2} \tag{3.11}$$

$$(\overline{p})_{out} = \frac{p_{out,t} + p_{out,t+\Delta t}}{2} \tag{3.12}$$

The term $\overline{v}$ should be the mean axial velocity which the species have in the moment they enter the PEN structure. Thus the velocity has to be averaged in time and space.

$$\overline{v} = \frac{v_{in,t} + v_{out,t} + v_{in,t+\Delta t} + v_{out,t+\Delta t}}{4} \tag{3.13}$$

The term $F_{friction}$ is evaluated with the equation presented in section 2.2.3. The right-hand term of equation (3.7) is discretized as follow.

$$V[(\rho v)_{t+\Delta t} - (\rho v)_t] \tag{3.14}$$

Where (ρv) is a mean value inside the channel CV. As explained for the mass balances, the variables are not evaluated inside the CV, but just on its faces. Therefore, equation (3.14) becomes:

$$V\{\frac{[(\rho v)_{in}+(\rho v)_{out}]_{t+\Delta t}}{2}-\frac{[(\rho v)_{in}+(\rho v)_{out}]_{t}}{2}\} \tag{3.15}$$

Also in this case, the finer the grid, the more accurate this last passage.

As usual, inlet values and the ones evaluated at instant t are known. Therefore, the unknowns are $\dot{m}_{out,t+\Delta t}$, $v_{out,t+\Delta t}$, $p_{out,t+\Delta t}$, $\rho_{out,t+\Delta t}$. The variable $v_{out,t+\Delta t}$ has already be seen in the mass balances, whereas $p_{out,t+\Delta t}$ is an independent variable. Thus one should relate $\dot{m}_{out,t+\Delta t}$ and $\rho_{out,t+\Delta t}$ to the independent variables as:

$$\rho_{out,t+\Delta t}=\sum_i C_{i,out,t+\Delta t}\cdot MM_i \tag{3.16}$$

$$\dot{m}_{out,t+\Delta t}=\rho_{out,t+\Delta t}\cdot v_{out,t+\Delta t}\cdot A_{cross} \tag{3.17}$$

Therefore, 2 (air and fuel) unknown outlet pressures has been added together with 2 equations. Thus until now the balance is 14 equations and 16 unknowns.

3.2.3 Energy balances

Channels energy balances

The following is the differential equation defining the fuel energy balance, the air one is totally similar.

$$(\dot{n}h_{tot})_{in}-(\dot{n}h_{tot})_{out}+\dot{Q}_{PEN\to f}+\dot{Q}_{int\to f}+\dot{H}_{PEN\to f}-\dot{H}_{f\to PEN}=V\frac{d(C\cdot h_{tot})}{dt} \tag{3.18}$$

$$h_{tot}=h+\frac{v^2}{2}MM \tag{3.19}$$

Where C and h_{tot} are the average total molar concentration and the average total molar enthalpy inside the CV. The terms $\dot{H}_{PEN\to f}$ and $\dot{H}_{f\to PEN}$ represent the enthalpy flows of species exchanged by the fuel channel and PEN structure.

$$\dot{H}_{PEN\to f}=\sum_i \dot{n}_{i,PEN\to f}\cdot h_i(T_{PEN}) \tag{3.20}$$

$$\dot{H}_{f\to PEN}=\sum_i \dot{n}_{i,f\to PEN}\cdot h_i(\overline{T}_f) \tag{3.21}$$

The heat exchanged by convection with the PEN and interconnection structures is evaluated with the following relations:

$$\dot{Q}_{PEN/int\rightarrow f} = h_f \cdot A_{contact} \cdot (T_{PEN/int} - \overline{T}_f) \tag{3.22}$$

$$A_{contact,PEN} = L_{CV} \cdot W \tag{3.23}$$

$$A_{contact,int} = L_{CV} \cdot (W + 2 \cdot H) \tag{3.24}$$

$$h_f = \frac{Nu_f \cdot k_f(\overline{T}_f)}{D_h} \tag{3.25}$$

Where k_f is the thermal conductivity of the fuel mixture, and D_h is the hydraulic diameter of the channel. The Nusselt numbers (fuel and air) are set, and they can be taken for instance from reference [4].

The discretization gives the following left-hand term:

$$[(\dot{n}h_{tot})_{in} - (\dot{n}h_{tot})_{out} + \dot{Q}_{PEN\rightarrow f} + \dot{Q}_{int\rightarrow f} + \dot{H}_{PEN\rightarrow f} - \dot{H}_{f\rightarrow PEN}]\Delta t \tag{3.26}$$

Where the time averaging should be performed as follow:

$$(\overline{\dot{n}h}_{tot})_{in} = \frac{[\dot{n} \cdot (h + \frac{v^2}{2}MM)]_{in,t} + [\dot{n} \cdot (h + \frac{v^2}{2}MM)]_{in,t+\Delta t}}{2} \tag{3.27}$$

$$(\overline{\dot{n}h}_{tot})_{out} = \frac{[\dot{n} \cdot (h + \frac{v^2}{2}MM)]_{out,t} + [\dot{n} \cdot (h + \frac{v^2}{2}MM)]_{out,t+\Delta t}}{2} \tag{3.28}$$

$$\overline{T}_f = \frac{T_{f,in,t} + T_{f,out,t} + T_{f,in,t+\Delta t} + T_{f,out,t+\Delta t}}{4} \tag{3.29}$$

$$\overline{T}_{PEN} = \frac{T_{PEN,t} + T_{PEN,t+\Delta t}}{2} \tag{3.30}$$

$$\overline{T}_{int} = \frac{T_{int,t} + T_{int,t+\Delta t}}{2} \tag{3.31}$$

Where the fuel temperature has been averaged both in time and space. On the other hand, the discretized right-hand term of equation (3.18) is:

$$V \cdot [(Ch_{tot})_{t+\Delta t} - (Ch_{tot})_t] \tag{3.32}$$

In which the energy content per unit volume must be interpolated using the faces values.

$$V\{\frac{[(Ch_{tot})_{in} + (Ch_{tot})_{out}]_{t+\Delta t}}{2} - \frac{[(Ch_{tot})_{in} + (Ch_{tot})_{out}]_t}{2}\} \tag{3.33}$$

Writing the same equations also for the air channel one can conclude that the last 4 independent variables have been introduced, namely $T_{f,out,t+\Delta t}$, $T_{a,out,t+\Delta t}$, $T_{PEN,t+\Delta t}$, $T_{int,t+\Delta t}$. Of course one has to express the dependent variables seen in the above equations in a consistent way:

$$C_{out,t+\Delta t} = \sum_i C_{i,out,t+\Delta t} \tag{3.34}$$

$$h_{out,t+\Delta t} = h(T_{out,t+\Delta t}, x_{i,out,t+\Delta t}) \tag{3.35}$$

$$x_{i,out,t+\Delta t} = (\frac{C_i}{C})_{out,t+\Delta t} \tag{3.36}$$

Where the fuel enthalpy h is a function of both temperature and composition, and it can be evaluated with equations (2.37) and (2.38). Thus 4 equations are missing to close the system. These will be 2 energy balances e 2 equations of state.

PEN structure energy balance

The discretized equation used to define the PEN energy balance in the n^{th} CV is:

$$(\dot{H}_{f/a\rightarrow PEN} - \dot{H}_{PEN\rightarrow f} - \dot{Q}_{PEN\rightarrow f/a} - \dot{Q}_{PEN\rightarrow int} - V_{cell}I + \dot{Q}_{ax,n-1\rightarrow n} - \dot{Q}_{ax,n\rightarrow n+1})\Delta t = (Mc_p\Delta T)_{PEN} \tag{3.37}$$

The terms accounting for energy exchange between PEN structure and channels have already been presented with equations (3.20), (3.21) and (3.22). The term $\dot{H}_{a\rightarrow PEN}$ is only made up by oxygen entering the PEN structure from the air channel.

$$\dot{H}_{a\rightarrow PEN} = \frac{\dot{n}_{H_2,f\rightarrow PEN} + \dot{n}_{CO,f\rightarrow PEN}}{2} h_{O_2}(\overline{T}_a) \tag{3.38}$$

The heat exchange between the PEN structure and the interconnetion in a certain CV is evaluated by using the transversal thermal resistance of equation (2.29):

$$\dot{Q}_{PEN\rightarrow int} = \frac{T_{PEN} - T_{int}}{R_{trans}} \tag{3.39}$$

Finally, The axial conduction heat is computed by making use of the thermal resistances explained in section 2.2.2.

$$\dot{Q}_{ax,n-1\rightarrow n} = \frac{T_{PEN,n-1} - T_{PEN,n}}{R_{PEN,n-1,n}} \tag{3.40}$$

An analogous equation is used between n and $n+1$. All the variables used are averaged in the time step as done up to now. The only exception is made for the temperatures appearing in the axial conduction, which can limit the accuracy of the simulation with high time steps. The reason for doing that is readily explained. Considering a the n^{th} CV in the middle of the channel one could easily consider that:

$$\overline{T}_{PEN,n-1} = \frac{T_{PEN,n-1,t} + T_{PEN,n-1,t+\Delta t}}{2} \tag{3.41}$$

This can theoretically be done because the $(n-1)^{th}$ CV has just been solved. Likewise, one can use the averaged PEN temperature of the considered CV, as done with equation (3.30). The problem is that the temperature of the $(n+1)^{th}$ CV cannot be averaged, because neither it has been already solved or it is being solved. Therefore, when solving the $(n+1)^{th}$ CV one cannot use its averaged temperature because it was not used when solving the n^{th} CV. The reason is that the energy exiting a CV during the time step should entirely go to the adjacent one to avoid unphysical energy generation or destruction, thus neither the averaged PEN temperature of the CV which is being solved can be used. Terefore, one may think of using just the previous CV averaged temperature to increase the accuracy of the simulation (or to allow higher time steps). The problem is that if the n^{th} CV cannot use its own averaged temperature, the $(n+1)^{th}$ CV solution must not use the n^{th} CV averaged temperature as well, for the energy unbalance problem just explained.

Thus, with the actual implementation of the channel solution, it is not possible to time-average the temperatures involved in axial conduction calculations. A possible solution to that could be to solve the channel altogether to better account for CVs interactions. A problem that may arise with the implementation of this solution are the troubles that the non-linear solver may encounter in solving a system larger by a factor

N_{CVs}, which can be of the order 10^2.

The fact that the axial conduction temperatures are not time-averaged may give other problems. For instance, if PEN or interconnection temperatures of two adjacent CVs are too close, each of those temperatures would be likely to oscillate over time. Indeed, at time t the colder CV gets heat from the hotter one, possibly raising its temperature above the adjacent one. At the next time step the opposite happens and so on. This may happen as the exchanged heat should get lower if the temperatures approach each other during the time step, this would be the case if temperatures were averaged. Usually at the cell inlet the CVs should be little compared with the outlet ones, because of higher gradients. Thus, to avoid space variable oscillation at the beginning, little CVs should be present. This may give problems of time oscillation because the CVs temperatures are very close to each other, and the problem explained above may arise. The solution to that is putting a tiny CV before the others (which can be larger), to smooth the spacial variations of variables. Therefore, spacial and time oscillation can be avoided.

Finally, the right-hand term of equation (3.37) has to be considered in deeper detail. The mass of the PEN structure is computed with the following equations:

$$M_{PEN} = \rho_{PEN} \cdot V_{PEN} \tag{3.42}$$

$$V_{PEN} = A \cdot t_{PEN} = L_{CV} \cdot (W + 2 \cdot t_{int}) \cdot (t_{an} + t_{cat} + t_{elec}) \tag{3.43}$$

Thus the term ρ_{PEN} is computed by calculating the mass contained in V_{PEN}. To do that, values for anode, cathode and electrolyte densities have been taken from the literature and the following equations have been applied:

$$\rho_{PEN} = \frac{t_{an}(1-\epsilon_{an})\rho_{an} + t_{cat}(1-\epsilon_{cat})\rho_{cat} + t_{elec}\rho_{elec}}{t_{PEN}} \tag{3.44}$$

Where ϵ is the porosity, and the area A has been simplified as it was common term. Likewise, the specific heat of the PEN structure is computed starting from specific heat of anode, cathode and electrolyte:

$$c_{p,PEN} = \frac{c_{p,an}\, t_{an}(1-\epsilon_{an})\rho_{an} + c_{p,cat}\, t_{cat}(1-\epsilon_{cat})\rho_{cat} + c_{p,elec}\, t_{elec}\rho_{elec}}{\rho_{PEN} \cdot t_{PEN}} \tag{3.45}$$

Where the area A has been again simplified since it was a common factor. The actual values of anode, cathode and electrolyte specific heat and density have been taken from the literature. Specifically, the values found in the following references, valid for high temperature SOFC, have been averaged [21][22][23][24][25][26]. Thus the resulting figures are:

Parameter	Value	Unit
ρ_{an}	5300	$\frac{kg}{m^3}$
$c_{p,an}$	550	$\frac{J}{kg \cdot K}$
ρ_{cat}	5025	$\frac{kg}{m^3}$
$c_{p,cat}$	530	$\frac{J}{kg \cdot K}$
ρ_{elec}	5675	$\frac{kg}{m^3}$
$c_{p,elec}$	550	$\frac{J}{kg \cdot K}$

Interconnection energy balance

The discretized equation which governs the temperature variation of the interconnection is the following:

$$(\dot{Q}_{PEN \rightarrow int} + \dot{Q}_{ax,n-1 \rightarrow n} - \dot{Q}_{ax,n \rightarrow n+1} - \dot{Q}_{loss})\Delta t = (Mc_p \Delta T)_{int} \tag{3.46}$$

$$\dot{Q}_{loss} = 4 \cdot q_{loss} \cdot L_{CV} \cdot H \cdot H_{int} \tag{3.47}$$

The term $\dot{Q}_{PEN \rightarrow int}$ is the same of equation (3.39). The axial terms are different from the ones seen in the PEN balance, but all it was said can be directly applied to this case using interconnection temperatures and thermal resistance. The axial thermal resistance is the one of equation (2.27).

The heat loss term has been already explained in section 2.2.2, and it just depends on the exposed surface of the CV. Equation (3.46) applies as it is just in the case one is simulating one channel. If 2 channels are simulated, the term $\dot{Q}_{loss}$ present in each channel interconnection balance would be half compared to the one-channel case. That is because the exposed surface of each channel is less. Moreover, the balance equation of the two channels would have one more component, because of the channels interconnections heat exchange. The resistance used to evaluate this heat exchange is the one of equation (2.30).

$$\dot{Q}_{ch1\rightarrow ch2} = \frac{T_{int,ch1} - T_{int,ch2}}{R_{int,ch}} \tag{3.48}$$

When more than a channel is simulated, the correspondent CVs of the different channels are solved together to account of this heat exchange. The interconnection temperatures of all channels are averaged in the time step as in equation (3.31).

Moreover, in the first and last CVs of each channel a loss as the one of equation (2.50) is added. If more than one channel is simulated, then the middle channels does not present the heat loss term in their balance, but they do have heat exchange with adjacent channels interconnections in both sides.

The averaging process to find density and specific heat of the interconnection has been performed, and the following are the results:

Parameter	Value	Unit
ρ_{int}	5515	$\frac{kg}{m^3}$
$c_{p,int}$	525	$\frac{J}{kg \cdot K}$

3.2.4 Equations of state

Considering the above sections, the non-linear system is now composed by 20 unknown variables and 18 equations for each channel. Thus 2 equations are missing, those are the equations of state at the outlet of the considered CV at the end of the time step.

$$p_{f,out,t+\Delta t} = R(CT)_{f,out,t+\Delta t} \tag{3.49}$$

$$p_{a,out,t+\Delta t} = R(CT)_{a,out,t+\Delta t} \tag{3.50}$$

Where the outlet total concentrations of both the fuel and air streams are found as the summation of the respective species concentrations, as stated by equation (3.34).

Chapter 4

Results and discussion

In this chapter the validation, results and discussion of the models proposed in the last two chapter will be presented. The stationary and dynamic models will be evaluated separately. Unfortunately, the literature lacks of suitable works to make a comparison for the carbon monoxide electroxidation and the dynamic model. Thus, the validation of those models will just show the physical consistency and validity of the results.

4.1 Stationary model validation

After all the changes explained in the first chapter, the validation of the stationary model general functioning is thought to be appropriate. An already validated code will be used for that. This same code will also be used to check the axial conduction implementation. After that, the discussion on the validity of the CO electroxidation model will be presented.

4.1.1 General validation of the code

A code at which the access was made available has been used to validate the stationary results of the code. The reference code was used to write several work in the past, thus it is believed to be established and well-validated. The aim of the validation is to reproduce the results of the reference code, using the same input parameters and models. The details of the electrochemical, chemical and heat exchange model implemented in the reference code are explained in the first part of reference [4]. The chemical and electrochemical models have been introduced in the actual code to reproduce the reference code results.

At the moment, the relevant differences with the reference code are: the fact that in the new code each channel CV has just one interconnection temperature, and the enthalpy linearization of the reference code. As explained in section 2.2.2, in the new code the enthalpy of a species is computed with a high-grade polynomial expression.

The input values of the simulation are the ones presented in the second part of reference [4] (tables 1 and 4), apart from the fact that just one channel is simulated and the *heat loss is set to zero* (both in the actual and in the reference code). This is done to avoid discrepancies due to the eventual different exposed surface. As a matter of fact, it has been difficult to understand where the heat loss was applied in the reference code. Moreover, note that without heat loss the number of channels is not really important. In the following tables the parameters and input values of the simulation are summarized.

Parameter	Value	Unit
Anode thickness	$50{\cdot}10^{-6}$	[m]
Cathode thickness	$50{\cdot}10^{-6}$	[m]
Electrolyte thickness	$150{\cdot}10^{-6}$	[m]
channel active area	5.56 x 100	[mm]
Pore diameter of anode	$1 \cdot 10^{-6}$	[m]
Pore diameter of cathode	$1{\cdot}10^{-6}$	[m]
Porosity of anode	50	[%]
Porosity of cathode	50	[%]
Tortuosity of anode	3.0	[-]
Tortuosity of cathode	3.0	[-]
L1	1.28	[mm]
L2	3.0	[mm]
L3	1.28	[mm]
L4	2.5	[mm]
L5	1.0	[mm]

Table 4.1: *Geometrical parameters of fuel and air channels*

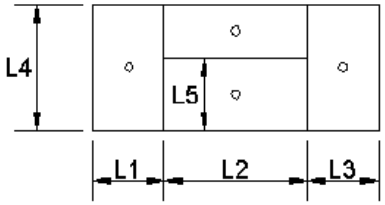

Figure 4.1: *Channels schematisation [4]*

The electric and thermal conductivities used to computed the resistances of sections 2.2.2 and 2.3.2 are reported in the following table.

Parameter	Value	Unit
Specific resistivity anode	$1 \,/\, [9.5{\cdot}10^7 / T_{PEN} \exp(-1150/T_{PEN})]$	[Ωm]
Specific resistivity cathode	$1 \,/\, [4.2{\cdot}10^7 / T_{PEN} \exp(-1200/T_{PEN})]$	[Ωm]
Specific resistivity electrolyte	$1 \,/\, [3.34{\cdot}10^4 \exp(-10300/T_{PEN})]$	[Ωm]
Specific resistivity interconnection	$1 \,/\, [9.3{\cdot}10^6 / T_{PEN} \exp(-1100/T_{PEN})]$	[Ωm]
Conductivity of anode	2.0	$[\mathrm{W\,m^{-1}K^{-1}}]$
Conductivity of cathode	2.0	$[\mathrm{W\,m^{-1}K^{-1}}]$
Conductivity of electrolyte	2.0	$[\mathrm{W\,m^{-1}K^{-1}}]$
Conductivity of interconnect	2.0	$[\mathrm{W\,m^{-1}K^{-1}}]$

Table 4.2: *Materials properties*

The chemical model substantially refers to the method used to compute the MSR and WGS rates. The WGS is supposed to be at equilibrium throughout the channel, thus its rate is computed with the model explained in section 2.3.5. On the other hand, the MSR rate is computed via the following equation [4]:

$$r_{MSR}[\frac{mol}{s}] = K_r \cdot (\frac{P_{CH_4}}{P_{ref}})^{\alpha} \cdot (\frac{P_{H_2O}}{P_{ref}})^{\beta} \cdot \exp(-\frac{E_{CH_4}}{RT_f}) \cdot A_n \tag{4.1}$$

$$A_n = L_{CV} \cdot (W + 2 \cdot t_{int}) \tag{4.2}$$

Parameter	Value	Unit
E_{CH_4}	82	[kJ mol^{-1}]
coefficient α	1.0	[-]
coefficient β	0.0	[-]
coefficient K_r	4274	[mol m$^{-2}s^{-1}$]

Table 4.3: *MSR rate parameters*

Note that in the present model, the electrochemically and chemically active surfaces are equal and equivalent to the PEN geometrical surface. The electrochemical model uses the usual equations (2.74) and (2.75) to compute the concentration losses, whilst the anodic and cathodic activation overpotentials are evaluated with the following Butler-Volmer equations [4]:

$$i_{H_2} = i_{0,H_2} \cdot \{\exp(\beta \frac{n_{e,H_2} F \eta_{act,H_2}}{RT}) - \exp[(1-\beta)\frac{n_{e,H_2} F \eta_{act,H_2}}{RT}]\} \tag{4.3}$$

$$i_{0,H_2} = \gamma_{an} (\frac{p_{H_2}}{p_{ref}})(\frac{p_{H_2O}}{p_{ref}}) \exp(-\frac{E_{act,an}}{RT}) \tag{4.4}$$

$$i_{O_2} = i_{0,O_2} \cdot \{\exp(\beta \frac{n_{e,O_2} F \eta_{act,O_2}}{RT}) - \exp[(1-\beta)\frac{n_{e,O_2} F \eta_{act,O_2}}{RT}]\} \tag{4.5}$$

$$i_{0,O_2} = \gamma_{cat} (\frac{p_{O_2}}{p_{ref}})^{0.25} \exp(-\frac{E_{act,cat}}{RT}) \tag{4.6}$$

Parameter	Value	Unit
$E_{act,an}$	100	[kJmol^{-1}]
$E_{act,cat}$	117	[kJmol^{-1}]
γ_{an}	5.5·10^8	[A m^{-2}]
γ_{cat}	7·10^8	[A m^{-2}]
n_{e,H_2}	2	[-]
n_{e,O_2}	2	[-]
β	0.34657	[-]

Table 4.4: *Kinetic parameters of electrochemical reactions*

Actually, in order to get as close as possible to the results produced by the reference code, the approximated relations for the activation overpotential will be used. The difference with using the complete equations is small, but still it can be detected.

$$\eta_{act} = \frac{RTi}{nFi_0} \tag{4.7}$$

$$\eta_{act} = \frac{RT}{nF\beta}\ln(\frac{i}{i_0}) \tag{4.8}$$

The former equation is used when low electrode polarization occurs, namely when $\eta_{act} < \frac{2RT}{F}$. On the other hand, with high polarization the second equation is employed. The parameter β has been selected to guarantee the continuity of the function $\eta_{act}(i)$ defined by equations (4.7) and (4.8). Eventually, the following are the general operating conditions:

Parameter	Value	Unit
Pressure	1	[atm]
Fuel mass flow	$1.17298{\cdot}10^{-4}$	[g s^{-1}]
Air mass flow	$3.1659{\cdot}10^{-3}$	[g s^{-1}]
Cell Potential	0.7	[V]
Inlet fuel temperature	900	[$^{\circ}C$]
Inlet air temperature	900	[$^{\circ}C$]
Heat loss at cell periphery	0.0	[W m^{-2}]
Fuel Nusselt number	3.6	[-]
Air Nusselt number	5.0	[-]
H_2	0.2626	[-]
H_2O	0.4934	[-]
CO	0.0294	[-]
CO2	0.0436	[-]
CH4	0.171	[-]

Table 4.5: *Operating conditions and inlet flows characteristics*

The first thing to be checked has been the implementation of the axial conduction. To do that, a comparison between the two codes with and without axial conduction has been performed. The actual results are not important now, also because the reference

code simulation has not been run in the grid-independency region. What is important is the impact that introducing the axial conduction has on the results.

reference code	ax off	ax on
$\eta_{el,LHV}$ [%]	56.08	56.98
Power [W]	0.886	0.9
U_f [%]	85.36	86.74
U_{ox} [%]	14.23	14.46
i $[\frac{A}{m^2}]$	2274	2311

Table 4.6: *Axial conduction effect on the reference code*

new code	ax off	ax on
$\eta_{el,LHV}$ [%]	54.54	55.60
Power [W]	0.8974	0.9148
U_f [%]	86.49	88.16
U_{ox} [%]	14.41	14.69
i $[\frac{A}{m^2}]$	2306	2350

Table 4.7: *Axial conduction effect on the new code*

The entity of the performance improvement is totally similar in the two cases, thus axial conduction is believed to be implemented correctly. This improvement is probably due to the higher temperatures at the inlet, which busts the electrochemical performance of the hydrogen-rich part of the channel.

Finally, axial conduction has been switched-on and the results of the two codes have been compared. After a lot of investigation and comparison of the two codes, some inaccuracies have been found in both. For instance, the porous diffusion coefficient in the new code has been discovered to be wrong, as explained in section 2.3.2. On the other hand, also in the reference code a couple of inaccuracies have been found. For instance, the current in equations (2.76) - (2.79) was not specific to the active area, which implied a practically null concentration loss. After correcting those discrepancies and using an adequate number of CVs to reach the grid-independency in both codes, the matching of the results has been satisfying:

	reference	new code
$\eta_{el,LHV}$[%]	56.15	55.60
Power [W]	0.9236	0.9148
U_f[%]	89.01	88.16
U_{ox}[%]	14.84	14.69
i [$\frac{A}{m^2}$]	2373	2350
$T_{max,PEN}[^\circ C]$	1028	1023

Table 4.8: *Final result of the validation*

The intrinsic differences between the codes, such as the different treatment of the interconnection, justifies the mismatch of the results. Thus the general functioning of the code is now believed to be alright. Moreover, the electric efficiency computed using the complete Butler-Volmer equations would be 55.30%. Therefore, the approximated equations could be used to speed up the simulation. Actually, the non-linear solver used to solve the electrochemical system of equations does not benefit so much from the use of the approximated equations, in terms of required computational time. Nevertheless, equations (4.7) and (4.8) would allow to use a more efficient IMSL function to solve the system, the one which finds the zero of a function. This would be possible as all the involved voltage losses could be written as a function of the current density. This would very likely speed up the simulation and improve the overall code efficiency. Finally, figures showing the distribution of some variables of interest are available in section 4.3, as stationary results of the dynamic simulation.

4.1.2 CO electroxidation

The majority of the SOFC models available in the literature do not account for carbon monoxide oxidation. The reason is that WGS reaction is supposed to be so fast to readily convert the available carbon monoxide into hydrogen, so that the oxidation proceeds via hydrogen electroxidation. As a matter of fact, WGS is often considered to be at equilibrium throughout the channel length, as explained in section 2.3.5. Thus, it is hard to find a reliable and complete model to make a comparison of results. Moreover, the results of the works present in the literature can even do not match at all [5][27].

The Butler-Volmer equations used in reference [6] have been employed in their

whole form, together with the model explained in section 2.3.3. Unfortunately, this work is not suitable to be used for comparing, since it models a cross-flow configuration. The first step is to simulate the same case of section 4.1.1 (same models and input parameters, axial conduction switched on) with *CO* electroxidation switched-off, using the hydrogen elctrochemistry of reference [6]. This is done to check the consistency of hydrogen and oxygen elctrochemical models. The following are the results of the simulation.

CO off	[6]	[4]
η_{el}[%]	55.78	55.30
U_f[%]	88.45	87.69
U_{ox}[%]	14.74	14.62
i [$\frac{A}{m^2}$]	2358	2338

Table 4.9: *Comparison between hydrogen and oxygen elctrochemistry of [4] and [6]*

Therefore, one concludes that oxygen and hydrogen electrochemistry of reference [6] is reliable, as the results are not sensibly different from the ones obtained in the previous validation. On the other hand, activating the carbon monoxide oxidation gives the following results:

WGS eq	CO off	CO on
η_{el}[%]	55.78	55.92
U_f[%]	88.45	88.68
U_{ox}[%]	14.74	14.78
i [$\frac{A}{m^2}$]	2358	2364

Table 4.10: *Results with and without CO oxidation, with WGS at equilibrium*

The performance gets better as expected. The improvement is not very high because of the low content of carbon monoxide, thus the model behaves as expected until now. Another reason which justifies the little improvement may be related to the hypothesis made on WGS reaction, which has been considered to be at equilibrium. It is trivial that the faster the WGS kinetics, the lower the incidence that would have introducing carbon monoxide oxidation. Therefore, the WGS rate is now lowered by setting $\frac{Kp}{Keq} = 0.8$ as explained in section 2.3.5.

WGS 0.8	CO off	CO on
η_{el}[%]	55.28	55.50
U_f[%]	87.66	88.00
U_{ox}[%]	14.61	14.67
i [$\frac{A}{m^2}$]	2337	2346

Table 4.11: *Results with and without CO oxidation, with almost equilibrated WGS*

The results generally do not change much, meaning that considering the WGS always at equilibrium may be a good approximation. However, it is important to note that the performance of the case without *CO* oxidation has worsened more. Therefore, the WGS rate is now further increased by setting $\frac{Kp}{Keq} = 0.6$. One expects that the only-hydrogen case would be the more penalized again.

WGS 0.6	CO off	CO on
η_{el}[%]	54.54	54.86
U_f[%]	86.48	87.00
U_{ox}[%]	14.41	14.50
i [$\frac{A}{m^2}$]	2306	2319

Table 4.12: *Results with and without CO oxidation, with WGS not at equilibrium*

The trend of the only-hydrogen case is confirmed, as its performance keeps being the more penalized. On the other hand, considering carbon monoxide as an active species attenuates the impact of WGS rate on the solution (as expected). This conclusion means that considering the carbon monoxide oxidation is likely to make the solution less prone to be affected by the WGS model, which has been seen not to be really studied in the literature.

The model behaves as expected, predicting a little improvement with respect to the only-hydrogen case when the input *CO* is low, and increasing that improvement when making the WGS reaction slower.

The last check is concerned with the energy balance (2.102), which takes the form of a voltage balance. The balance is referred to the overall current (which simplifies), for this reason it is not very intuitive as far as activation loss is concerned. Thus, the

following energy balance check is performed in the CVs. The maximum work which can be extracted is:

$$V_{rev,H2} i_{H_2} + V_{rev,CO} i_{CO} \tag{4.9}$$

Which must be equal to the actual work extracted plus the loss terms.

$$(V_{cell} + \eta_{ohm} + \eta_{act,O_2} + \eta_{conc,O_2}) i_{tot} + (\eta_{act,H_2} + \eta_{conc,H_2}) i_{H_2} + (\eta_{act,CO} + \eta_{conc,CO}) i_{CO} \tag{4.10}$$

The relative difference between (4.9) and (4.10) is always lower than 10^{-14}, thus the model gives energy-consistent results.

4.2 Low temperature model validation

Unfortunately, it is rather difficult if not impossible to find in the literature complete models of well-functioning low temperature cells. One of the main problems is the development of an anode capable of performing at low temperature while catalyzing both chemical and electrochemical reactions. The model proposed in section 2.4 does not get into the detail of species transport inside the electrolyte, thus it is necessary to understand whether it can produce results in a realistic way. To do that, the model will try to reproduce the polarization curves of reference [7]. The cited article considers a button cell with SDC as electrolyte, producing polarization curves for various hydrogen concentrations. The cathode is commericial, made by LSCF-GDC thus it is expected to perform well. On the other hand, the Cu-Pd-CZ80 anode performance has been investigated, and it has been discovered that it actually limits the cell performance.

The model is not generally capable of simulating an isothermal button cell, but still one can use the electrochemical non-linear solver to solve the button cell set of equations together with the assumption to have just one constant temperature. First of all, the assumption on the electrode loss should be checked. Thus, the following graphs show the comparison between the reference and the model under different operating condition and electrodes ohmic loss assumptions. These assumption are:

- Only electronic loss: assumption of electrochemical reactions occuring just at electrode/eletrolyte interface. This is equivalent to assuming that just electric

current (the drawn current) flows in the electrodes, with no ionic loss. This has been seen to be almost equal to setting null electrode loss (low electronic loss).

- Null anodic ionic loss: the above assumption applies just within the anode (remember that its ionic conductivity was not really available). In the cathode the assumption of linear ionic and electronic currents has been made.
- Linear currents: linear electronic and ionic currents in both electrodes. The electrolyte ionic conductivity and the anode one are assumed to be equal.

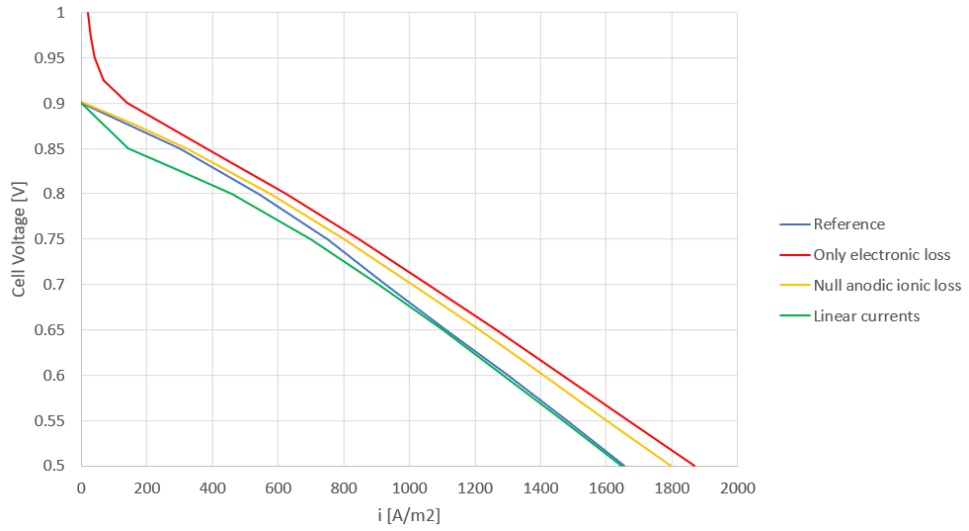

Figure 4.2: *Electrodes loss assumption effect. 97% H_2, 3% H_2O, 650°C*

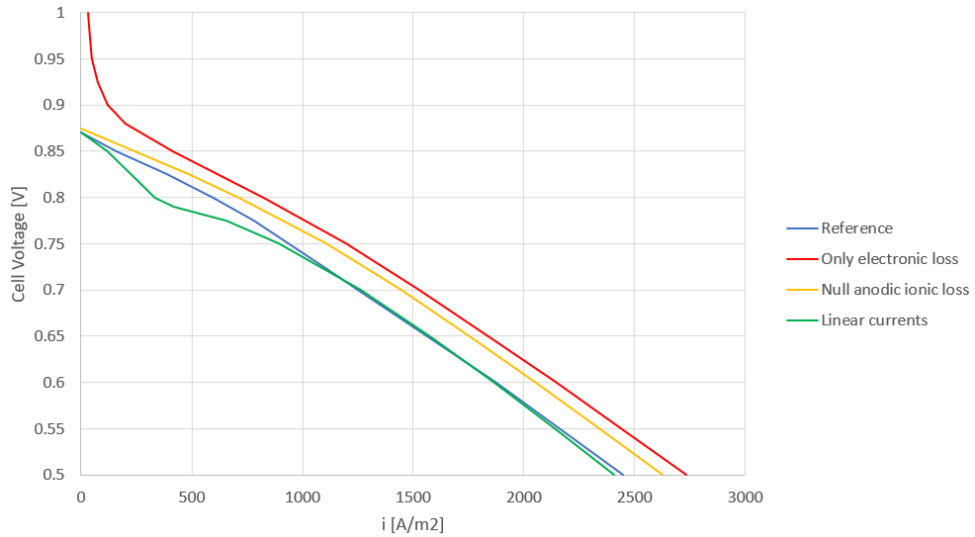

Figure 4.3: *Electrodes loss assumption effect. 100% H_2, 700°C*

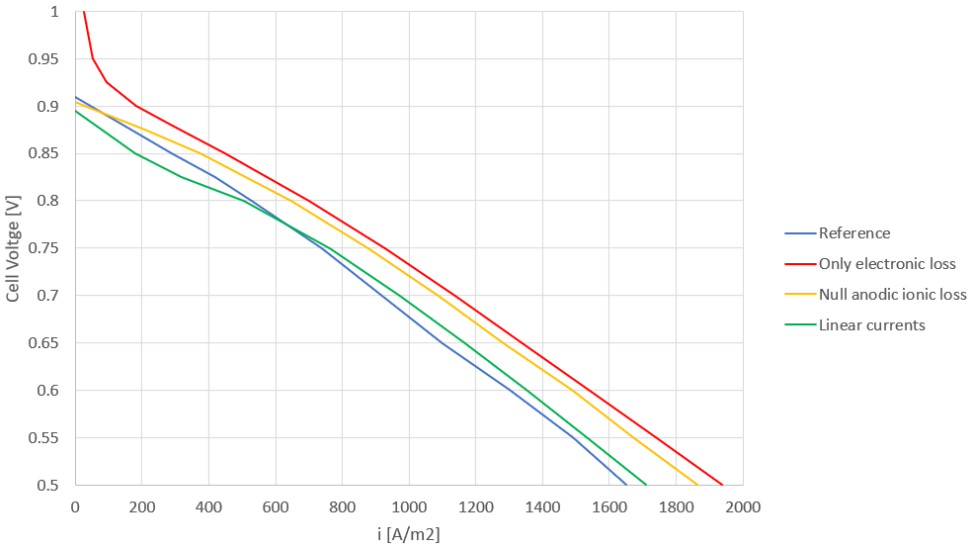

Figure 4.4: *Electrodes loss assumption effect. 100% H_2, 650°C*

One can see that the assumption used for high temperature SOFC simulation of electrochemical reactions occurring just at the electrode/electrolyte interface does not seem to be very realistic. The red curve is the further from the reference one, plus near the OCV it diverges, whereas all the other curves actually get to the zero-current point at a reasonable voltage. This suggests that it is really important to evaluate the electrodes ionic loss at the OCV point. For instance the following is a possible current distribution at OCV:

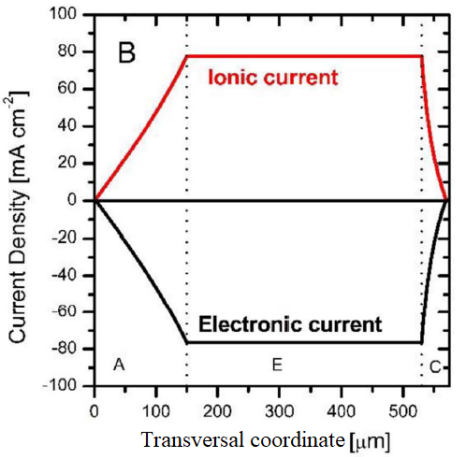

Figure 4.5: *Ionic and electronic currents at OCV point [7]*

The ionic current within the electrodes assumes values ranging between 0 and 800 $\frac{A}{m^2}$, thus it is not negligible. Terefore, the electrodes ionic loss should somehow be

considered, as in the green and yellow curves of figures 4.2 - 4.4. In general, it seems that considering the ohmic ionic loss in both electrodes gives the best matching with the reference. Nevertheless, the correspondent curves always show some instabilities, this may due to the assumption on the anodic ionic conductivity. Probably, the best assumption until now is to consider the ionic loss just in the cathode, as it does not diverge and it gets closer to the reference compared with the red curve. Plus it does not show any instability as the green one. A possible solution which may tackle the mismatch, instability and divergence problems once and for all would be to discretize the electrodes solving the charge-transport equations. Thus, the ionic and electronic current distributions would be known, and more accurate results may be given by the model.

Finally, the following figures, show the capability of the code to catch the effects of temperature and fuel composition variations. The comparison will be made between the reference and the model which considers ionic ohmic loss just within the cathode, since it is thought to be the more reliable one. Nevertheless, the conclusions upon the capability of reproducing temperature and fuel composition variations can be extended to the other elctrode loss models, thus it is a general feature of the model itself.

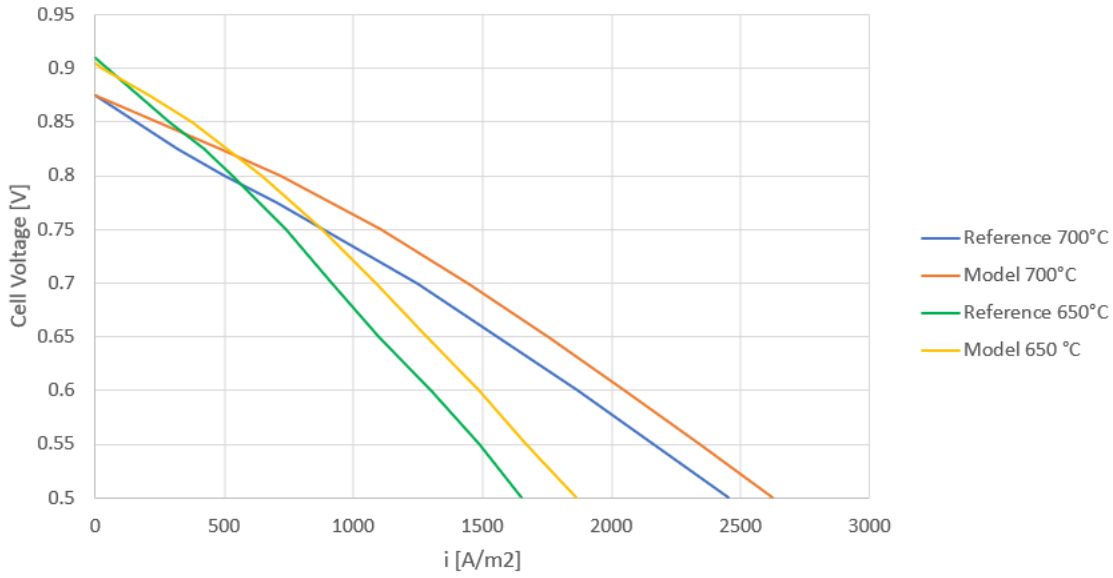

Figure 4.6: *Temperature effect, 100% H_2*

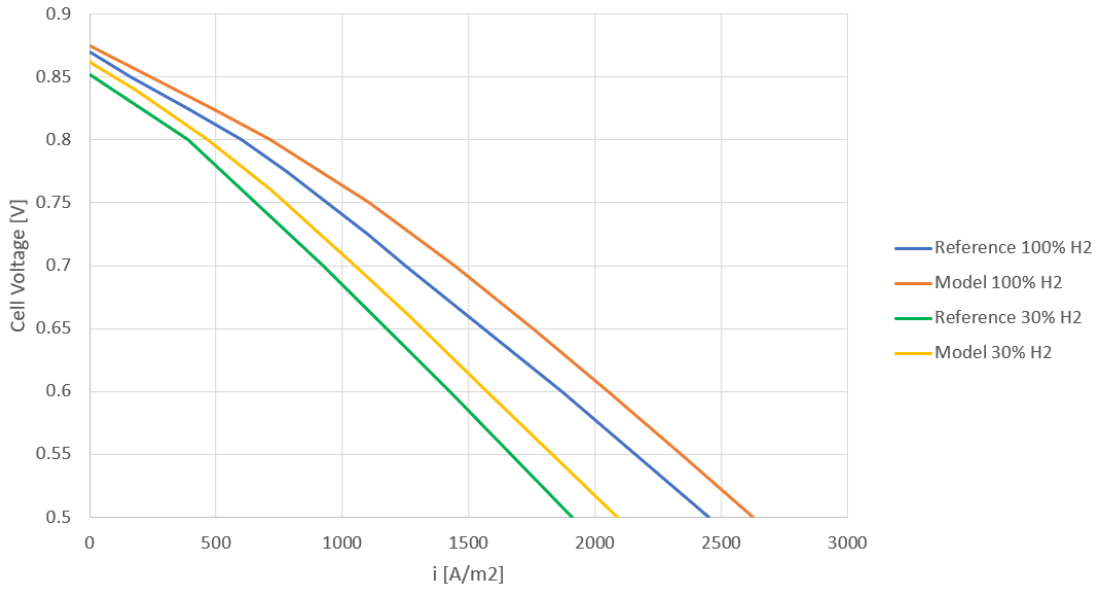

Figure 4.7: *Hydrogen concentration effect, 700°C*

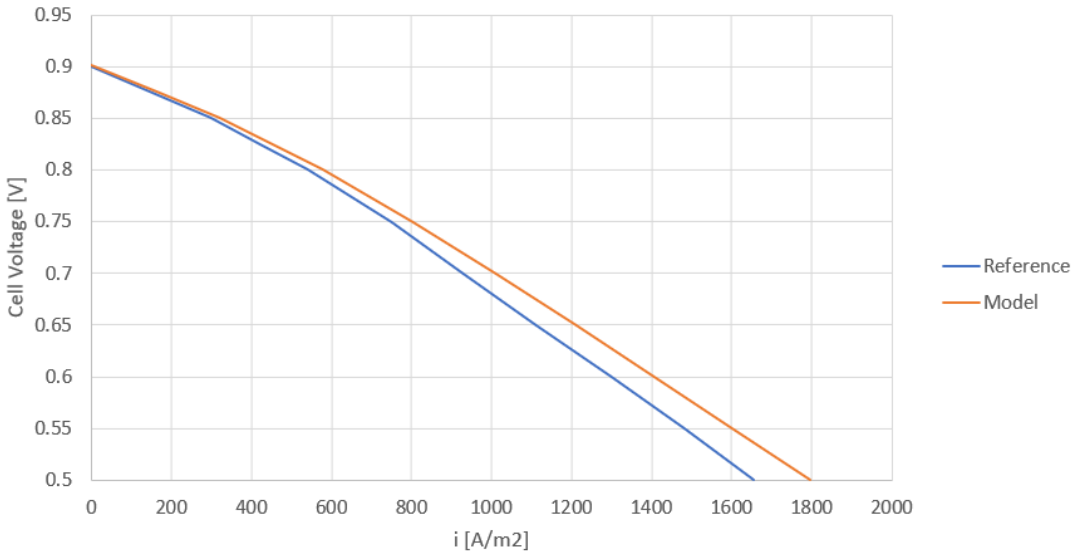

Figure 4.8: *Fuel composition effect, 97% H_2, 3% H_2O, 650°C*

The above figures show how temperature and fuel composition effects can be well accounted by the model. As said above, this conclusion does not depend on electrodes ohmic loss assumption. Nevertheless, the actual mismatch between model and reference is not negligible, thus a detailed model of charge transport within the electrodes may be really beneficial.

4.3 Dynamic simulation

To check the consistency of the dynamic model the results obtained at the end of a transient simulation will be compared with the ones obtained from the simple stationary model. Obviously, the results should closely match each other. For the sake of simplicity, the input geometry, the boundary conditions, and the models used in section 4.1.1 will be employed. The final stationary condition should then be the same one as in table 4.8. During the transient simulation, the complete Butler-Volmer equations have been used instead of equations (4.7) and (4.8).

In the following figures, the distribution along the channel of some variables of interest through the simulation is shown. The distribution is recorded every 500s, until the stationary condition is reached. As expected, the composition distribution transient is the quicker one, almost stop changing after about 2000s. The current density distribution almost reaches the stationary distribution after about 3000s. As expected, the thermal transient is the longest one, lasting more than 4000s.

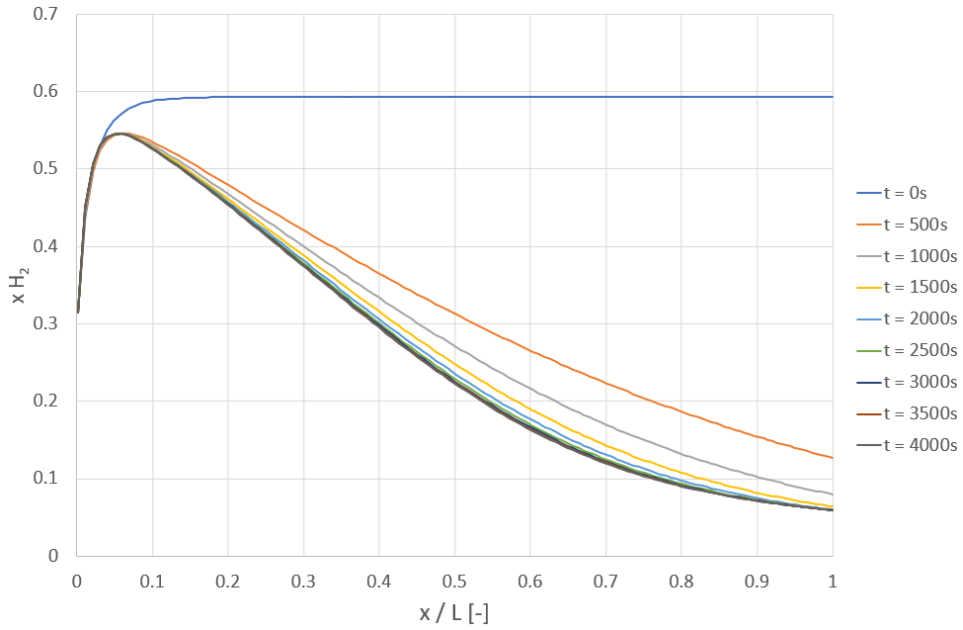

Figure 4.9: *Hydrogen molar fraction distribution throughout the simulation*

The distribution of hydrogen grows until about 10% of the channel because of the rapid steam reforming kinetic. This kind of hydrogen molar fraction distribution using a methane-rich fuel is also confirmed by graphs shown at the end of reference [4].

Moreover, in reference [13] it is claimed that methane is generally consumed in the very first part of the channel in high-temperature SOFCs, which is what happens here. At $t = 0$, when the fuel runs out of methane, the hydrogen composition stop changing. During the simulation, the molar fraction in the part of the channel where methane is not present drops sensibly until stationary condition is reached. This is obviously due to hydrogen electrochemical oxidation.

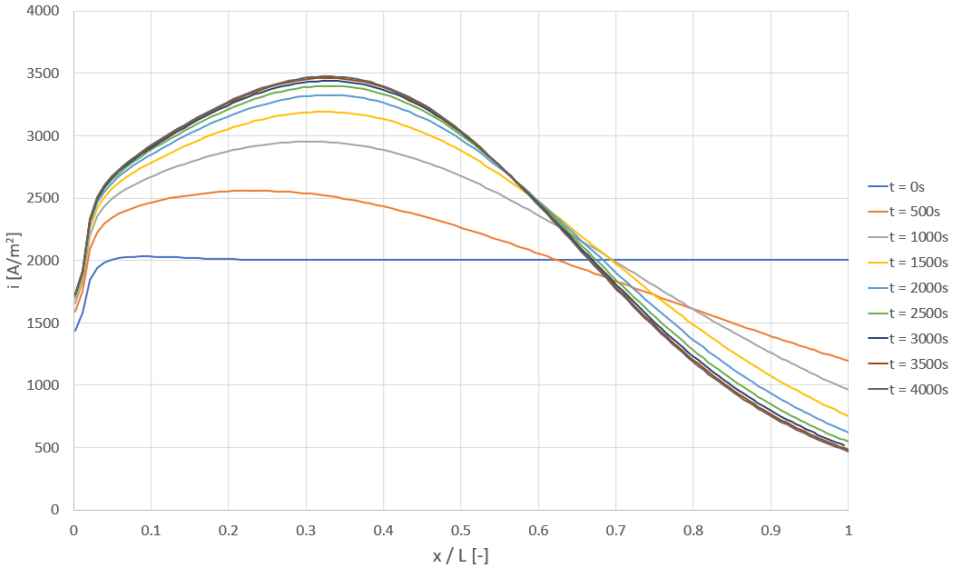

Figure 4.10: *Current density distribution throughout the simulation*

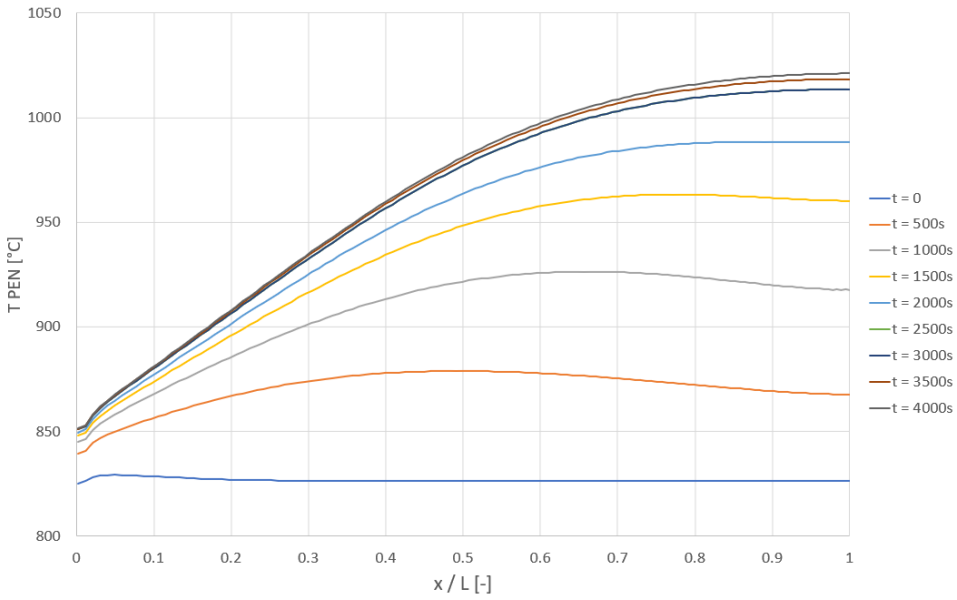

Figure 4.11: *PEN temperature distribution throughout the simulation*

The initial distribution of current density (right after the voltage step from OCV condition to 0.7 V) is plain throughout the cell except from the very beginning, where it is sensibly lower. The steep current increase at the inlet is actually a common feature to all the current distributions recorded in the simulation. The current is generally higher where the temperature and the presence of hydrogen is larger. The temperature increase at the inlet of the cell does not justify the rapid current increase, thus it must be due to the rapid increase of hydrogen molar fraction due to steam reforming. Nevertheless, the maximum of the current density occur considerably after the hydrogen molar fraction one. This may due to temperature, which generally increases along the channel. This is confirmed by the fact that the current maximum keeps moving towards the end of the channel and to grow in value, even if the hydrogen molar fraction drops and remains constant after a while. This is because of the continuous spacial temperature gradient increase, which determines higher temperatures far from the channel inlet. Nevertheless, after the plateau the current sensibly decreases, this must be due to the lower hydrogen concentration, since the temperatures are generally the highest. Moreover, thanks to the general temperature increase, the mean current density tends to grow throughout the simulation:

t [s]	i [$\frac{A}{m^2}$]
0	1998
500	2076
1000	2282
1500	2350
2000	2364
2500	2364
3000	2362
3500	2360
4000	2359

The above results seem physically realistic. Another check can be done verifying the consistency between the results of the stationary model and the dynamic model ones which has reached the stationary condition: the variables profiles should perfectly match. For instance, this is the current profile computed with both models:

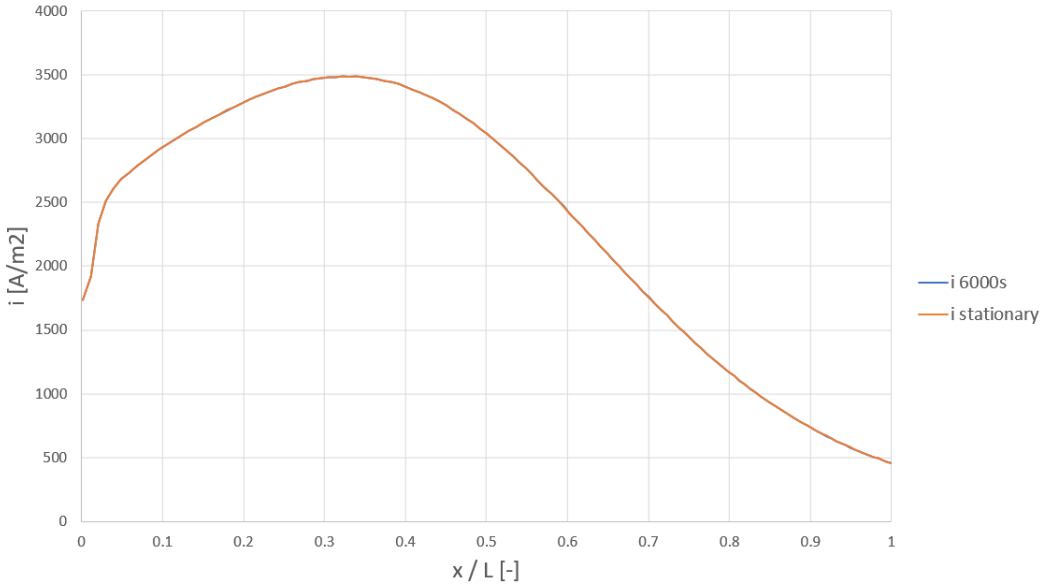

Figure 4.12: *Comparison between current profile at 6000s and the the stationary one*

The matching is flawless, thus the two models are consistent. It is not necesseary to show the PEN temperature profile along with the hydrogen molar fraction as the current is dependent from these two variables, as said above.

Chapter 5

Conclusions

An existing SOFC stationary model capable of simulating a co-flow configuration has been revised and extended to run dynamic simulations. The revision process has been really time-consuming, but it brought major benefits regarding the efficiency point of view, the correctness of the models used, and the updating of the code as a whole.

The general efficiency of the code has been deeply improved as in the future it will be integrated in a wider program to simulate advanced power cycles. The required computational time has become 20-200 times lower, depending on the type of simulation run. Nevertheless, there is still margin for improvement, for instance by refining the algorithm for axial conduction iterations.

Axial conduction was not accounted in the initial version of the code, thus an iterative method has been added to account for it (the user can choose whether to consider it or not). The validation of the method implemented has been performed by comparison with an already validated code, the outcome of the validation has been rather satisfactory.

Two new electrochemical models have been added within the code, regarding carbon monoxide electrochemical oxidation and low temperature SOFC operation. The former has the characteristic of defining a single reversible voltage, from which the voltage losses has to be subtracted. Its validation with literature works was not really possible, thus the validation has been limited to show its results alignment with expectations. For instance it showed little difference with the case of only active hydrogen

when CO content in the fuel was limited. Moreover, a lower WGS rate penalized the performance of the case with CO oxidation less than the other one, as expected.

The Macro-scale low temperature model polarization curves has been compared against the ones of a literature work. The matching achieved was good if one did not consider the ionic ohmic losses within the anode (whose ionic conductivity was not really known). Thus, a possible code development in the future would be to solve the charge conservation equations within the electrodes, which would likely enhance the model accuracy and stability.

Finally, a dynamic model capable of simulating the transient after the load connection starting from the hot cell has been implemented. Nevertheless, the model can be easily adapted to simulate other kind of transients. Suitable literature work to make a validation has not been found, thus it has just been shown that the model gives physically realistic results consistent with the stationary model ones.

Nomenclature

Acronyms

CV Control Volume

LHV Lower Heating Value

MIEC Mixed Ionic and Electronic Conducting (material)

MSR Methane Steam Reforming

OCV Open Circuit Voltage

PEN Positive-Electrolyte-Negative

SOFC Solid Oxide Fuel Cell

WGS Water Gas Shift

Physical constants

F Faraday's constant 96487 [C mol^{-1}]

R Universal gas constant 8.314 [J $mol^{-1}K^{-1}$]

Symbols

A_n PEN geometrical surface within the $n^{th} CV$ [m^2]

A_{cross} Fuel and air passage surface [m^2]

a_v	Electrochemically active area per unit volume of electrode [m^2 m^{-3}]
C	Total concentration [mol m^{-3}]
C_i	Concentration of species i [mol m^{-3}]
$c_{p,i}$	Specific heat of species i [J mol^{-1} K^{-1}]
$c_{p,int}$	Specific heat of interconnection [J kg^{-1} K^{-1}]
$c_{p,PEN}$	PEN specific heat [J kg^{-1} K^{-1}]
C_f	Friction factor [-]
D_i	Diffusion coefficient of species i [m^2 s^{-1}]
E_{act}	Activation energy [J mol^{-1}]
h_f	Fuel convective heat transfer coefficient [W $m^{-2}K^{-1}$]
h_a	Air convective heat transfer coefficient [W $m^{-2}K^{-1}$]
h_i	Enthalpy of species i [J mol^{-1}]
H	Channel height [m]
H_{int}	Interconnection height after channel height [m]
i	Current density [A m^{-2}]
i^{ely}	Current density within the electrolyte [A m^{-2}]
i_0	Exchange current density [A m^{-2}]
K_{eq}	Equilibrium constant [-]
L_{CV}	CV length [m]
MM_i	Molar Mass of species i [kg mol^{-1}]

$\dot{m}_i$ mass rate of species i [mol s^{-1}]

$\dot{n}_i$ molar rate of species i [mol s^{-1}]

$N_{sp,a}$ Number of species in the air

$N_{sp,f}$ Number of species in the fuel

P_a Air pressure [Pa]

P_f Fuel pressure [Pa]

P_i Partial pressure of species i [Pa]

$P^0_{O_2}$ Oxygen partial pressure in the anode, at anode/electrolyte interface [Pa]

$P^I_{O_2}$ Oxygen partial pressure in the electrolyte, at anode/electrolyte interface [Pa]

$P^{II}_{O_2}$ Oxygen partial pressure in the electrolyte, at cathode/electrolyte interface [Pa]

$P^L_{O_2}$ Oxygen partial pressure in the cathode, at cathode/electrolyte interface [Pa]

Po Posuille number [-]

$\dot{Q}_{a\to b}$ Heat flowing from a to b [W]

q_{loss} Heat loss specific to exposed surface [W m^2]

Re Reynolds number [-]

t time instant [s]

t_{an} Anode thickness [m]

t_{cat} Cathode thickness [m]

t_{PEN} PEN thickness [m]

T_a Air temperature [K]

T_f	Fuel temperature [K]
T_{int}	Interconnection temperature within the CV [K]
T_{PEN}	PEN temperature within the CV [K]
U_f	Fuel utilization factor [%]
U_{ox}	Oxygen utilization factor [V]
v	Stream velocity [m s^{-1}]
V	Volume of discretized fuel (or air) channel within a CV [m^3]
V_{cell}	Cell voltage [V]
W	Channel width [m]
$x_{i,b}$	Bulk flow molar fraction of species i [-]
$x_{i,r}$	Active site molar fraction of species i [-]
β	Electron transfer coefficient [-]
ΔG	Gibbs free energy of reaction [J mol^{-1}]
$\Delta V_{rev,comb}$	Reversible voltage when considering CO direct oxidation [V]
Δt	Time step of dynamic simulation [s]
ϵ	Electrode porosity [-]
τ	Electrode Tortuosity [-]
γ	Pre-exponential factor of exchange current density [A m^{-2}]
η_{act}	Activation overpotential [V]
η_{conc}	Concentration overpotential [V]

η_{ohm}	Ohmic overpotential [V]
ϕ	Electric potential [V]
σ	Electric conductivity [S m^{-1}]
σ_{th}	Thermal conductivity [W m^{-1} K^{-1}]
η_{el}	Electric efficiency [%]
ρ	Density [kg m^{-3}]

Bibliography

[1] J. Larminie, A. Dicks. "Fuel Cell Systems Explained Second Edition", Wiley, 2003.

[2] T. Matsui, M. Inaba, A. Mineshige, Z. Ogumi. "Electrochemical properties of ceria-based oxides for use in intermediate-temperature SOFCs", *Solid State Ionics*, 176, 647 - 654, 2005.

[3] J. Li, T. Lv, X. Dong, J. Yu, B. Yu, P. Li, X. Yao, Y. Zhao, Y. Li. "Linear discharge model, power losses and overall efficiency of the solid oxide fuel cell with thin film samarium doped ceria electrolyte. Part II: Power losses and overall efficiency", *International Journal of Hydrogen Energy*, 1 - 6, 2017.

[4] S. Campanari, P. Iora. "Comparison of Finite Volume SOFC Models for the Simulation of a Planar Cell Geometry", *Fuel Cells*, 5, 34 - 51, 2005.

[5] V. Spallina, L. Mastropasqua, P. Iora, M.C. Romano, S. Campanari. "Assessment of finite volume modeling approaches for intermediate temperature Solid Oxide Fuel Cells working with CO-rich syngas fuels", *International Journal of Hydrogen Energy* 40, 15012 - 15031, 2015.

[6] O. Razbani, M. Assadi, M. Andersson. "Three dimensional CFD modeling and experimental validation of an electrolyte supported solid oxide fuel cell fed with methane-free biogas", *International Journal of Hydrogen Energy*, 38, 10068 - 10080, 2013.

[7] M. Rahmanipour, A. Pappacena, M. Boaro, A. Donazzi. "A Distributed Charge Transfer Model for IT-SOFCs Based on Ceria Electrolytes", *Journal of the Electrochemical Society*, 164 (12), F1249 - F1264, 2017.

[8] S. Shen, Y. Yang, L. Guo, H. Liu. "A Polarization Model for a Solid Oxide Fuel Cell with a Mixed Ionic and Electronic Conductor as Electrolyte", *Journal of Power Sources*, 2014.

[9] S. Shen, M. Ni. "2D segment model for a solid oxide fuel cell with a mixed ionic and electronic conductor as electrolyte", *Internetional Journal of Hydrogen Energy*, 40, 5160 - 5168, 2017.

[10] P. Iora, S. Campanari. "Development of a Three-Dimensional Molten Carbonate Fuel Cell Model and Application to Hybrid Cycle Simulations", *Journal of Fuel Cell Science and Technology*, 4, 501 - 510, 2007.

[11] D. Mogensen, J.-D. Grunwaldt, P.V. Hendriksen, K. Dam-Johansen, J.U. Nielsen. "Internal steam reforming in solid oxide fuel cells: Status and opportunities of kinetic studies and their impact on modelling", *Journal of Power Sources*, 196, 25 - 38, 2011.

[12] K. Ahmed, K. F*ö*ger. "Approach to equilibrium of the water-gas shift reaction on a Ni/zirconia anode under solid oxide fuel-cell conditions", *Journal of Power Sources*, 103, 150 - 153, 2001.

[13] P. Aguiar, C.S. Adjiman, N.P. Brandon. "Anode-supported intermediate-temperature direct internal reforming solid oxide fuel cell. II. Model-based dynamic performance and control", *Journal of Power Sources*, 147, 136 - 147, 2005.

[14] D. P. Xenos, P. Hofmann, K. D. Panopoulos, E. Kakaras. "Detailed transient thermal simulation of a planar SOFC (solide oxide fuel cell) using gPROMS^{TM}", *Energy*, 1 - 19, 2014.

[15] E. S. Hecht, G. K. Gupta, H. Zhu, A. M. Dean, R. J. Kee, L. Maier, O. Deutschmann. "Methane reforming kinetics within a Ni-YSZ SOFC anode support", *Applied Catalysis A*, 295, 40 - 51, 2005.

[16] https://en.wikipedia.org/wiki/Solid_oxide_fuel_cell

[17] S. Campanari, P. Iora. "Definition and sensitivity analysis of a finite volume SOFC model for a tubolar cell geometry", *Journal of Power Sources*, 132, 113 - 126, 2004.

[18] B. Poling, J. Prausnitz, J. O'Connell. "The Properties of Gases and Liquids", 5th edition, McGraw-Hill, 2001.

[19] B.A. Haberman, J.B. Youg. "Three-dimensional simulation of chemically reacting gas flows in the porous support structure of an integrated-planar solid oxide fuel cell", *International Journal of Heat and Mass Transfer*, 47, 3617 - 3629, 2004.

[20] H. Timmermann, W. Sawady, R. Reimert, E. Ivers-Tiffée. "Kinetics of (reversible) internal reforming of methane in solid oxide fuel cells under stationary and APU conditions", *Journal of Power Sources*, 195, 214 - 222, 2010.

[21] R. S. Gemmen, C. D. Johnson. "Effect of load transients on SOFC operation—current reversal on loss of load", *Journal of Power Sources*, 144, 152 - 164, 2005.

[22] Y. Huangfu, F. Gao, A. Abbas-Turki, D. Bouquain, A. Miraoui. "Transient dynamic and modeling parameter sensitivity analysis of 1D solid oxide fuel cell model", *Energy Conversion and Management*, 71, 172 - 185, 2013.

[23] P. Iora, M. A. A. Taher, P. Chiesa, N. P. Brandon. "A one dimensional solid oxide electrolyzer-fuel cell stack model and its application to the analysis of a high efficiency system for oxygen production", *Chemical Engineering Science*, 80, 293 - 305, 2012.

[24] V. M. Janardhanan, O. Deutschmann. "Numerical study of mass and heat transport in solid-oxide fuel cells running on humidified methane", *Chemical Engineering Science*, 62, 5473 - 5486, 2007.

[25] L. Petruzzi, S. Cocchi, F. Fineschi. "A global thermo-electrochemical model for SOFC systems design and engineering", *Journal of Power Sources*, 118, 96 - 107, 2003.

[26] X. Xue, J. Tang, N. Sammes, Y. Du. "Dynamic modeling of single tubular SOFC combining heat/mass transfer and electrochemical reaction effects", *Journal of Power Sources*, 142, 211 - 222, 2005.

[27] R. Suwanwarangkul, E. Croiset, E. Entchev, S. Charojrochkul, M.D. Pritzker, M.W. Fowler, P.L. Douglas, S. Chewathanakup, H. Mahaudomc. "Experimental and modeling study of solid oxide fuel cell operating with syngas fuel", *Journal of Power Sources*, 161, 308 - 322, 2006.